Simulation of Portable Gamma Radiation Detectors for Virtual Reality based Training applications

PhD Thesis

Teófilo Moltó Caracena
Author

Eduardo Vendrell Vidal
Director and Tutor

November 2015

Acknowledgements

I would like to express my deep gratitude to my scientific and academic supervisors: Dr. Gonçalves, Dr. Peerani and Dr. Vendrell Vidal, for their guidance, expertise, patience and encouragement throughout the whole time it has taken me to elaborate this PhD.

Also I would like to thank my colleagues of whom I have learned the ropes of some of the techniques necessary for the work done in this thesis.

Finally I would like to thank my parents for a lifetime of unconditional support, dedication and effort. Without them, most likely I could not be writing these words right now.

Abstract

This thesis focuses on the development of a simulator of a gamma radiation portable detector. The aim is to determine the feasibility of such a software tool in a virtual reality (VR) based application, with the purpose of using it in training tasks in the framework of nuclear safeguards and security activities.

The work starts with the definition of the series of technical requirements which are necessary to achieve a working prototype of an application of the kind aforementioned.

In order to achieve these requirements, a series of incremental prototypes of a VR based simulator are devised, implemented and tested. Each of these prototype versions tries to improve on its predecessor by introducing new concepts aimed at better satisfying the requirements set.

The thesis is structured in several main chapters which divide the bulk of the PhD work in independent sections. Therefore, first the problem is introduced and then the current state of the art analysed. Next the first solutions are explained and following these introductory chapters the main contribution of the author is found in the development chapter. This chapter explains the ideas and methods created in a chronological manner, taking the reader through the steps the author took in the same order as he did.

Logically, the next chapter deals with the testing of these methods in order to assess their validity and last a conclusion chapter evaluates if the objectives set at the beginning of the thesis have been met according to the results obtained.

Resumen

Esta tesis trata el desarrollo de un simulador de un detector portátil de radiación gamma. El objetivo es determinar si una herramienta software basada en técnicas de realidad virtual como esta es factible. Con la intención de utilizarla en tareas de entrenamiento de personal en el sector de la salvaguarda y seguridad nuclear.

El trabajo empieza con la definición de la serie de requisitos técnicos que son necesarios para conseguir un prototipo funcional de una aplicación como la anteriormente descrita.

Para conseguir cumplir estos requisitos, se han desarrollado, implementado y probado una serie de prototipos incrementales de un simulador basado en realidad virtual. Cada uno de estos prototipos intenta mejorar a su predecesor introduciendo nuevos conceptos con el objetivo de satisfacer mejor los requisitos planteados.

La tesis está estructurada en varios capítulos principales que dividen el grueso del trabajo en secciones independientes. Por lo tanto, en primer lugar se introduce el problema y luego se analiza el estado del arte. A continuación se explican las primeras soluciones probadas seguidas del capítulo de desarrollo que contiene la contribución principal del autor. Este capítulo explica las ideas y métodos creado en orden cronológico, llevando al lector por los mismos pasos que el autor dio.

De manera lógica, el siguiente capítulo trata con el testeo de estos métodos para evaluar su validez y un último capítulo de conclusión analiza si se cumplieron los objetivos propuesto al inicio de la tesis según los resultados obtenidos.

Resum

Esta tesi tracta el desenrotllament d'un simulador d'un detector portàtil de radiació gamma. L'objectiu és determinar si una ferramenta software basada en tècniques de realitat virtual com esta és factible, amb la intenció d'utilitzar-la en tasques d'entrenament de personal en el sector de la salvaguarda i seguretat nuclear.

El treball comença amb la definició de la sèrie de requisits tècnics que són necessaris per a aconseguir un prototip funcional d'una aplicació com l'anteriorment descrita.

Per a aconseguir complir estos requisits, s'han desenrotllat, implementat i provat una sèrie de prototips incrementals d'un simulador basat en realitat virtual. Cada un d'estos prototips intenta millorar el seu predecessor introduint nous conceptes amb l'objectiu de satisfer millor els requisits plantejats.

La tesi està estructurada en diversos capítols principals que dividixen el total del treball en seccions independents. Per tant, en primer lloc s'introduïx el problema i després s'analitza l'estat de l'art. A continuació s'expliquen les primeres solucions provades, seguides del capítol de desenrotllament, que conté la contribució principal de l'autor. Este capítol explica les idees i mètodes creats en orde cronològic, portant al lector pels mateixos passos que l'autor va fer.

De manera lògica, el següent capítol tracta el testeig d'estos mètodes per a avaluar la seua validesa i un últim capítol de conclusió analitza si es van complir els objectius proposats a l'inici de la tesi segons els resultats obtinguts.

Table of Contents

List of Figures

1 Introduction

What is a portable radiation detector? What does it have to do with Virtual Reality? And what is the point of simulating its usage? These are questions that might come to a reader, who has no background on these topics, after reading the title of this thesis.

This introductory chapter is aimed at answering these questions by giving the reader an overview of the working context, the different areas of science involved, the main objective of this work and the structure of this thesis document.

1.1 Historical Working Context

The development of nuclear science and technology during the first half of the twentieth century and specifically the creation of military nuclear devices led to a worldwide struggle to control nuclear and radioactive materials.

With this objective in mind, the United Nations Organisation (UNO) established the International Atomic Energy Agency (IAEA) as an independent entity in 1957 [1]. The IAEA's task is to assist its member countries in developing civilian uses to nuclear science and technology and to verify that the non-proliferation agreements are respected.

One of the branches in this field of work is Nuclear Safeguards and Security activities (NS&S). The aim of NS&S is to ensure that nuclear material is used only for peaceful purposes such as energy production and medical treatments. This is achieved by controlling nuclear and radioactive materials and detecting their illicit transfer.

Part of this thesis project work was performed at the European Commission's Joint Research Centre, Institute for Transuranium Elements (JRC-ITU) Nuclear Security Unit. JRC-ITU provides scientific and technical assistance to the implementation of two international

treaties: EURATOM treaty for the European Union (implemented by the European Commission, Luxembourg) and the Non-Proliferation Treaty (implemented by the International Atomic Energy Agency, Vienna, Austria).

1.2 Radiation Detectors

In order to achieve the goals noted previously, it is evident that nuclear and radioactive materials must be controlled with care. To control a nuclear or radioactive material, first it needs to be detected and identified. Many kinds of apparatus exist to facilitate the detection of nuclear and radioactive materials. Depending on the type of radiation, the accuracy required, the time available and other factors, a type of detector is better suited than other. In safeguards and security one of the most used tools is the main character of this work, the portable radiation detector, also called survey meter.

These instruments measure primarily the gamma radiation received by the user. Some provide gamma spectral measures that can be used to identify the material.

Naturally it is not straightforward for the new user how to use these instruments, especially if her/his background is not related to radiation physics, which is a fairly common type of user in most real life cases. Therefore, previous training is required. This leads to the next topic which deals with this concept.

1.3 Training

Survey meters are used by many kinds of users around the world, among them first responders like police or firemen, officers at customs in border crossings and airports, medical personnel, nuclear industry workers etc.

Obviously in order to be able to properly use detectors these users need to be trained, to be able to locate a nuclear or radioactive

source and characterise the source intensity and type. Nowadays training is performed in a traditional on-site way. This implies the use of real detectors, real nuclear sources and a facility where it is possible to perform this kind of training.

There are three important disadvantages with this classical training method.

First, the *availability of nuclear sources*. Having access to nuclear sources valid for training is not possible everywhere, often the users need to travel to another country where such a facility exists.

Second, the *cost associated to training*. International travelling, accommodation, expert instructors, interpreters, high tech material (detectors) etc. requires finding a sizeable budget for all of this and represents a difficulty for the organisers.

Third, *time*. Such a complex organisation requires planning courses well in advance making it a slow process to train new users or regularly refresh the knowledge of the current ones.

1.4   Virtual Reality based computer simulation

When trying to find a solution to the shortcomings of traditional on-site training the option of Virtual Reality (VR) training comes up. A VR based computer application could simulate the tasks performed at training, without the need of nuclear sources, survey meters or a special facility. Training could be held at the user's location on standard PCs, where the scenario, tools and procedures are simulated. This VR based approach overcomes all three disadvantages of the traditional method. This approach may thus complement training sessions based with real sources and equipment. Furthermore, it would allow the user to train for cases that due to unavailability of sources or even cases that would represent a physical hazard (and therefore are impossible to train for) but still can actually happen in the real world.

Therefore it is established as a goal of this thesis to develop a VR based prototype application to be used for training purposes, this practical goal translates into a series or technical requisites when trying to implement such a tool, these are of two kinds: VR related, and radiation transport related.

To be successful, VR based applications need to "immerse" the user into the virtual world, making him/her feel like in the real world. This requires that images reach the user at a rate that convinces the brain of the user into believing the series of images are actually a realistic view of the world. In other words the first requirement is that frame refresh rate of the rendering process must be high enough to provide this fluidity of movement.

The second requirement is also time related. The measuring time that real survey meters require must be respected in the virtual simulation, this is not a fixed value since it depends on the instrument, and even for a given instrument it may vary depending on the energy range being measured.

The last requirement is related to the fact this is a dosimetry application, therefore the accuracy of the dose rate value provided must be in line with the accuracy of the real survey meter. This represents the biggest challenge of the thesis considering the starting point was an application that did not provide a real dose rate value at all, let alone one which is within the required accuracy. In order to tackle this problem, the first step was to evaluate what kind of solutions already existed for this problem. In other words evaluating the state of the art in radiation transport methods, in order to judge their applicability to VR based tools.

Therefore the main task of this PhD thesis is to develop methods for radiation transport simulation which will meet the requirements of VR based applications simulating the use of survey meters.

1.5 Thesis structure

The thesis is structured in seven chapters, dividing the project in well-defined steps in order to simplify the reader's task, with this introduction being the first of the seven.

The second chapter investigates the state of the art of the different branches of science and technology which this work is based on. These are radiation transport simulation, radiation detectors, virtual reality, nuclear safeguards training and geometry decomposition. The aim is to determine what are the limitations and possibilities of these technologies at their current state in order to know which paths of research to follow.

The third chapter deals with the first approaches taken to achieve the objectives set. It explains the paths that were explored and why they were not a valid solution to meet the objectives.

The fourth chapter covers the bulk of the work done, it starts with the simplest solution found, which is the cornerstone on which all the following work is based, going through the iterative process that lead to the final version of the method which is the most significant scientific contribution of this thesis.

The fifth chapter focuses on the results obtained in the experiments done to test the validity of the code. Comparing these results with those obtained using other benchmark codes and real life experiment data.

The sixth chapter is dedicated to the conclusions that are extracted from evaluating the results obtained in the last chapter and addressing the issue of future work, what could be done in order to improve the method created, what other uses or research directions might be worth to explore.

Finally the last chapter includes a bibliographical reference list to all the research resources cited in this thesis.

1.6 Motivation

Within the frame of the Joint Research Centre's (JRC) programme on Nuclear Safeguards and Security, precursory work for this thesis was started under the traineeship program during 2008, consisting in the development of Virtual Reality (VR) based software tools with the aim of demonstrating the possible uses of VR in the fields of nuclear safeguards and security.

This work led to the development of several applications [2]. Among them, a VR prototype aimed at training users how to use gamma radiation detectors. This simple prototype was just a showcase of the advantages of applying VR to training applications in this field. Nevertheless the potential of this prototype to become a real useful tool to be used in training, made it worth to continue its development.

The challenge arose when trying to find a way to implement the physics behind the behaviour of the elements involved (radiation sources, detectors, behaviour of gamma radiation with the aforementioned and other objects) while respecting the requirements of VR applications (real time behaviour).

As the next chapters of this thesis will show, matching gamma radiation transport simulation and VR is not a straightforward task. Several methods exist for radiation transport computation, but they are not capable of real time performance. On the opposite end, some VR applications treat the issue of radiation detectors but lack a solid physics base to provide sufficiently accurate results, therefore none of them has successfully achieved both requirements. This conundrum motivated this PhD project.

All the work for this PhD thesis has been carried out within the ITU (Institute for Transuranium Elements) NUSEC Unit at the Ispra site (Italy), part of the European Commission's JRC, under the direct supervision of Dr. João Gonçalves, the nuclear physics expert aid of

Dr. Paolo Peerani and the guidance and tuition of my thesis director Dr. Eduardo Vendrell Vidal from the Universitat Politècnica de València (Spain).

2 Radiation detection, Virtual Reality and Simulation

The aim of this chapter is to introduce the concepts, definitions and procedures which are relevant to the fields of science pertinent to the thesis and their current state of development.

The first step performed was to study the state of the art of all the branches of science and technology which are involved in the topic of the thesis. Only after a thorough analysis of the current situation, it is possible to properly define a line of research, reducing the chance of following paths already explored by other researchers and known dead ends.

This thesis involves several fields of study. In first place types of radiation and detectors were studied, to properly understand what had to be simulated exactly. This led onto training and Virtual Reality (VR) to answer the question of what VR training options are there currently available. The next relevant issue is how to simulate the physical concepts involved, therefore a careful analysis of dosimetry applications and the latest radiation transport methods was undertaken. Finally several methods and theories involving efficient modelling, which were useful to develop solutions for this thesis were examined.

Therefore this chapter is divided into the following main sections:

- Radioactivity and radiation detectors.
- Virtual Reality and its use for training.
- Radiation transport simulation methods.

2.1 Radiation Physics Basics

This thesis research focuses mainly on computer science methods applied to the field of nuclear science, there is no pure physics research per se and none is pretended. Nevertheless due to the extensive use of nuclear physics concepts throughout the work, the author considers it necessary to introduce some basic nuclear physics definitions and concepts.

2.1.1 Characterization of Atoms

For a long time atoms where be considered the cornerstone of physics, the general consensus up to the beginning of the 20th century was that all the materials known were built by atoms, the smallest entity of matter which could not be divided.

This theory was proved wrong by the discovery of the electron in 1897 by J.J Thompson and the other sub-particles neutron (discovered by James Chadwick in 1932) and proton (discovered by Ernest Rutherford in 1920). For the purposes of this thesis, the classical Rutherford-Bohr model [3] is sufficient and we will not deepen into the intricacies of the Standard Model for particle physics [4]. This thesis will only consider atoms as defined by the Rutherford-Bohr model, that is considering a positively charged nucleus containing a determined amount of protons (dubbed Z or atomic number) and neutrons (dubbed N) surrounded by a cloud of electrons.

Using this nomenclature the atomic mass number (A) is defined as the addition number of sub-particles in the nucleus (protons and neutrons) as stated in the following equation.

Equation 2-1

$$A = N + Z$$

The atomic mass (A) and atom number (Z) allows us to unambiguously define every nuclide by using the following notation $^A_Z X$ or X-A, e.g. the isotope of the element Plutonium with atomic number 94 and atomic mass 241 will be referenced in this text as $^{241}_{94} Pu$ or Pu-241.

2.1.2 Radiation

Radiation can be defined as the emission of sub-atomic particles and/or energy. It is a very broad term which encompasses several types of radiation that are of no interest in the field of nuclear safeguards, such as radio waves or heat.

Therefore we take the more restrictive term "ionizing radiation" which in its classical definition includes alpha, beta and gamma radiation types. To these three, neutron radiation is added which is also a significant indicator of nuclear material presence. These four kinds of radiation are the primary concern in nuclear safeguards as they originate from atomic or nuclear processes.

Alternatively other authors [5] propose to classify these relevant kinds of radiation according to their charge as shown in the following figure.
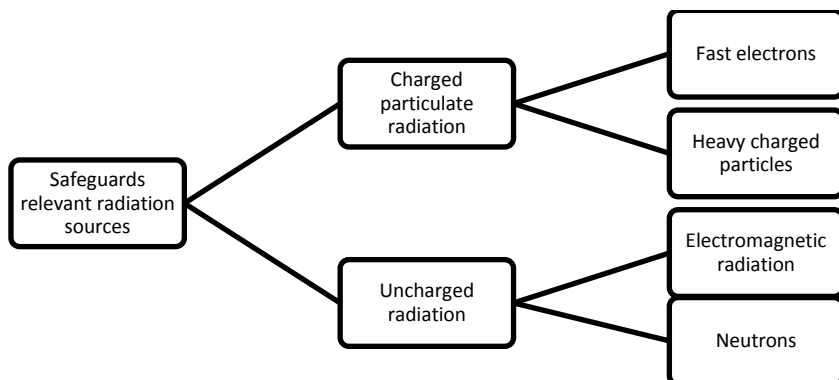
Figure 2-1 Types of nuclear safeguards relevant sub particles

In the Fast electrons category beta particles both negative and positive are included from whichever origin, though in nuclear safeguards it will most likely be the standard negative kind. The Heavy charged particles category includes alpha particles (Helium nucleus), protons and any other ion with atomic mass equal or greater to one. The neutron category is self-explanatory as it just considers this sub-particle (albeit sometimes can be distinguished in slow or fast neutron subcategories). Finally the electromagnetic radiation category is in this field limited to gamma rays and X-rays with gamma being the main subject of study of this thesis.

The most obvious characteristic that tells apart these kinds of radiation is their different penetrating power. Alpha particles have a very limited ability to penetrate through matter and can be blocked by a sheet of paper or the skin, therefore external contact is not dangerous but if inhaled they can represent a safety threat. Next (in terms of penetrating power) are the beta particles, these can pass through human skin but they are stopped by a thin sheet of metal or plastic. Gamma and X-rays have a much stronger penetrating ability, managing to pass through human tissue easily. In order to shield this type of radiation a considerable thickness of dense materials (like lead or concrete) is necessary. Finally neutrons are strongest penetrating radiation, requiring very thick hydrogen containing materials (water most notably) to shield effectively neutrons.

Considering the objective of this thesis is to simulate a gamma radiation detector, the research will focus on computer methods to simulate the transport of gamma radiation, leaving aside the other types mentioned.

2.1.3   Radioactivity

Radioactivity is the rate of decay of a radioisotope (a radioisotope is a non-stable atom which emits radiation in a process called radioactive decay). Technically speaking it is defined as the number of atoms

decaying per unit time. This must not be confused with the number of particles emitted from the atom.

Historically the unit used to measure activity has been the *curie* (Ci) named in honour of Marie and Pierre Curie. It corresponds to 3.7 x 10^{10} disintegrations per second, which is the activity of one gram of the radium isotope Ra-226 which the Curies used in their experimentation.

Though still used in literature, it has been substituted for the SI (International System of Units) unit *becquerel* (Bq) also named in honour of another radioactivity research pioneer, Henri Becquerel. A becquerel is equivalent to one disintegration per second. This unit and its multiples kilo becquerel (kBq) and mega becquerel (MBq) will be used throughout this thesis to define the activity of a nuclear source.

2.1.4   Energy

In nuclear physics the SI unit for energy; the *joule* (J), is rarely used. A much more practical and quantitatively smaller unit for this purposes is the *electron volt* (eV), which is defined as the kinetic energy gained by an electron by its acceleration through a potential difference of one volt, one eV equates to 1.602 x 10^{-19} J.

The energy of the emission lines of the radioisotopes used during this thesis will be quantified using the multiples of the eV: *kilo electron volt* (keV) and *mega electron volt* (MeV), which are more convenient for the magnitudes usually found in this kind of research work.

The energy emissions can be used to identify a radioisotope, as the gamma-ray photon energy is directly related to the frequency by the following formula.

Equation 2-2

$$E = h \cdot v$$

Where *E* stands for the energy of the emitted photon, h is Planck's constant (4.135 x 10^{-15} eV · s) and h is the frequency in h*ertz* (Hz). For example the radioactive isotope of cobalt Co-60 emits two gamma rays in its decay, with energies of 1.173 MeV and 1.332 MeV respectively.

2.2   Gamma Radiation Detectors

Radiation detectors exploit the capacity of gamma-ray photons to interact with the electrons of the detecting element. They ionize the atom, giving the electron its energy. These electrons are then collected directly or indirectly (depending on the type) by the detector which acknowledges the presence of the gamma ray and may measure its energy, in that case providing an electrical pulse whose voltage is proportional to the energy carried by the photon.

There are several types of detectors; they can be categorized by the physical principle upon which they work. The three most relevant types for Safeguards according to [6] are: Gas-filled detectors, Scintillation detectors and Solid-state (also known as semiconductor) detectors.

2.2.1   Gas-filled detectors

Gas-filled detectors consist of a closed housing containing two electrodes and a sensible gas, which fills the housing separating the electrodes. Usually the casing is metallic and acts as the negative electrode and a wire in the centre acts as an anode in the electric circuit as shown in the following figure.

When incident gamma radiation ionizes the gas, the resulting electrons are driven by the electric field into the anode, creating a charge in the circuit for each incident photon which can be detected.
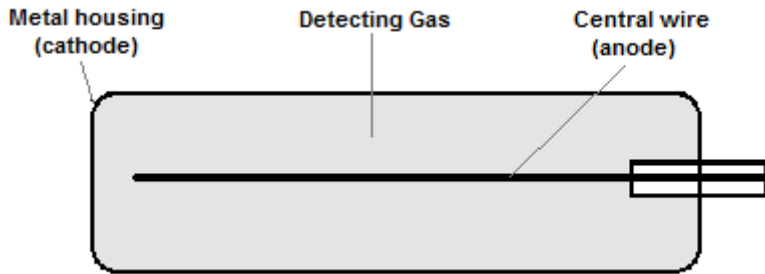
Figure 2-2 Gas-filled detector scheme

Depending on the strength of the electric field applied we can distinguish three cases:

- *Ionization chamber*: This is the lowest voltage case, only the primary ionization charge is collected, there is no secondary ionization.

- *Proportional counter*: This case considers a higher voltage than an ionization chamber, this results in secondary ionization which follows the initial single ionization event. The output signal generated is proportional to the energy transferred by the incident photon to the gas, hence the name proportional counter.

- *Geiger-Müller* (GM): GM detectors have the strongest electric field of the three kinds of gas-filled detectors, this causes a larger secondary ionization effect which ends up saturating the field, and in this case the response is no longer proportional to the incident gamma ray photon energy. Therefore a GM tube detector cannot distinguish radiation type or energy magnitude. Another disadvantage is that after each pulse the GM detector is inactive for periods of time of several microseconds, limiting the detector to low frequency applications.

2.2.2 Scintillation detectors

The gamma ray detecting element of a scintillation detector is a luminescent material, which produces pulses of light when gamma radiation reaches the material. Subsequently this light pulse is converted into an electrical signal due to the photoelectric effect, via a photomultiplier tube (PMT). This electron flow is then largely amplified by a series of electrodes in the PMT. Finally this amplified flow of electrons reaches the output electrode with a magnitude that is proportional to the initial gamma ray photon. Many materials (both organic and inorganic) can be used to build the scintillator like for example thallium doped sodium iodide (NaI), caesium iodide (CsI), zinc sulphide, lithium iodide (LiI) bismuth germanate (BGO) or more recently cerium doped lanthanum tribromide $LaBr_3(Ce)$. The thallium doped NaI is one of the most used due to its good efficiency for gamma radiation. The following figure shows the scheme of a scintillator detector.
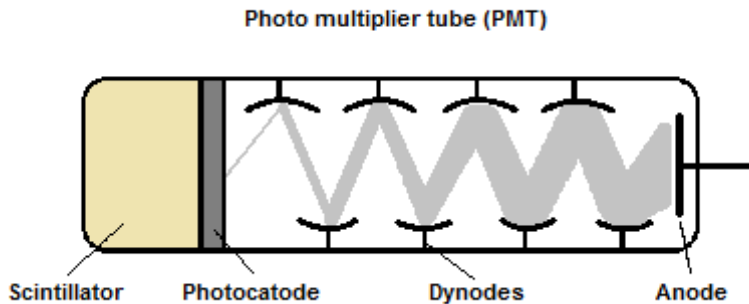
Figure 2-3 Elements of a Scintillation detector

2.2.3 Semiconductor detectors

This kind of detectors (sometimes called solid-state) use as a detecting element the depleted region of a semiconductor material. This depleted region allows electrons and holes to move freely, therefore if a charge is produced by an incoming gamma ray photon, the flow reaches the electrodes producing a measurable electrical

signal which is proportional to the energy of the incident gamma ray. The most commonly used materials used to build the semiconductor are silicon (Si) and germanium (Ge). Initially lithium was used to 'dope' the crystal to compensate for the impurities in it, nowadays high purity crystals are available like high purity germanium (HPGe) which eliminate the need to dope with lithium. These detectors offer a much higher resolution that scintillator detectors, unfortunately they require cumbersome cooling systems like liquid nitrogen, this limits their range of application. Other materials can be used which need no cooling and therefore can be used for portable detectors, among them there is Cadmium Telluride (CdTe), Cadmium Zinc Telluride (CZT), mercuric iodide (HgI2) or gallium arsenide (GaAs) the downside is they are not as accurate as the HPGe detector. This lack of efficiency of portable detectors is of utmost importance for the work being developed in this thesis as it establishes the amount of deviation the simulation will be allowed to have in order to be realistic. The following figure shows the main parts of the detecting element in a semiconductor detector, the depleted region in the centre is the detecting element.
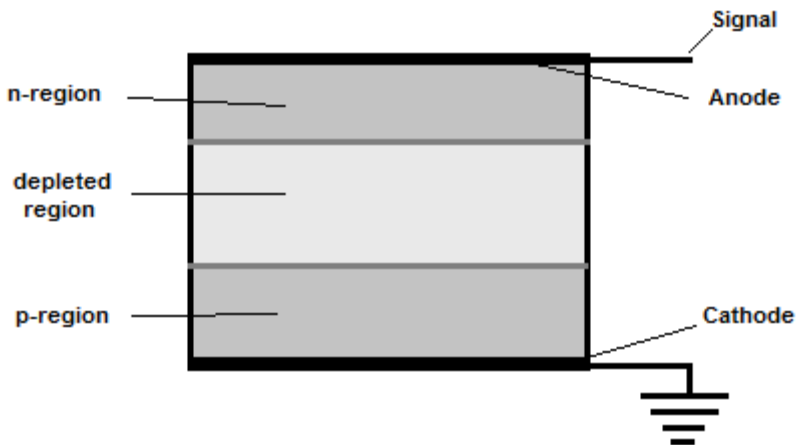
Figure 2-4 Scheme of a semiconductor detector

2.3   Virtual Reality

It is not evident how to define Virtual Reality (VR). One of the first definitions of VR was given by one of the pioneers of computer graphics, Ivan Sutherland [7]: "A looking glass into a mathematical wonderland". A much less poetic but much more practical definition is given in [8]: "A VR experience is any in which the user is effectively immersed in a responsive virtual world. This implies user dynamic control of viewpoint". This definition introduces a few key concepts of this field such as immersion, dynamic and viewpoint.

For this thesis purposes we can consider VR a technology which aims at representing the real world by electronic means, with as much realism as possible. In an ideal perfect VR system the user should not be able to tell the difference between VR and reality.

The following points will analyse what a VR system is, what are its purposes and how could it be useful for the objectives set in this thesis.

2.3.1   VR Systems

VR includes all kind of media and graphics technology available, there are no limitations to how the immersion objective can be reached, although there are four technologies that are crucial to VR (according to [9]) and are found in most VR systems, these are:

- The interface: It potentially can target all of the user's senses, not just the sight (common visual interface via PC screen) but also aural and haptic, responsible of immersing the user in the virtual environment. Among the most characteristic VR interfaces we can find HMDs (Head mounted displays) and CAVEs (Cave automatic Virtual Environment) but also panoramic displays, workbenches and sound systems are other used devices.
- Graphics rendering systems: These provide real time (at least 15 to 20 frames per second) representation of the environment. This

systems evolve rapidly, with dedicated graphics cards (GPU) improving their speed and reducing their cost, driven by the video game market.

- Tracking Systems: In VR systems where the position and/or aim of the user and other relevant items need to be known, a tracking system is needed. There are several types of tracking systems. We can distinguish by technology type, radio frequency (RF), optical or acoustic.

- Database managing system: This takes care of the 3D model storage. Trying to represent objects realistically requires very precise models with an enormous amount of polygons; a lot of effort goes into reducing the computational load trying to keep the images realistic.

2.3.2   Haptic Interfaces and devices

Considering the myriad of visual interfacing devices and considerable number of audio options available in standard computer applications and hardware, what mostly pulls apart VR from the rest of computer areas is haptic interfaces which are almost exclusively a trademark of VR.

The objective of haptic interfaces is to use human sensory-motor skills to improve communication between human user and machine, making it a more realistic experience.

Haptic interfaces differ from traditional visual or sound interfaces because they provide mechanical signals that stimulate the human kinaesthetic and touch senses. Also they allow the user to interact physically in their environment. A distinguishing characteristic of haptic interfaces is the bidirectional information channel between the human user and the machine. Another difference with the visual interface is the minimum working frequency, for video purposes a rate of 24 frames per second is enough, the sense of touch requires update rates of 1 kHz or more to satisfy the signal representation theorem and to minimize interaction delay [9].

Haptic devices can be classified in two broad groups; passive or active. Passive (or inert) devices can only dissipate mechanical energy, though the dissipation can usually be programmed as a function of position or time.

In active devices, the energy exchange between user and machine is completely a function of the feedback control which is implemented. This leads into two sub-categories. First the isotonic ones were actuators act as a force source and the position is measured and second, the opposite case, the so called isometric devices: where actuators act as a position source and force is measured.

We can consider three main activities which make up the principle of operation of haptic interfaces. First we have the tactile sensations which include, pressure, temperature, surface texture, elasticity, wetness etc. Second we have the local geometrical features that we can identify like for example, shape, edges and recessed features. Finally we can define vibro-tactile sensations as the perception through touch of oscillating objects.

The components of a haptic interface are:

- Interface hardware: This includes the electromechanical transducers (sensors and actuators) that are physically in contact with the user. These provide a bi-directional communication; they can apply mechanical signals on the user (i.e. force feedback in a steering wheel) and also "read" the mechanical input created by the user's movement.
- Interface computer: The function of this computational system is to provide haptic rendering capabilities. This means producing signals that are relevant to a particular application. There are many ways to implement this task. For example, a model may be used to represent the environment, and its equations solved computationally to find forces as a function of displacements and their derivatives (or vice versa). The model may be developed

from first principles, or parameterized to represent only certain desired aspects (example extracted from MacLean, 1996).

2.3.3 Application of VR in Science and Industry

Virtual Reality is quite a new discipline compared to other science fields, despite that it has already passed the experimental period and has been successfully applied to different fields of industry, proving its validity as the following examples show:

- Vehicle Simulation: This was the first field where VR was applied and is still by the most developed one, many examples can be found of simulation of car driving ranging from simple low cost home systems (closely linked to the video game industry) which use standard video game interfaces up to prototype simulators with hydraulic/mechanical simulation of physics [10] [11]. This systems allow to both train the drivers of the vehicles and the vehicles themselves (to a certain extent) reducing costs, improving safety and saving time.

  Logically VR simulation of other similar transport means followed suit and well known are flying simulators for both commercial and military aircraft [12] and navigation simulators for ships [13]. All of these are usually created with the aim of providing a safe learning environment for the apprentices before taking command of the real aircraft or ship respectively.

- Medical applications: VR can be used also in the field of medicine, thanks to the use of augmented reality and the force feedback of haptic devices physicians can tele-operate a patient [14], and benefit from the precision of the computer controlled system. Also it is possible to use VR based applications to train surgeons or students [15] successfully improving their skills. Another medical use of VR is the treatment of mental diseases like acrophobia [16], spider phobia [17], claustrophobia [18].

- Design review: Reviewing a design by traditional means (blue prints, mock ups, scaled replicas etc.) is expensive, time

consuming or error prone. VR brings users a new way to review their designs in many fields such as hospital room equipment [19], automotive design [20], aircraft design and others.

- Others: Some tasks are trained on VR systems not just because of economical or safety issues but sometimes there just is not an alternative like for example NASA has simulator for training astronauts for extra-vehicular-activity [8].

These examples highlight some of the main advantages of VR systems: cost reduction, safety and time saving. The next point of this chapter illustrates how these advantages translate to the field of interest of this thesis, Nuclear Safeguards and Security.

2.3.4 VR applied to Nuclear Safeguards and Security

Virtual Reality has expanded into many fields of industry and science, and nuclear safeguards and security is not an exception. There are several examples of proposed applications that benefit from VR technology.

One of the first proposed applications was for training dismantling nuclear weapons and what the author called "hypermedia access" [21] which consists of a virtual navigation of a nuclear installation, a sort of information review. In this case VR was chosen because compared to other training methods like reading or watching, learning on VR is actually like doing the real task and it is therefore much more effective according to the authors.

Subsequent proposals covered topics such as: simulating generic nuclear sources and detectors, training operators to correctly handle nuclear materials within a source safe and evaluating diversion scenarios in nuclear facilities [22]. In this case the authors conclude that "VR technology is viable for safeguards analysis, design, and system evaluation". Furthermore the necessity of an efficient method to simulate sources is highlighted and some solutions proposed, these will be studied in a later chapter of this thesis.

Other more computer science oriented works show some interesting prototype applications based on open source 3D engines for simulating emergency and operational routines within a nuclear power plant (NPP) [23], [24]. Albeit being innovative proposals, they lack a proper radiation physics simulation, this limits their applicability to mostly demonstration purposes.

Nevertheless other researchers have gone one step further in this particular application (route planning in NPPs), and several more scientifically sound examples can be found, like for example the Visiplan tool [25] or the Halden Planner [26]. These aim at guaranteeing useful accurate enough data. This thesis focuses on the same target, aiming at accuracy.

Other examples of nuclear related applications are training inspections of nuclear facilities [27] by virtual inspection, and evaluation and gathering augmented reality tools [28].

Some of the latest developments in this field cover training activities such as replicating in VR scenarios relevant to the nuclear industry like a pressurized heavy water reactor [29], or teaching nuclear criticality safety program concepts [30]. Other recent work involves the simulation of video control systems in nuclear storage sites (or other facilities subject to safeguards control) [31]. This application aims also at training but in this case of future nuclear inspectors which need to learn the basics of camera installations and has recently passed the demo phase and has been tested with real trainees [32]. Also not forgetting the work associated to this thesis, simulation of radiation detectors in efficient ways to optimise its implementation on VR applications [33] has been a very active issue recently.

From all the information gathered in the contents of the previous examples, which represent the state of the art in VR applied to Nuclear Safeguards, it can be concluded that VR can provide advantages in terms of:

- Safety: In many activities real radioactive sources are used for training purposes. Nuclear sources are complicated to handle and can potentially be a health risk, virtualising them could offer a great advantage from this point of view.
- Cost saving: The technology used in nuclear safeguards devices is very expensive due to several reasons, among them, the fact the market is very small and the technology, state of the art. Furthermore training activities are now restricted to a few places around the globe, making it imperative for the users to travel to these special centres. The cost of bringing users and experts and transporting material adds up making it affordable not as often as desired.
- Time saving: The preparation of conventional training courses in this field is cumbersome and requires in many cases international cooperation. VR based training could provide and easy accessible source of training without the limitations of traditional training (availability of sources, availability of experts, etc.)
- Visualization: VR interfaces are able to show things to the user which cannot be shown by other more conventional means or even not possible to see in reality. This is very helpful for design review applications.

Another conclusion reached is that in order to obtain realistic results, the VR application must implement accurate radiation transport methods so that virtual sources and detectors can be used. In order to achieve this, the next step is to analyse the available computer simulation methods for radiation transport; this is covered in the next section.

2.4   Radiation transport simulation methods

Radiation transport methods can be divided in two broad categories these are: probabilistic (also called stochastic) and deterministic methods.

Probabilistic methods are based on the tracking of the physical events that affect a sizeable number of randomly chosen individual particles and from that sample deriving the average behaviour of all the system. The most significant method of this type is **Monte Carlo** (**MC**).

Deterministic methods are based on solving the Boltzmann transport equation and discretizing in space, angle and energy. The two methods of this type applicable to this task are the **Discrete Ordinates** method (**S$_N$**) and the **Point Kernel** method (**PK**).

The inherent characteristics of each method translate into performance differences which can be considered advantages or disadvantages depending on the aim of the simulation. These differences need to be taken into account when choosing a method for the objective of this thesis, real-time hand held detector simulation.

2.4.1   The Monte Carlo Method

The origins of the Monte Carlo method can be traced back to the forties, at the Los Alamos scientific laboratory in the US where Stanislaw Ulam conceived the idea of using a stochastic approach for radiation transport problems [34], due to the association to probability calculus they decided to name it Monte Carlo after the well-known casino located in that principality where a relative of Ulam used to spend his time. The method promptly proved its worth treating complicated particle transport systems [35]. A series of small MC codes for tracking a single kind of particles (neutron, photon, electron, gamma etc.) were released during the sixties and seventies. These later were merged into a general MC code, Monte Carlo N-Particle (MCNP), which has been used during the benchmarking phases of this thesis in its fourth version (MCNP 4).

Other equivalent codes where developed by other entities elsewhere in the world, such as the GEANT series [36] developed by the

European Organisation for Nuclear Research (CERN) now at its fourth version [37], the Organisation for Economic Co-operation and Development (OECD) brought forward PENELOPE [38], FLUKA [39] also by CERN in collaboration with the Italian National Physics Institute (INFN), TRIPOLI [40] by the French Alternative Energies and Atomic Energy Commission (CEA), the EGS series by Stanford Linear Accelerator Center [41] and several others.

Nowadays Monte Carlo methods are a well-established technology for nuclear physics computations and many other fields of science such as medical physics [42] or astronomy [43], where a determinist method is not a pertinent approach due to its lack of accuracy in certain conditions (see the following points of this chapter about deterministic methods), particularly those involving multiple independent variables.

The basic principle upon which Monte Carlo methods work is the use of random numbers to pick random particles (in this case photons) which will be given a weight and tracked until an interaction event ends the simulation of that particular particle.

The trajectory of that particle is ruled by a series of possible events which each have associated a probability. By tracking the path and events of each particle for a sufficient amount of particles the general behaviour of the whole system can be deduced. The accuracy of this simulation is proportional to the number of particles tracked, the more particles tracked the higher the accuracy.

The mathematical explanation for the method is the following. First calculating the probability of a collision of the tracked particle in the volume of matter being analysed, this probability is given by the following expression.

Equation 2-3

$$Pl\ (dl) = \sum_t e^{-(\sum_t l)dl}$$

Where *dl* is the length travelled until the collision and Σ_t is the macroscopic total cross section of the medium. Introducing a variable random (λ) in the range zero to one we redefines the expression as:

$$\lambda = \int_0^1 P(s)ds = \int_0^1 \Sigma_t \, e^{(-\Sigma_t s)ds} = 1 - e^{(-\Sigma_t s)}$$

From that equation it is possible to infer the expression for the distance to next collision:

$$l = -\frac{ln(\lambda)}{\Sigma t}$$

Subsequently taking into account the type of collision event, the direction of flight and energy of the resulting particle will be determined by the nuclear physics laws and the associated probabilities. Fig 2-5 illustrates Monte Carlo particle tracking, showing the possible events MC code must handle.
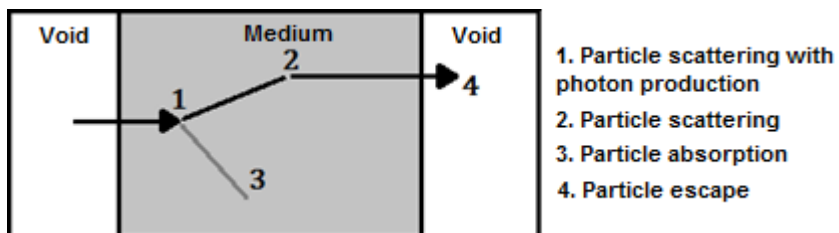
Figure 2-5 Tracking of a particle

The main drawback of this method is the high computational cost associated with calculating all the particle histories. Work has been done to provide solutions to this problem, producing the so called variance reduction schemes (such as nested Dxtran spheres [44], weight dependent variance reduction [45], pulse height tallies [46] Russian roulette etc.), which are techniques to speed up Monte Carlo

by biasing the particle choice, the direction choice or limiting other random dependent input variables. Despite these, the general consensus is that it is a slower method than deterministic approaches as acknowledged by the scientific community [47] [48] [49] [50].

2.4.2   The Discrete Ordinates Method

The Discrete Ordinates method (DOM), usually noted S_N, falls in the category of deterministic methods. It was originally developed by the astrophysics community to study radiation transfer in stellar and planetary atmospheres [52]. Later it was applied to study neutron transport in nuclear physics applications in sixties [53]. Nowadays it is widely used for particle transport (neutron and photon) problems in many software tools such as TORT [54], DOT [55], ANISN [56] or XSDRNPM [57].

The method is based on the evaluation of the Boltzmann transport equation, discretizing its differential form at a series of angular directions (ordinates) and the use of quadrature sets to substitute the angular integrals by summations over the discrete ordinates. The key elements of the method are the choice of ordinates, quadrature weights, difference schemes and iterative solution procedures.

In the general case two angular coordinates are necessary to specify the direction of motion of the particle travelling. This direction (usually dubbed vector Ω) is expressed by the cosines μ, ζ and η with respect to the coordinate axis (x,y,z) respectively. Due to the fact that Ω is a unit vector, the following expression applies to the direction cosines:

Equation 2-5

$$\mu^2 + \zeta^2 + \eta^2 = 1$$

 A two-dimensional quadrature is used to approximate the integrals in angular variables, so for the positive quadrant it can be written as the following expression as shown in [58].

46

Equation 2-6

$$\frac{\pi}{2} \int\limits_{0}^{1} d\mu \int\limits_{0}^{\frac{\pi}{2}} d\varphi \; f(\mu, \mathfrak{z}, \eta) \cong \sum_{n=1}^{M} W_n \, f(\mu_n, \mathfrak{z}_n, \eta_n)$$

Where $\eta = (1 - \mu^2)^{\frac{1}{2}} \times \cos\varphi$, $\mathfrak{z} = (1 - \mu^2)^{\frac{1}{2}} \times \cos\varphi$, M is N(N+2)/8 and the weights (W_n) and the base points ($\mu_n, \mathfrak{z}_n, \eta_n$) are those of the Gauss-Legendre polynomial. The following figure illustrates an octant of a sphere where a quadrature set S_6 has been drawn.
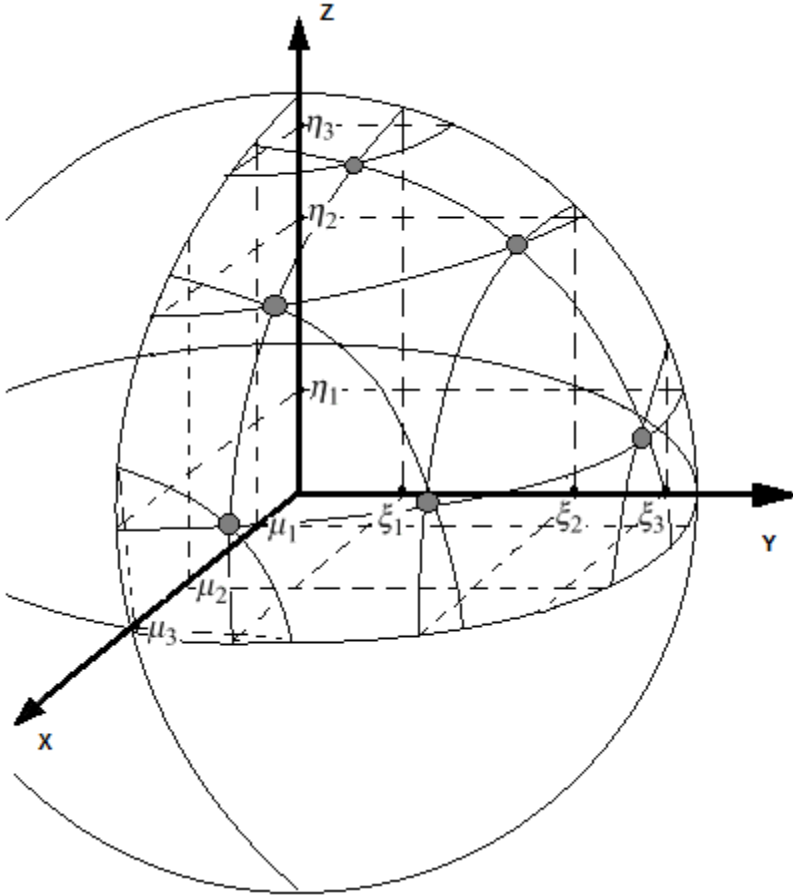
Figure 2-6 Level symmetric S_6 discrete ordinates quadrature set

The weight scheme for each base point (grey dots) in this case is one for the points in the edges of the triangle and two for the rest. The set of ordinates is symmetric in every octant of the sphere, therefore the direction cosine set (μ_n, ζ_n, η_n) for the rest of the octants can be obtained just by changing the sign of each cosine element.

Summing up the characteristics of this method it can be said that the main advantage of the S_N method is its ability to treat deep penetration problems.

On the other hand the disadvantages of the S_N method are the limitations to deal with complex geometries and accurate source modelling [59] [48] resulting in inaccuracies and a slow performance in these cases.

Despite representing a speed increase over the Monte Carlo method it is not the fastest method, it is surpassed in this domain by the Point Kernel method [60].

2.4.3 The Point-Kernel method

The fastest simplest method available for calculating flux or dose at a certain volume-less point of interest is the Point-Kernel (PK) method, which falls in the deterministic methods category. This method has the limitation of only taking into account the direct path uncollided radiation disregarding the scattered radiation coming from nearby solid objects such as ground walls or ceiling. This is a valid approach in many cases because the importance of this scattered radiation is minimal. The advantage is that it is the fastest method available, and therefore the best suited candidate for the purpose of this thesis.

The concept behind the PK method in its simplest form is to calculate the uncollided dose at a certain point (P) coming from a monoenergetic (only one energy line considered) point source (S_p) which has no volume or matter. The following figure illustrates this scheme, detector position denoted by (P) is at a distance (d) from source (Sp).
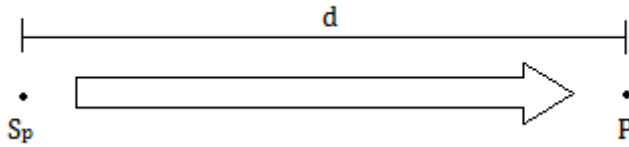
Figure 2-7 PK calculation scheme

The theoretical background of this method considers a point-isotropic (same amount of radiation emitted in all directions) radiation source which emits a certain amount of particles (S_p). An imaginary sphere centred on this point will be crossed by the outgoing particles; every unit area of this sphere will be crossed by the same amount of particles due to the source's isotropy. The concept of fluence (F) can be inferred by this explanation and the following expression relates the flow of particles at a certain distance (I).

Equation 2-7

$$F(d) = \frac{S_p}{4\pi d^2}$$

In order to convert a radiometric quantity like fluence into a dosimetric value (more useful for our purposes), the previous expression needs to be modified by including a conversion constant (C) which accounts for this fluence-to-dose conversion, leaving the expression as follows.

Equation 2-8

$$D(d) = \frac{S_p C}{4\pi d^2}$$

This formulation (figure 2-3), though true is very unrealistic as in most real cases the radiation will travel through material (medium) which causes an attenuating effect. The source itself will be made of a material which will cause this effect and additionally other

49

materials (shielding) could be found between the source and the detector point. Each material according to its composition will have a different attenuation effect, this effect is defined by the material's attenuation coefficient (μ) and the energy of the particle ($_i$). The following figure illustrates the shielding scenario where a slab of a certain material of thickness (t) is in-between the point source (S_p) and detection point (p).
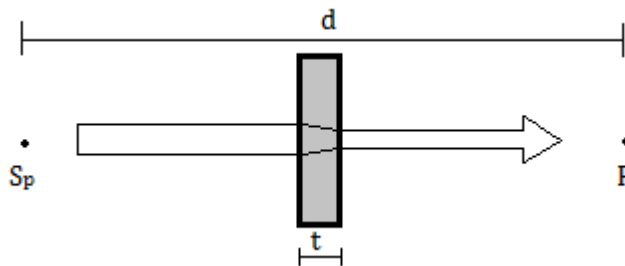
Figure 2-8 Shield attenuates the dose received at detection point

In this case, in order to take into account the attenuation caused by the slab, the previous equation needs to be modified. The probability of particles travelling though the shield without collision is $S_p e^{-\mu t}$, including this parameter in equation 2-8 the following expression is obtained.

<div style="text-align:right">Equation 2-9</div>

$$D(d) = \frac{S_p C}{4\pi d^2} e^{-\mu_i t}$$

If instead of a slab shield we are considering a homogenous medium which is the source's volume material (as shown in the following figure). The same formula can be applied to obtain the dose at a point inside of the spherical volume simply by substituting the thickness (t) in the previous equation by the radius (r) of the point inside the source volume.
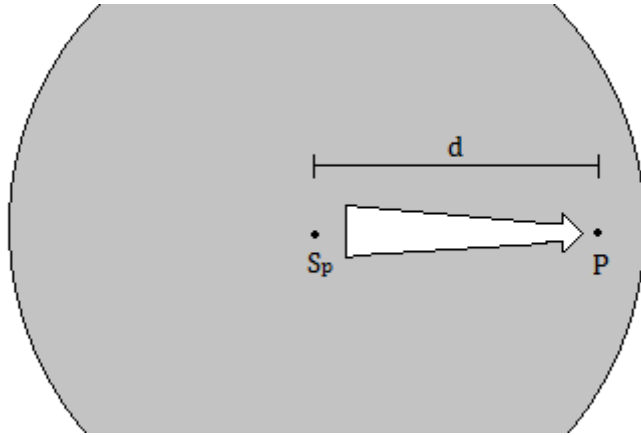
Figure 2-9 Radiation travelling through attenuating medium

If the material is not a single homogenous volume but instead it is made of a series of different materials (i) of different thicknesses (t_i) and different attenuation coefficients (μ_i), the shielding parameter of equation 2-9 is updated as shown in the following equation.

Equation 2-10

$$D(d) = \frac{S_p C}{4\pi d^2} e^{(\sum_{i=1}^{\#materials} -\mu_i t_i)}$$

The method as described up until this point only considers the uncollided radiation. Ignoring the scattered radiation might be acceptable in some cases but in others, this radiation can add up to a significant amount of the total fluence or dose.

There exist several types of scattered radiation, among them we can distinguish buildup radiation caused by particles scattered in a shield which end up directed to the detection point, albedos (radiation reflected from surfaces around the source) and line-beam response functions such as skyline (radiation bounced off the atmosphere). The following figure illustrates how the scattered radiation can reach the point of detection.
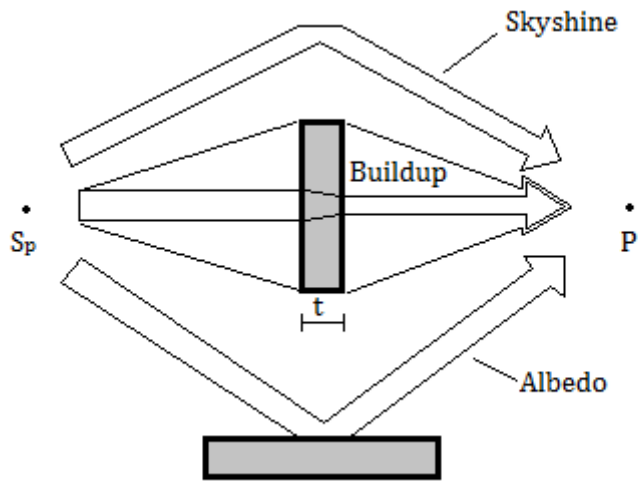
Figure 2-10 Different types of scattered radiation fluxes

Buildup radiation can be accounted for in PK photon calculations by including a *buildup* factor. The concept behind the buildup factor is to add to the uncollided radiation the radiation from the homogenous medium being crossed by the uncollided component due to physical processes such as: Compton scattering, secondary photons (X-rays and annihilation gamma rays), fluorescence and Bremsstrahlung. The buildup factor datum used in this project, taken from the American National Standards Institute (ANSI) [61] accounts for the mentioned processes.

The total particle fluence received at the detection point is the summation of the direct uncollided flow (already accounted for in the previous equation) plus the indirect flow coming from the buildup, therefore the Buildup factor can be defined as the ratio of the total fluence/dose to the direct unscattered flow. For measures such as kerma, absorbed dose or absorbed equivalent dose, the ratio is not very sensitive to the type of response; because of that buildup factors for air kerma can be applied for exposure or dose equivalent with little error [58].

Buildup factors can be measured empirically, like for example the set of data from Eisenhauer and Simmons [62], alternatively mathematical methods have been devised to try to approximate buildup factors (for point-isotropic monoenergetic sources). Three methods can be distinguished, the older Taylor [63] and Berger [64] forms which date back to the seventies are still in use but the more modern Geometric Progression (GP) [65] form provides a much more accurate result and has superseded the previous forms in modern calculations. The GP form is defined by the following expression

<div align="right">Equation 2-11</div>

$$B(E_o, \mu r) = \begin{cases} 1 + \dfrac{(b-1)(K^{\mu r}-1)}{K-1}, & K \neq 1 \\ 1 + (b-1)\mu r, & K = 1 \end{cases}$$

Where:

$$K(\mu r) = c(\mu r)^a + d \frac{\tanh\left(\frac{\mu r}{\xi} - 2\right) - \tanh(-2)}{1 - \tanh(-2)}$$

in which $B(E_o, \mu r)$ is the buildup factor for a material with attenuation coefficient μ, for photons with energy E_o. The parameters a, b, c, d and ξ are related to energy of the photon, attenuating medium and nature of the response.

In order to apply buildup radiation in a point kernel computation, a buildup factor must be included in the formula. Taking equation 2-9 we include the buildup factor which is a value of the ratio of total radiation over direct flow radiation. The following expression for PK dose calculation includes this buildup factor.

<div align="right">Equation 2-12</div>

$$D(d) = \frac{B \, S_p \, C \, e^{-\mu_i t}}{4\pi d^2}$$

In order to quantify the amount of particles S_p, the PK method will have as inputs the activity (A) of the source, its energy (E) lines and its yield (probability of gamma emission (P_i)). Some sources might have more than one energy line; therefore it is necessary to summate the dose produced of all individual energy lines (denoted n in the equation) of the source. Substituting the amount of particles S_p by the aforementioned parameters the following expression is obtained.

Equation 2-13

$$D(d) = \frac{C\ A\ \sum_{i=1}^{i=n} B_i E_i P_i\ e^{-\mu_i t}}{4\pi d^2}$$

This expression will provide the absorbed dose (assuming charged particle equilibrium), which is a magnitude that does not give any information about the harmfulness of the energy absorbed. It is necessary to convert this magnitude to equivalent dose, which does quantify the harmfulness of each type of radiation and is expressed in *Sieverts* (Sv) the same unit the real handheld detectors use to inform the user. Considering in this case the type of radiation is gamma, the conversion is straightforward because the weighting coefficient for this kind of radiation is one, and multiplying by this coefficient does not alter the equation as shown in the previous expression. Nevertheless for the purpose of this work it is necessary to assess the effect of radiation on tissue particular material (normally air, human tissue or silicon), therefore to the previous equation an energy absorption coefficient (μ/ρ) ^{material} must be added to account for this particular effect. This energy dependent coefficient can be obtained from sources such as [61]. Including this factor in the previous equation results in the following expression.

Equation 2-14

$$D^{eq}(d) = \frac{C\ A\ \sum_{i=1}^{i=n} B_i E_i\ P_i\ e^{-\mu_i t} \left(\frac{\mu}{\rho}\right)_i^{material}}{4\pi d^2}$$

2.4.4 Hybrid methods

Hybrid methods are not a different type of method *per se*, they actually use a combination of deterministic and stochastic methods, described in the previous sections, with the aim of exploiting the advantages of both depending on the characteristics of the problem to be solved.

Some examples exist of these codes [66], designed with the purpose of simulating gamma-ray spectroscopy scenarios or other tasks requiring sometimes speed and sometimes accuracy.

An example of a hybrid code is DOMINO [67] which stands for (Discrete Ordinates Monte Carlo Interface Operation) which combines a two dimensional discrete ordinates method results with a Monte Carlo Code. This hybrid code takes the results of a discrete ordinates computation with the DOT [68] code and transforms them to become an input of the MORSE [69] Monte Carlo Code.

A different strategy on hybrid methods also aims at combining discrete ordinates and Monte Carlo, with the objective of improving the computational cost and reliability of the solution for real-world shielding applications such as in reactor cavity dosimetry calculations. The strategy of this code [70] is to apply the deterministic method as a variance reduction option of a standard Monte Carlo package code. The method is based on biasing the source and the transport mechanism with the weight window technique. This technique implies the division of space in windows or cells each with a weight (i.e. a factor which accounts for the number of particles being transported) which biases the chance of survival of a particle reaching that point.

The drawback of this method is that in some conditions the disadvantages of both kinds of methods might appear in the problem resolution. Furthermore for simple straightforward problems it does not provide any advantage over an only deterministic approach.

3 Precursory development

Before a clear path of research justified the realisation of a doctoral thesis work, a series of developments were undertaken with mostly practical objectives targeted. These first developments aimed mostly at demonstrating the capabilities of Virtual Reality (VR) applications in the field of Nuclear Safeguards and Security. Nevertheless they are the origin of the thesis and represent the foundation upon the rest of the work was elaborated.

When the idea of developing a VR based simulator for a handheld radiation detector arose, the first consideration was to evaluate the feasibility of a VR application of such kind. Therefore before deepening into the intricacies of programming detailed radiation physics algorithms, the requirement was to achieve standard VR immersion features.

This first prototype had as objectives, 3D modelling of real handheld detectors, real venues at which they might be used, and a crude approximation of radiation physics basic with only the aim of showing a possible data output interface.

Once the practicality of such an application was demonstrated by this first prototype, the obvious next step was to provide the application with a gamma dose rate output. Consequently a second prototype was developed upon the basis of the first one, but implementing a gamma dose rate output system.

This system employed a so called map of data points, where dose rates had been measured or computed previously. This static solution was valid for some cases but had some significant drawbacks which stemmed the following research that lead to the bulk of the thesis work.

This chapter will cover three main points. Firstly the basic VR application structure which all the future prototypes use. Secondly

the first prototype with no dose rate computation and thirdly the second prototype with a static dose rate output.

3.1 Characteristics of a VR based Simulator of a Radiation Detector.

VR applications have in common a series of characteristics with non-VR applications such as programming of functions and procedures and standard input/output features. In addition VR applications have some elements which are specific of this category of computer science which help achieve the concept of immersion. Among these we can distinguish the 3D models (objects, characters, scenarios) or the specific VR interfacing hardware which is the most well-known trade mark of VR. These elements are structured in a common way for all VR applications, and all the prototype application versions presented in this thesis follow that structure.

The elements of a generic VR based training application are the following:

- 3D Model: The 3D model of the scenario and the different objects present in it is one of the most important elements of a VR application. The aesthetic quality and precision of the model are vital for the success of the application.
- Human-Machine Interface: The complex task of connecting the virtual world to the real user is achieved via the human-machine interface which is composed of a hardware and software elements which have as aim facilitating the use of the system in a way that it seems as simple and natural as the real world.
- Learning task: The purpose of the application, or in other words the reason why the VR system is made, it could be showing something, demonstrating or as in this case teaching.

In the case concerning a Radiation detector simulator the specific elements which correspond to the general categories above are:

- 3D Model: In first place a scenario must be designed, where the virtual action must occur. In this particular case, scenarios of typical working areas where radiation detectors are used were devised. Among them a customs border control area, a dry storage building for spent fuel, a truck container box and a general purpose laboratory (this one provided by the development software kit).

  Second the detector themselves must be modelled, so based on pictures of currently used models three detectors were modelled in a previous application and one of them re-used for this project. The 3D model was complemented with a 2D replica of the screen of the detector.

  Other objects were modelled which were necessary to demonstrate the attenuation concept, such as wooden cranes, metal doors, and walls (concrete, metal).

- Human-Machine interface: In previous work developed at JRC some sophisticated VR hardware was used (Head mounted display with infrared motion sensor) and wireless controllers. For the current work a more flexible and practical approach was applied and the prototype is implemented to run on PCs, using standard computer screens and mouse and keyboard as interfacing hardware. This choice is justified because the scope of the thesis is not in VR hardware tools, and keeping the most simple interface allows for the application to be demonstrated anywhere. Nevertheless the software development environment used is a very flexible tool that would allow to interface the application to many sophisticated VR hardware thanks to its library of drivers.

- The learning objectives for this application would be to teach the user to properly use a hand held radiation detector to detect nuclear material and in a latter second stage identify the radio-isotope detected.

  Other secondary objectives would be to teach in a very practical manner radioprotection basics such as the effects of distance

(moving towards or away from the source in the virtual scenario), attenuation and time in radiation exposure.

3.2 Structure of a VR based Simulator of a Radiation Detector.

The application is developed on a VR specific software development environment (SDE) called Virtools [71] which was found an appropriate tool for the projects requirements.

This kind of VR oriented SDE provides necessary elements such as a 3D engine, a library of drivers to interface VR specific hardware, database functionalities, a series of pre-built functions common for any kind of application.

Upon this layer of basic functionalities the application per se has to be built. The developer must include the media to be used (in this case 3D models and 2D textures) and integrate it in the application structure so the 3D engine will properly render it, via the setup menus provided by the SDE.

Secondly the standard application characteristics need to be programmed. For this task the SDE provides a visual blocks programming language with several pre-programmed modules for common programming necessities which represent the backbone of the application.

Furthermore specific programming needs can be accomplished in this SDE by programming scripts in a C-like programming language which can be compiled by the SDE and integrated as a module in the visual programming language. This allows the developers to program any kind of functions without being limited to the visual blocks.

The VR application can be structured in the following parts:

First, underlying layer of functionality provided by the SDE (3D engine, hardware drivers, etc.). This is not part of this thesis'

contribution because it is used without any own-made development, but the developed work rests upon it, as it is in charge of linking the application layer to the hardware layer.

Secondly we can distinguish the media elements: 3D models, 2D textures, sounds or other elements which are necessary to build the virtual world. These elements were created externally to the SDE using specific 3D modelling software or obtained from general purpose libraries. These were then imported into the SDE project. Despite they do not represent scientific work (actually artistic) they are a very important element for the success of a VR application. These objects which were originally purely aesthetic were later complemented with attributes to define physical properties necessary for the radiation transport simulation calculus.

Third, there are the task behaviours, this part dictates the flow of the application and is the backbone of the programming work, the rest of elements are linked to it and their execution is controlled by this part. Just like the previous point (media elements) it does not represent either a scientific development work because it is just a series of standard programming techniques, already well proven and do not represent a breakthrough in computer science. Nevertheless it is a completely necessary element of any working VR based application and it does represent a fair amount of working time.

The last part of the application structure (physics behaviours) is the most significant for the thesis work, as it contains most of the scientific development. This part requires the programming of radiation transport methods that will be used by the simulator to calculate the gamma dose rates. This element of the application will be developed in each prototype version seeking to improve the performance of the application, unlike the rest of elements which remain fairly unchanged.

The following figure illustrates the different layers into witch the application is structured. The next sections in this chapter cover the

top layer elements: 3D Model, task behaviours and physics behaviours.
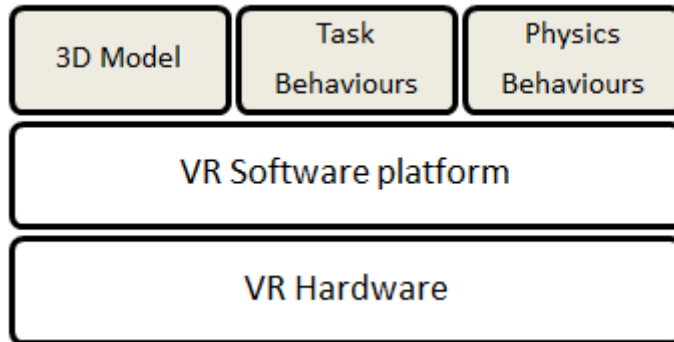
Figure 3-1 Application layer structure

3.3   3D Modelling

During the whole length of the thesis, the same 3D elements where used for the prototype application, most of them being created at the beginning of the project in house at JRC.

The elements modelled are the following:

- Scenarios

Two complete scenarios were modelled to be used in VR based applications, a third one was modified from an existing model available in the SDE.

The first scenario represents a dry storage site for spent nuclear fuel casks which can be used for Nuclear Safeguards exercises. The second scenario represents an international road border customs area. This scenario is intended for the use of customs agents training. A view of both can be seen on the following figure.

Finally a third scenario was used represented a general purpose laboratory. The following figure shows the first two scenarios described above.

Scenarios may contain elements dynamic elements such as doors, hoods etc. The state in which these elements are may affect the radiation transport computation.
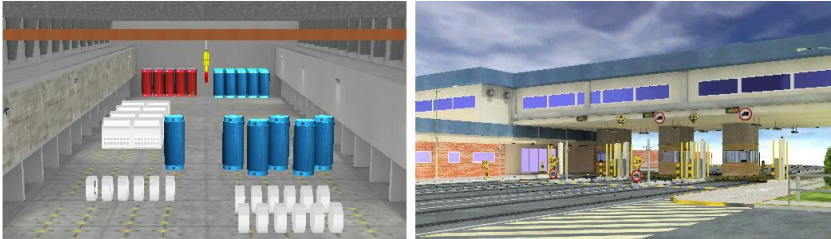
Figure 3-2 Application scenarios: Storage site and Customs area

- Detector

The modelled detector is based on a RadFinder model from the manufacturer Thermo Electron Corporation. It is a handheld survey meter of the semiconductor type (see chapter two for further information on detector technologies) with a CZT (Cadmium Zinc Telluride) detecting element. The performance of the detector in terms of energy ranges, dose rate ranges and acquisition time will be simulated in the virtual version.

It is rather small (1.5kg heavy, 19cm long, 12cm wide, 27cm high) and can be carried in one hand without any supporting straps. It features a VGA (Video Graphics Adapter) colour display of 320 by 240 pixels. This screen has been replicated to be used In the application, offering the user not only the 3D view of the detector from a first person perspective but also a replica of the 2D display on the corner of the screen to offer the user a better view of the information displayed by the detector.

Other characteristics of the detector have been also included in the virtual model, such as battery duration, colours, aesthetical decoration etc. The following figure compares the real detector picture to the 3D model rendered in the application.

This perspective reflects realistically the view the user has if she/he is carrying the detector in hand. Nevertheless this view is not optimal to read the information in the display. Therefore the display is replicated on screen in the application in real size.

The elements of the 2D display are:

- Battery life indicator: It shows the amount of battery energy left.
- Dose rate: it shows the gamma dose rate received by the detector in µSv/h (micro Sieverts per hour) by default.
- Neutron count rate: In the virtual model this element is left blank as neutron radiation simulation is not part of the work.
- Direction to source: tells the user in which direction lays the source with respect to where the detector is pointing at. It shows the information both graphically (horizontal bars) and numerically (percentages of the angle).
- Waterfall chart: This feature stores the dose rate values of the last few iterations.

The following figure shows the 2D replica display and its different sections.
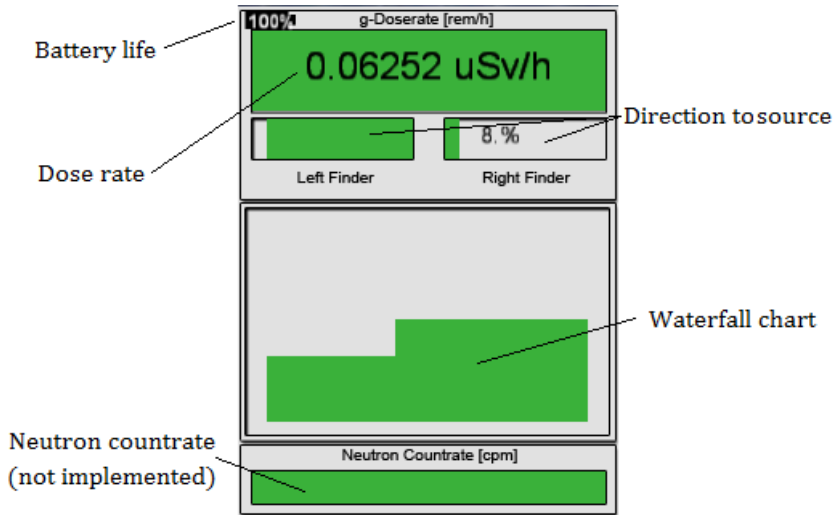
Figure 3-4 Display of the detector

3.4 Task Behaviours

The second element which is inherent to VR based training applications is the task behaviour programming or in other words, what the user must do. As shown in Fig 3-1 this is element belongs to the highest programming level layer, and it is one of the three elements along with 3D model and Physics behaviours which fall under the developer's responsibility.

This part converts the learning tasks from a paper basis to interactive computer training. The approach taken is: step by step accomplishing of partial objectives guided by text and multimedia elements.

For a training application to be successful a series of issues related to the task have to be clearly specified in terms of workflow, decision making process, alternatives to be considered, etc. The different actions and the correct order in which they must be completed are the basis of the learning experience and must be controlled by the application. Among other we can distinguish the following main issues which define the behaviour of the user with the application:

- Workflow: A virtual training application must consider all the possible flow of alternatives the task execution can generate. It is important that the situation is properly studied beforehand, creating workflow diagrams that cover all the possible alternatives the user might attempt to take in the virtual scenario, so that the application is ready to handle unexpected behaviours.

  The figure below shows the flow of actions for an example application targeted to train customs officers in detecting radioactive sources and nuclear materials in border monitoring activities [72]. The aim is to let customs officers learn how to use a simple radiation detection instrument such as the one being simulated in the context of a radiation detection exercise. Each functional block can be further specified in terms of sub-blocks, alternative workflow diagrams, etc.
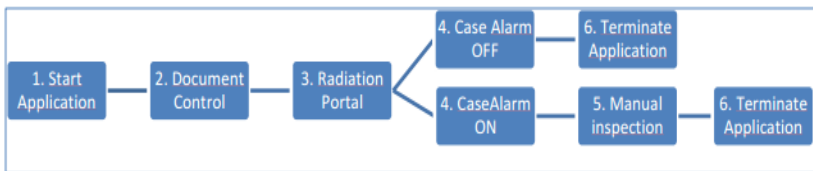
Figure 3-5 Task flow of a training application

  To be realistic and consistent, the VR application matches the flow of actions done by the user with the real procedures customs officers need to face on a daily basis.

- Difficulty: The difficulty of the virtual task must be tuned so that the user does not find it too easy, and consequently loses interest, nor too hard and the user feels frustrated and inadequate.
  This might not be an easy target to reach, in fact given users of different levels of expertise it might be impossible to find a single level of difficulty that works for all. In this case, for the

application to be fulfilling for all users, different levels of difficulty can be set to the task.

Taking as an example a safeguards surveillance simulation application [31], it considers two cases, beginners and experts. This software lets the user chose at the start between a guided mode (intended for beginners) and an expert mode intended for more proficient users. Even though the target is the same, set up a video surveillance system, the guided mode takes the user in a step by step process with visual, text and audio guidance, meanwhile the expert mode leaves the user complete freedom of action.

• Multimedia usage: Virtual training offers the developer a broad choice of elements to use. Choosing which ones to use and how to combine them define the behaviour in which the application conveys information to the user. This depends on factors such as the activity being simulated and the target audience.

We can distinguish several types of multimedia elements such as camera walkthroughs, voiceover explanations, text messages, visual, sound and tactile effects.

Taking as an example the application from the previous point, if the aim is to show a beginner user how a spent nuclear fuel storage site is, it is most convenient to use a camera walkthrough which shows visually what the site looks like. On the other hand to an expert user who knows already the facility it could be more convenient to show a text message with the particular elements this facility has without having to waste time "watching a movie".

• Progress control: In order to control the progress a user makes, some sort of control mechanism must be engineered into the application. This necessity influences the behaviour of the user in the virtual world. Several types of progress control elements exist, three of the most used ones are:

Spatial control: The position of the user in the virtual world is constantly tracked by the application. When the user reaches a certain location a trigger can be activated to let the application know of the user's position. For example if the user is instructed to reach a certain place in the scenario, the application will wait until the user finds it and reaches it, consequently the next activity in the application can start.

Timer control: This kind of control mechanism launches successive steps of the program according to a timer mechanism. This kind of system complements one of the drawbacks of the spatial control mechanism, in case the user is stuck and doesn't know how to proceed, the application will wait for a period of time and then take the user to the next action. On the other hand this kind of mechanism might be frustrating for very experienced users who finish their tasks well in advance and have to wait for the timer to reach the end.

Event control: This is one of the most extended control mechanisms and it is activated when the user performs a certain activity that triggers the event control system. In the previous example of the detector training for customs officers, switching the detector on would trigger the functions that execute the radiation transport algorithms.

3.5 Physics Behaviours: First version- No Dose Rate Calculation

The first version of the prototype featured a 3D model of a Customs border control area as a virtual scenario [73]. The user's task (a customs officer) was to inspect the incoming vehicles with a virtual radiation detector if the alarm of the radiation portal detectors was activated.

This prototype's target was mainly to show that such a VR based tool was feasible and that there was a potential user group which could

benefit from it. This version did not provide a real dose rate calculation. The display of the virtual detector showed as a result the inverse of the distance between source and detector. The following figure shows the scheme of the computation implemented.
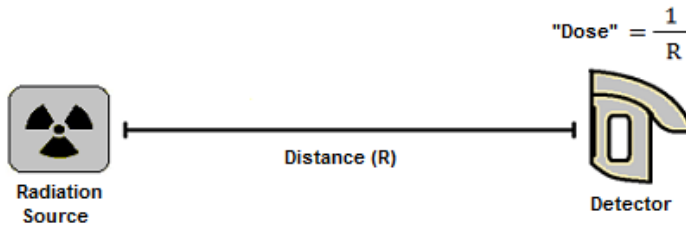
Figure 3-6 Scheme of fake Dose Rate computation implemented

This was achieved by defining the source as a point in the Cartesian space in the virtual scenario, and the detector as second point in space. By retrieving the position of both elements the distance between them was calculated. This simple function was executed iteratively to provide a real time result; this result was updated with a frequency which matched that of the simulated apparatus. The following pseudo-code describes the algorithm that computes the "false dose rate".

```
/******** Inverse distance algorithm********/

radpos= GetPosition (Rad_source);
period=RealMeasuringFrequency;
repeat-always;
        detpos= GetPosition (detector);
        dist=ComputeDistance(radpos,detpos);
        dose=1/dist;
        wait(period);
end-repeat-always;
end;
/*************************************/
```

Figure 3-7 Algorithm to calculate inverse distance reading

From the nuclear safety point of view this information might not have much value but it did prove that mathematical operations based on information extracted from the virtual scenario (position, distance) was possible in real time. The possibility of substituting the distance computation for a dose rate computation became a clear improvement which could be made. This work was the basis for the next prototype version.

3.6 Physics Behaviours: Second Prototype - Dose Rate mapping

Once the feasibility of a VR based radiation detector simulator was proven by the first prototype the evident target for the next version was to improve it by generating real dose rate data results in the virtual detector.

The first approach implemented, provided dose rate data from a 2D map of dose rate points [74]. This technique discretises the scenario volume into a series of equally spaced out points in space which form a 2D matrix. For each point a dose rate value is obtained either by a physical measurement in a real scenario with a real source of by a computer simulation offline.

In our case the map was obtained from a Monte Carlo simulation using MCNP 4 tuned for high accuracy (one million particles), at the expense of computing time (several minutes). The generated map was loaded offline into a database in the application.

To estimate the dose rate at a given point where the detector lies P(x,y) in the environment a bilinear interpolation was applied using the nearest four points on the 2D map (P1,P2,P3,P4) as shown on the following figure.
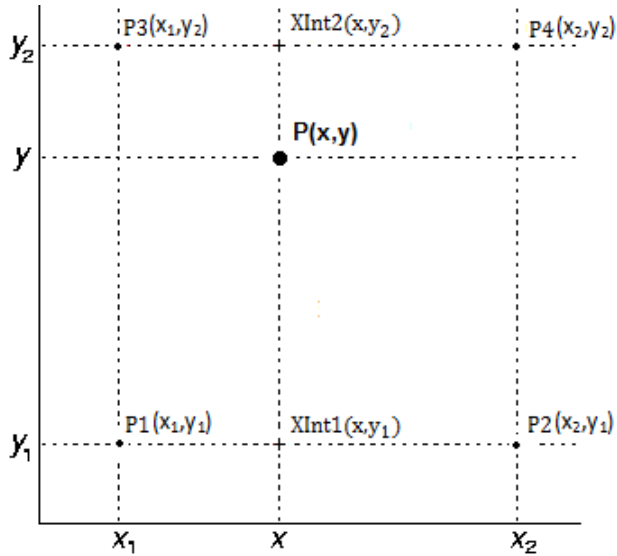
Figure 3-8 Bi-linear interpolation scheme on a 2D map

In order to obtain the bilinear interpolation, a two-step process is performed. Firstly the implemented algorithm linearly interpolates along the X-axis, taking the pairs of points with equal Y-axis value. In order to do this the standard linear interpolation equation shown in the following expression is used.

<div align="right">Equation 3-1</div>

$$XInt1(x, y_1) = \frac{x_2 - x}{x_2 - x_1} P1 + \frac{x - x_1}{x_2 - x_1} P2$$

Similarly, the second intermediate point XInt2 is obtained by the similar expression:

<div align="right">Equation 3-2</div>

$$XInt2(x, y_2) = \frac{x_2 - x}{x_2 - x_1} P3 + \frac{x - x_1}{x_2 - x_1} P4$$

With this operation, two intermediate points XInt1 and XInt2 (shown in the previous figure) are obtained. Subsequently these two

71

intermediate points are linearly interpolated along the Y-axis thus finally obtaining P(x,y) using the following expression.

<div align="right">Equation 3-3</div>

$$P(x,y) = \frac{y_2 - y}{y_2 - y_1} XInt1(x, y_1) + \frac{y - y_1}{y_2 - y_1} XInt2(x, y_2)$$

The following pseudo-code sums up the procedure implemented in this version of the application prototype.

```
/********* Dose mapping algorithm*********/

Map=LoadDoseMad(Rad_source);
period=RealMeasuringFrequency;

repeat-always;
        detpos= GetPosition (detector);
        P1=GetPointXX(p_d);
        P2= GetPointXY(p_d);
        P3=GetPointYX(p_d);
        P4=GetPointYY(p_d);

        Xtemp=Interpolate(P1,P2,detpos.x);
        Ytemp=Interpolate(P3,P4,detpos.x);
        Dose=Interpolate(XInt1,XInt2,detpos.y);
        wait(period);
end-repeat-always;
end;

/*************************************/
```

Figure 3-9 Algorithm to interpolate dose rate from a 2D data map

There are series of limitations associated with this type of method. On one hand the accuracy of the method greatly depends on the resolution (amount of data points) available. Though the implemented version obtained satisfactory results in terms of accuracy when tested, it was prone to significant errors in situations

where attenuation elements where interfering partially as shown in the following figure.
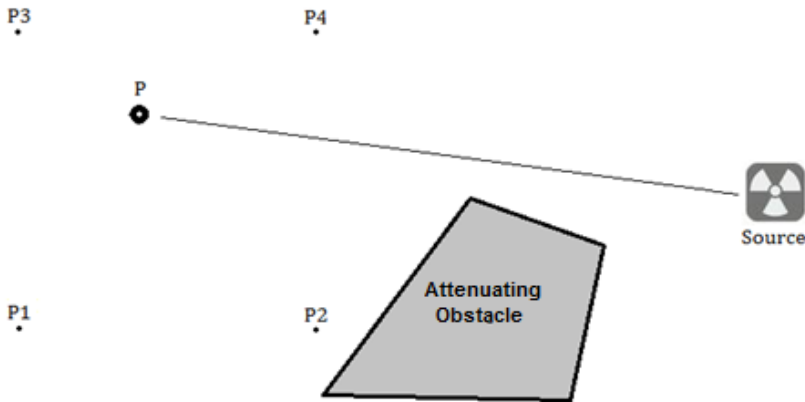
Figure 3-10 Partially attenuated error

In this case the dose rate values of points P1 and P2 are affected by the attenuation caused by the obstacle between them and the source, this attenuation effect is partially passed onto the bilinear interpolation when trying to calculate the dose at point P when it actually should not because the straight flow of radiation arriving at point P is not affected by the presence of the attenuating obstacle.

Another limitation of the method is that dose rate values can only be obtained for positions within the 2D map. Therefore either the map must be large enough to cover the whole scenario of the application or movement of the user in the virtual scenario must be limited to the area of the map.

But the most important limitation, the one which actually was unacceptable for the requirements of a VR based application, was the lack of interactivity.

This method relies on static data; any changes in the scenario which would vary the dose rate value map are not reflected in real time in the application. To update the data map would require to re-calculate offline the data points (which is a time consuming process)

73

and to reload them into the application. Therefore this method was discarded and a search for new interactive ways of obtaining dose rate values was started. This search led to the following chapter of the thesis.

4 Developed Methodology

The core scientific work of the thesis is the development of novel methods to **improve the performance of the Point Kernel (PK) radiation transport computation**. This chapter narrates the evolution of these methods within the simulator prototype from the initial single point kernel (PK) algorithm through the various versions up to the latest most evolved version.

The chapter starts with the description of the application structure developed which is common to all the versions. Subsequently it continues with each version implemented, in chronological order, starting with the motivation for each new idea and the implementation strategy. The versions developed are:

- Mono PK: The first version developed featured the single PK which is the simplest implementation.

- Mono PK with shielding and Build up radiation: The shielded Mono PK was improved again by taking into account the radiation deflected towards the detector.

- Multi PK regular Octree division: Due to the limitations of a single point representation of the kernel (source volume), a new version explored the multi-point kernel method.

- Multi PK non-regular Octree division: This version aims at reducing the computational cost of the multi PK approach via a non-regular model.

- Multi PK KD-tree division: This version substitutes the source representation strategy of the Octree division with a more aggressive approach based on KD-trees.

- Unlimited shape post processing: This version overcomes the limitation on source shape of the previous versions by using a Boundary Representation (BREP) method.

A series of tests were performed to evaluate these methods, the results obtained will be presented in the following chapter of the thesis.

4.1 Application Structure

When classifying the different functional elements that make up the VR prototype, we can clearly distinguish two parts implemented in separate modules:

The first module (hereafter called *Dosimetry module*) contains the functions related to running the radiation transport algorithm periodically.

In terms of data flow interfacing in this module, it can be said that the inputs are: the clock, the current status of the relevant 3D objects (sources, detector, obstacles) in the scenario and the parameters necessary for the radiation transport calculation which are obtained from tables stored in the PK database, while outputs are the 2D and 3D display rendered images.

The second module (dubbed *Movement module*) implements the user-interface functionality, translating input of hardware (keyboard, mouse) in movement in the virtual scenario. Input comes from the user's commands and the state of the 3D objects in the scenario. Output in this case only affects the 3D rendering and optionally other multimedia effects (sound).

To describe graphically the flow of information along the VR system, data flow diagrams will be used (DFD) [75]. These are purposely devised diagrams which indicate the flow of information via arrows and the actors or agents of the system via boxes or ovals depending

on their type. The following DFD sums up the highest level interaction, it is also called context diagram.
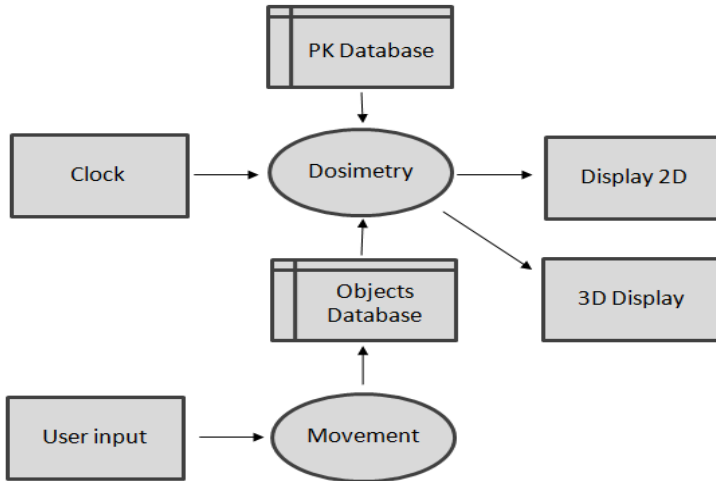
This diagram of the top level data flow is just an aid to give the reader an overview of the system with its two main areas of the application. It is necessary to take a closer look at the data flow within those two modules to explain the structure of the algorithms implemented.

Consequently we draw the attention now into the *Dosimetry module* which holds the functions relative to the radiation transport computation. The contents of this will vary in the successive prototype versions but the data flow interaction with the rest of the application agents remains unchanged. Below, this initial diagram shows the basic contents of the dosimetry method in its simplest form, in following versions more sub-modules will be added or some of the existing modified with the exception of the *2D Display manager* sub-module.
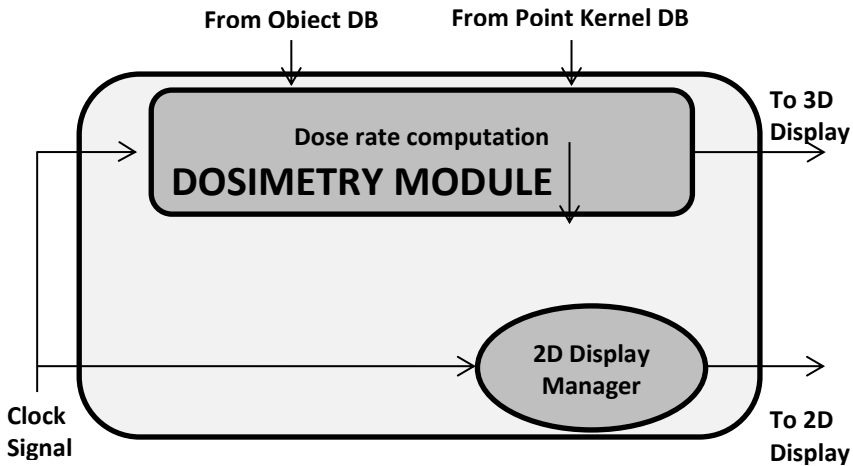
Figure 4-2 Dosimetry module DFD

This *2D Display manager* sub-module takes care of the rendering of the virtual display and the functions which provide its data (see display image in Fig 3-4). This sub-module will be presented at the end of the chapter as it is not related to the core of the research work.

4.2 First version: Mono Point Kernel (PK)

4.2.1 Rationale of Mono PK version

The starting point of this chapter's work on PK methods is motivated by the conclusion from the last chapter about dose maps: to compute gamma dose rate in the simulator a **fast, interactive, real-time method was necessary.** Given the available options analysed, only Point Kernel met the requirements. Therefore the first prototype version of this chapter implements a Mono PK algorithm which is the simplest and fastest kind of PK algorithm.

PK algorithms such as the one used in this version have already been implemented in the field of nuclear science and industry by a myriad of computer codes, for many purposes such as shielding calculations or radiation protection [76] [77]. All these codes require a setup of

the problem to simulate before performing the actual simulation (e.g. define position of source or detector), on the contrary this prototype automatically takes the necessary inputs from the system environment without requiring the input from the user, at the time this version was developed there was no other PK code in a VR based application which could run automatically on real-time. This characteristic represented a novelty in the field.

Furthermore the prototype provided dose rate data in real time. The following scheme illustrates the assumptions made such as the representation of the radiation source as a single point and the consideration of only direct radiation impinging on the detector.
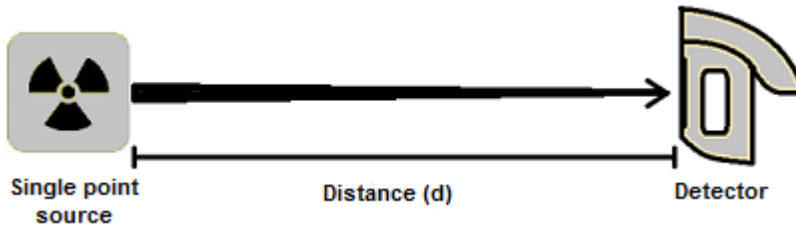
Figure 4-3 Mono PK computation scheme

4.2.2 Software architecture of the solution

Retrieving the equation 2-14 for equivalent dose rate from chapter two, and considering only the simplest mono point kernel situation and air as the absorption material we obtain the following expression. The application prototype must perform this calculation to obtain the equivalent dose rate value.

Equation 4-1

$$D^{eq}(d) = \frac{C\ A\ \sum_{i=1}^{i=n} E_i\ P_i\ \left(\frac{\mu_{en}}{\rho}\right)_i^{air}}{4\pi d^2}$$

In order to have a truly automatic system, it is necessary to abstract the user from selecting the parameters of the equation. The application will therefore have to obtain the parameter values from the virtual scenario by itself. This task will be performed in the so called *Data Retrieval* module which is shown in the following figure, as the reader can appreciate, the new module is encapsulated within the *Dosimetry* module; it is run by the computer clock and collects the necessary data, computes the necessary values and subsequently feeds them to the PK Calculus module. The following figure shows the updated data flow structure.
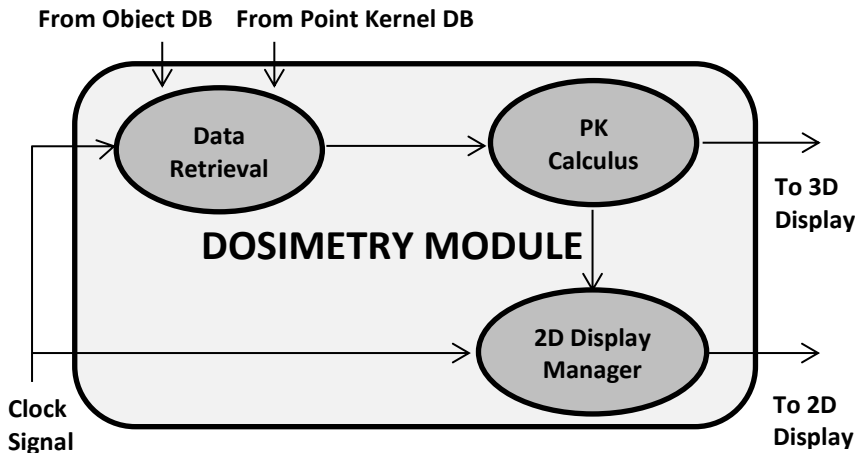
Figure 4-4 Mono PK dosimetry module DFD

The data that is needed to perform the computation can be classified in two types. First the 3D object dependent parameters (activity, energy lines, yield and distance) and second, the point kernel specific data (energy absorption coefficient) which is obtained from a database of tables containing the PK parameters for different materials and gamma ray energies.

Therefore in first place, the default object definition provided by the software development kit used (i.e. Virtools) needs to be extended with the necessary attributes to perform the gamma transport calculation, these are:

- Activity (A): This numerical attribute stores the activity of the source in Bequerels.
- Energy (E): Declared as an array (unlimited length), it contains the different energy line values which define the spectrum of the radiation source expressed in KeV (Kilo electron-volts).
- Yield (P): The emission probability of the gamma ray, they are associated to a particular energy line, therefore implemented in the same table.
- Energy absorption coefficient $(\frac{\mu_{en}}{\rho})^{medium}$: This factor is implemented as an array of data, ordered by energy of the incoming particle. It indicates the amount of energy that is captured by the medium per unit distance.
- Position: Each source has its position stored (x,y,z), trigonometrically the distance is obtained using this position and the detector's position, this attribute is already implemented by the SDK.

The other incoming flow of information comes from the PK database which is structured as sets of arrays (tables) of different lengths, ordered by energy line value from lowest to highest.

There are several parameter types, though for this first mono PK case only the air energy absorption coefficient table is used, this database includes other materials such as tissue and Si (Silicon) which are of common use in the dosimetry field. The rest of the table parameters will be explained in the following sections of the chapter which explain the following versions of the prototype.

The data of these tables comes from the American Nuclear Society's standard for gamma ray coefficients [61], which is a widely used reference material for PK calculations. The data has been implemented as an internal array in the SDK's database framework. The following figure shows partially the implemented database.

Energy (MeV)	Energy absorption coefficient
0.01	4.6400
0.015	1.3000
0.02	0.5255
0.03	0.1501
0.04	0.0669
0.05	0.0403
0.06	0.0300
0.08	0.0239
0.1	0.0232
0.15	0.0249
0.2	0.0267
0.3	0.0287
0.4	0.0294
0.5	0.0297
0.6	0.0295
0.8	0.0288
1	0.0279

Figure 4-5 Energy absorption coefficient table for air

4.2.3   Algorithm description

First, the *Data retrieval* module obtains the attribute values from the source object by directly consulting its definition attributes. The distance parameter is calculated trigonometrically from the retrieved position (x,y,z) of the source and the position of the detector which are updated in every iteration.

The energy absorption coefficients from the PK database are calculated by firstly performing a binary search within the corresponding table (which is indexed by increasing energy levels) to obtain the two closest energy values. The binary search method was chosen as it is the fastest search method in ordered lists and speed is a priority in an application which is expected to run in real time.

Secondly a linear interpolation is applied to obtain the required value associated to the energy level of the energy line of the current source using the retrieved closest points from the table. The table values

cover a range of values wide enough for the sources that will be
tested and wider than the measuring range of the real detectors
simulated, therefore the simulation is limited to sources within this
energy range. The following image shows the pseudo code for the
main algorithm in the *Data Retrieval* module.

```
/*********** Mono PK - Data Retrieval ***********/

Source = GetSource();

/************* 1. Get Activity ***************/
Activity=Source.Activity;

/****** 2. Get Energy*Yield*attcoef*en_coef ******/
Spectra=Source.SpectraArray;
while (i < number of energy lines) {
        temp = Spectra.Line[i]*Spectra.Yield[i];
        en_coef= BiSearch(Spectra.Line[i],En_coef Table);
        temp = temp* en_coef;
        sum = total+temp;
        i++;
        }

 /************* 3. Get distance **************/
SourcePos = Source.GetPosition();
DetPos = Detector GetPosition();
Distance = GetDistance(SourcePos,DetPos);

/*************************************/
```

Figure 4-6 Data Retrieval pseudo code algorithm

Once all the parameter values have been obtained, they are passed
onto the *PK Calculus* module which performs the mathematical
operation of equation 4-1. Once the dose rate equivalent has been
calculated, this module passes the value to the *2D Display Manager*

module which prompts the equivalent dose rate value on the virtual display on screen.

```
/************* Mono PK – PK Calculus ************/


/************** 1. Get Parameters ***************/
C = 5.77e-4 //Equivalent Dose Conversion constant
A=GetValue(Activity);
sumatory =GetValue(sum); //Σ E_i*P_i* en_coef_i
d = GetValue(Distance);


/************ 2. Apply formula *************/
EqDose = C*A*sumatory / 4 * π * d^2;


/*****************************************/
```

Figure 4-7 Pseudo code of the Mono PK algorithm

4.3   Second version: Mono Point Kernel with shielding and Build Up

4.3.1   Rationale of shielding & Build up calculation version

The first version of the prototype is not a very realistic representation of reality because it considers the source a volume less point in a vacuum, where the radiation travels from the source point to the detector point without any interaction.

Although in same cases it is workable, this overly simplified scheme might not be useful for many practical examples, as the source usually has a significant volume and the radiation will travel through some medium (air, water concrete or metal shield, etc.), both of which have an attenuating effect which might not be negligible.

Nevertheless the shielding introduces a new source of inaccuracy; this is due to the so called build up effect. This refers to the scattered radiation which after a series of interactions with the shielding medium ends up directed towards the detector, adding up to the direct radiation which passed straight through the shield. Therefore the build-up factor is a ratio of the total received radiation with respect to the uncollided radiation.

Therefore the second version of the prototype aims at including a more elaborated PK calculation with attenuation and build up included, to achieve this objective a mechanism to detect the presence and properties of the attenuating medium is necessary. This makes the prototype accurate enough to be a useful tool to be used in practical problems which may arise in real life training exercises.

Taking into account the shielding and build up factors, the scheme of the PK computation is as shown by the following figure.
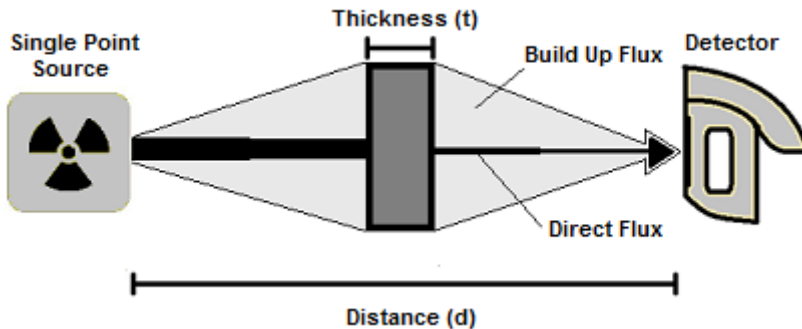
Figure 4-8 Mono PK with shielding and build up factor scheme

4.3.2 Software architecture of the solution

Taking the architecture of the first version shown by the data flow diagram (DFD) in fig 4-4 as a starting point for the second version, the main difference is that a new module is introduced to calculate if an object (shield) is placed between the detector and the source.

This module's task is to check if there is any obstacle (including the source itself) between the source and detector by using a ray tracing algorithm. If that is the case, the function fetches the data which are necessary for the PK computation with shielding and build up included.

Similarly to the *Data Retrieval* module, information flow is coming from two different sources, the obstacle object definition will provide the material and thickness (t), computed from its geometry definition and ray tracing intersection data. The other source is the PK database for total attenuation coefficients (μ_i) and build up factors (B_i). Hence the system will search in the table that matches the material specified in the object definition.

The modified DFD including the new module and its data connections is shown by the following figure.
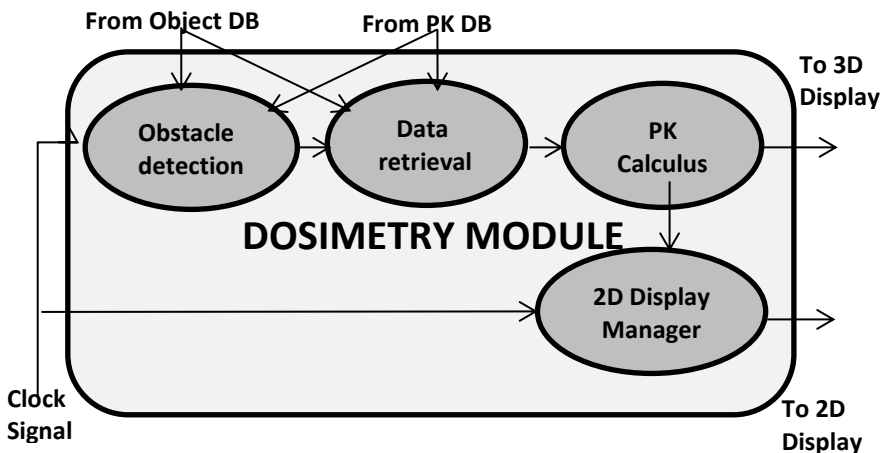
Figure 4-9 Mono PK with shielding dosimetry module DFD

The *Data Retrieval* module is slightly modified as now the summation includes the shielding parameter to account for the mono PK with shielding formula which includes the attenuation factor of a possible obstacle detected by the previous *Obstacle Detection* module and the build-up factor of that obstacle's material.

Unlike the rest of data tables in this database, the build-up parameter is a function of the total attenuation coefficient of the material and both the thickness of the obstacle and the energy of the gamma beam. Therefore the tables are matrices where the build-up parameter is ordered both by increasing energy and increasing distance (the unit in this case for distance is mean free paths).

The following equation shows the new formula implemented which stems from the inclusion of the three new factors: attenuation coefficient (μ_i), build up factor (B_i) and thickness (t) to equation 4-1:

<div align="right">Equation 4-2</div>

$$D^{eq}(d) = \frac{C\ A\ \sum_{i=1}^{i=n} B_i E_i\ P_i\ e^{-(\mu_i\ t)_{shield}}\left(\frac{\mu_{en}}{\rho}\right)_i^{air}}{4\pi d^2}$$

4.3.3   Algorithm Description

This mono PK with shielding and build up version is characterized by the new *Obstacle Detection* module which features a ray tracing algorithm to detect the presence of objects defined as obstacles in between the source and the detector.

Secondly if an obstacle has been detected the next phase of the algorithm fetches the relevant information from the interfering obstacle definition (material and thickness).

Consequently the *Data Retrieval* algorithm is modified to consult the PK Database to search for the corresponding material and compute the adequate total attenuation coefficient and build up factor for the energy ray of the source.

The following pseudo code describes the work done by the algorithm of the *Obstacle Detection* module:

```
/** Mono PK with shielding – Obstacle detection **/

Source = GetSource();
Detpos = GetDetectorPosition();
Obstacles[] = GetListOfObstacles();
Material = void;
Thickness = 0;

/*********** 1. Find obstacle ***************/
Ray = SetVector (source.GetPos(), detpos);
For (i=0; i<Obstacles[].length(); i++) {
        If (intersection(ray,Obstacles[i]) == true) {
                Material = Obstacles[i].GetMateria();
                Thickness = Obstacles[i].GetThick();
        }
}
/*************************************/
```

Figure 4-10 Pseudo code of the Obstacle Detection algorithm

The total attenuation coefficient is computed in the same fashion as the energy absorption coefficient presented in the previous point, that is first performing a binary search within the table and then performing a linear interpolation to obtain the value.

The build-up parameter is both dependant on energy level and thickness, it implies the use of a nested search which will be binary in both cases to keep computational cost as low as possible. The double intervals result obtained will be passed on to a double linear interpolation function which will take care of computing the final build up factor to be included formula.

Once the attenuation coefficient and build up factor are computed, the thickness of the obstacle parameter is inserted in the summation calculation as shown by equation 4-2.

Once the data necessary for the computation is obtained, the algorithm finishes by passing it on to the PK computation algorithm. The modified *Data retrieval* algorithm is shown below:

```
/**** Mono PK Shielding and Build up- Data Retrieval ***/

Source = GetSource();
Obstacle = GetObstacle();
Thick = GetThickness(Obstacle);

/************* 1. Get Activity ***************/
Activity=Source.Activity;

/****** 2. Get Energy*Yield*Bup*attcoef*en_coef ******/
Spectra=Source.SpectraArray;
while (i < number of energy lines) {
        temp = Spectra.Line[i]*Spectra.Yield[i];
        en_coef= BiSearch(Spectra.Line[i],En_coefTable);
        attco = BiSearch(Spectra.Line[i],AttcoTable);
        Bup_en = BiSearch(Spectra.Line[i],BupTable);
        Bup_mfp = BiSearch(Spectra.Line[i],BupTable);
        Bup = LinearInt(Bup_en,Bup_mfp);
        temp = temp* en_coef*Bup*e^(-attco*Thick);
        sum = total+temp;
        i++;
        }
/************* 3. Get distance **************/
SourcePos = Source.GetPosition();
DetPos = Detector.GetPosition();
Distance = GetDistance(SourcePos,DetPos);

/***************************************/
```

Figure 4-11 Data Retrieval algorithm (shielding version)

The *PK Computation* algorithm is modified by including the new parameters of attenuation and build up to the previous version (shown in fig. 4-8).

```
/***** Mono PK Shielding and Build up – PK Calculus ****/


/************** 1. Get Parameters **************/
C = 5.77e-4 //Equivalent Dose Conversion constant
A=GetValue(Activity);
Thick=GetValue(Thickness);
sumatory   =GetValue(sum);//ΣE_i*P_i*Bup_i*e^(-attco*thick)*
en_coef_i
d = GetValue(Distance);

/************ 2. Apply formula *************/
EqDose = C*A*sumatory / 4 * π * d^2 ;


/********************************************/
```

Figure 4-12 Pseudo code of the Mono PK algorithm

4.4 Third version: Octree based Multi PK with Shielding and Build Up

4.4.1 Rationale of multi PK version

The motivation to develop the third version of the prototype comes from the necessity to deal with the limitations of the previous version. The results in the following chapter will show that there is an accuracy loss in the dose computation at short distances or when increasing the size of the source (while maintaining the distance).

The mono point kernel paradigm is based in representing the source as a point. This paradigm is acceptable as long as the actual volume of the source is negligible in the problem set up. As soon as one of

the two situations described in the previous paragraph arises the representation of the source as a single point is problematic.

To overcome this problem the devised solution is to change the representation of the source from a single point to a multiple point representation, this set of points will be evenly spaced out within the volume of the source, organised as a three dimensional matrix. This model we will dub a Multi Point Kernel method. This has been used by several PK codes [76] . The following figure shows a two dimensional simplification of the new method.
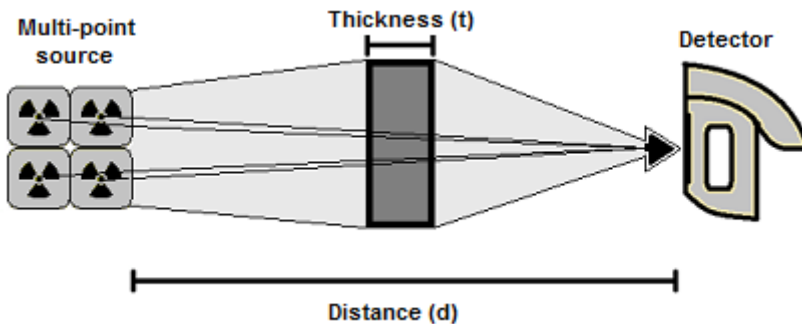
Figure 4-13 Multi PK with shielding and build up factor scheme

This scheme divides the original source in a series of identical sub-sources whose summation adds up to the total activity of the original source. The idea behind this concept is to better distribute the activity of the radiation source in order to achieve more accurate dose rate computations. In essence it is a repetition of the mono PK method for each sub-source created, therefore in terms of computational cost, the new method's cost increase is proportional to the amount of sub-sources created.

4.4.2   Mesh resolution in Multi PK

The question which naturally arises is; how many sub-sources the original source must be divided into to obtain the necessary degree of accuracy required for the simulation? This parameter will be called

the mesh resolution from here onwards, as in computer simulation terms each sub-source will be a point in a mesh that represents the volume of the original radiation source.

The answer is not straightforward as there are several factors which affect this parameter. In practice scientists and engineers use their knowledge of radiation physics and their experience to decide, and they may further refine their choice based on a trial and error process. This approach is not valid for our purposes because of two reasons; first the users will not be experienced radiation physics professionals, so they will not know about setting up point kernel simulations. Second, given the time restriction inherent in real time applications, a very high resolution with many points might incur in the violation of the time limit requirement.

In order to find a solution to deal with the issue of having an adequate mesh resolution, the factors that influence the method are analysed. These are:

• Distance: At long distances the mono PK method provides an acceptable performance for this task, but as the detector is moved closer to the source the accuracy error increases (without varying the size of the source), requiring a higher resolution mesh Multi PK method.
  This is because the self-attenuation of the source material becomes a more significant factor as the overall distance is reduced. The shorter the distance the higher the resolution of the mesh needs to be. The following figure illustrates this concept. The dot represents position of detector.

| Mono PK OK | Mono PK Insufficient | 8 point mesh OK | 8 point mesh Insufficient | 64 point mesh OK |
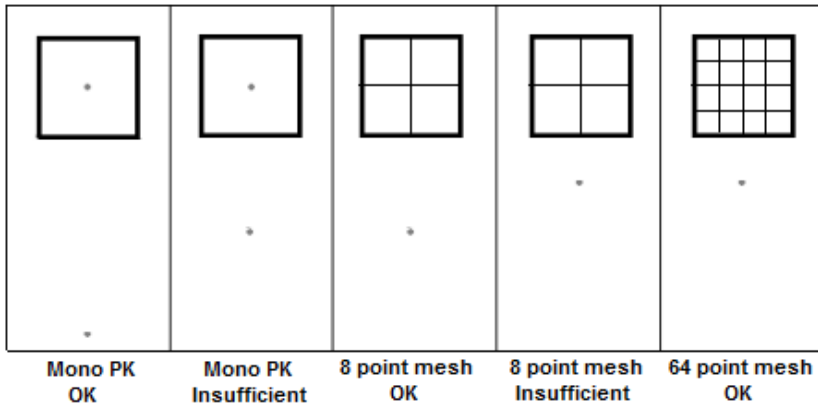
Figure 4-14 Effect of distance on accuracy

- Size: In a similar way as distance does, the size of the radiation source volume affects the accuracy of a PK computation (for a fixed distance), as the size of the source increases, so does the error of the Mono PK computation, requiring an increase in mesh resolution (implying a switch to Multi PK). The bigger the source is the higher the resolution of the Multi PK mesh needs to be. The following figure shows this effect on a source which increases size progressively.

| Mono PK OK | Mono PK Insufficient | 8p mesh OK | 8p mesh Insufficient | 64p mesh OK |
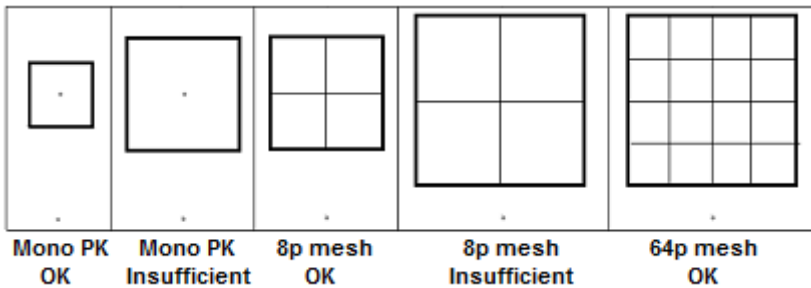
Figure 4-15 Effect of size on accuracy

- Orientation: Considering the source type being used is a parallelepiped, the angle at which the source is placed with respect to the direction of the detector has an effect on the accuracy of the mono PK method. In the worst case (detector on

93

a corner) the mono PK greatly amplifies the self-attenuation. This is because at different angles the mono PK does not account properly for the change in distribution of the radiation source volume, as shown by the following figure.

Mono PK	Mono PK	8 point mesh
OK	Insufficient	OK
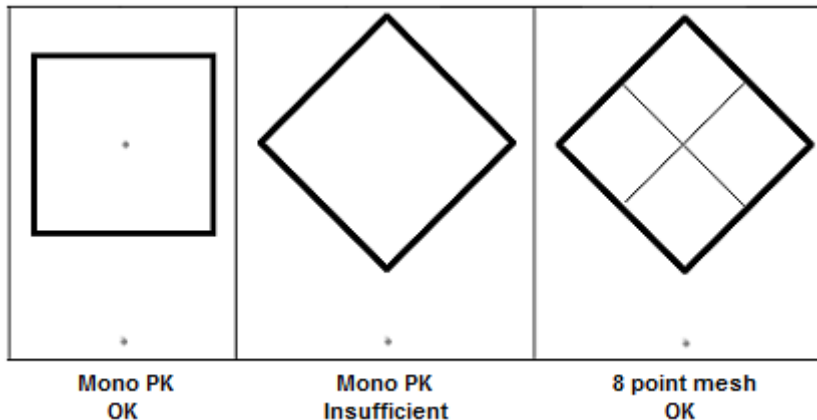
Figure 4-16 Effect of orientation on accuracy

Now that the necessity to divide the source volume has been shown, the next question which the reader might think off is: When to divide the source? A parameter which quantifies this need to divide the source must be established so that an algorithm can apply the division when necessary, the following point of the chapter explains what parameter has been chosen for this purpose.

4.4.3   The solid angle concept

Considering the effect of the parameters explained in the previous point, the aim is to come up with a solution that can detect these changes in order to automatize the selection of an adequate mesh resolution without requiring input from the user.

The chosen solution is to use the solid angle as a unified parameter to detect variations in the three relevant factors (distance, size and orientation). The solid angle can be defined as a measure of how large the source volume appears to an observer standing at the point

where the detector is, looking towards the source centre, or in other words the amount of the field of view occupied by the source volume.

The following figure shows how the variation in each of the three factors considered affects the solid angle of the source.
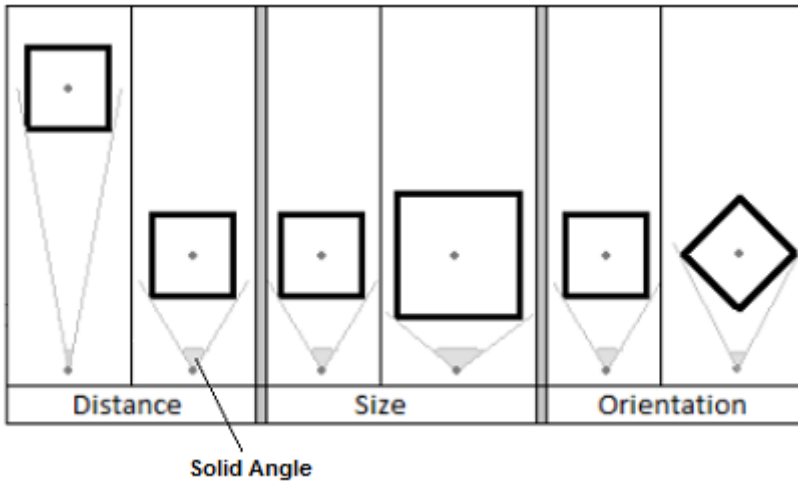
Figure 4-17 Effect of distance, size & orientation on solid angle

Therefore by monitoring the solid angle of the source we can assess the resolution of the mesh, by setting a threshold angle, if the computed angle is larger than this threshold, the resolution will be increased.

To calibrate the threshold angle the following process is performed. Given a standard case which will be presented in the next chapter (Results) different threshold limits are tested (a sequential series of angle increases), comparing the dose rate results with a high accuracy Monte Carlo simulation the smallest angle that meets the accuracy criteria of the problem is selected. Larger thresholds generate higher resolution meshes which of course also meet the accuracy requirements, but at a much higher computational cost. It must be noted the number of points increases exponentially as a

resolution is increased therefore unnecessary computational burdens must be avoided if possible.

4.4.4   Software architecture

Mathematically speaking the multi-point kernel method implies having a summation of the individual sub-sources which account for the whole original source. Taking as a starting point equation 4-2 for mono PK (with shielding and build up) the modification adds an outer summation loop from one to 'm', which stands for the number of sub-sources. This is represented by the following expression.

$$D^{eq}(d) = \sum_{j=1}^{j=m} \frac{C \, A_j \; \sum_{i=1}^{i=n} B_i E_i \, P_i \, e^{-(\mu_i \, t_j)_{shield}} \left(\frac{\mu}{\rho}\right)_i^{air}}{4\pi d_j^{\,2}}$$

The implementation of the solid angle concept introduces significant changes in the software structure of the application prototype. In first place a new module is created which will be in charge of selecting the adequate mesh resolution for the simulation. This will be called *model generator* as in fact selecting a mesh resolution is defining a model for the source. This module will in first place evaluate the solid angle of the original source, compare it with the threshold and subsequently proceed to establish a new mesh resolution if necessary. Once the source model is meeting the solid angle requirement, the points are then evaluated each as a mono PK and finally the individual flux of each sub-source point is added up to obtain the total dose rate.

The following data flow diagram shows where the *Model Generator* module is placed within the *Dosimetry module.*
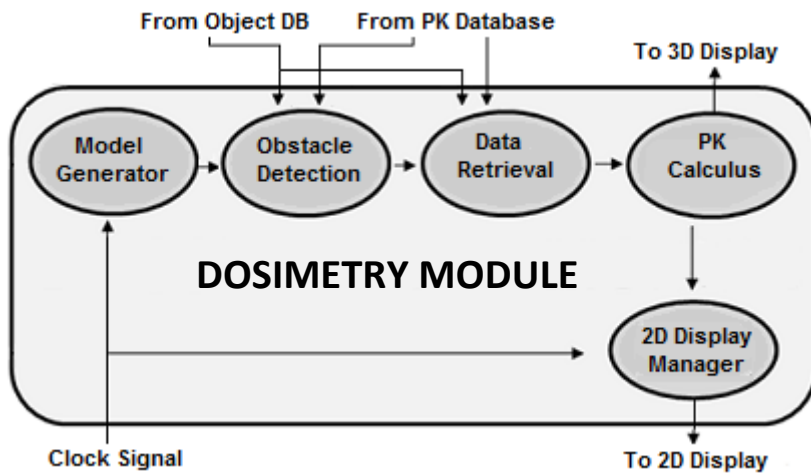
Figure 4-18 DFD for Multi PK with shielding method

4.4.5 Algorithmic description

The algorithm implemented in the *model generator* module performs two tasks. First, it computes the solid angle of the current source model; second, depending on the result of the comparison of the solid angle with the threshold, it may perform an increase of the mesh resolution of the source model.

To calculate the solid angle of the source volume the developed method first computes the position of the eight points corresponding to the vertices of the source parallelepiped (all sources considered up until now are parallelepipeds, other shapes will be dealt with further in the chapter), retrieving from the objects database the position of the barycentre, the orientation and the dimensions of the source. In the following step, it takes the position and aim direction of the detector. Then it computes the angle between the normalized vector going from the detector to the centre of the source and the vector going from the detector to a corner of the source. The algorithm calculates all eight angles and keeps the two largest ones on opposite sides of the source and adds them up.

The application compares the calculated angle with the threshold value. If the calculated angle is lower, the current model of the source is kept as it is; otherwise, the source will be divided to increase the mesh resolution.

The following figure illustrates this process simplified to 2D.
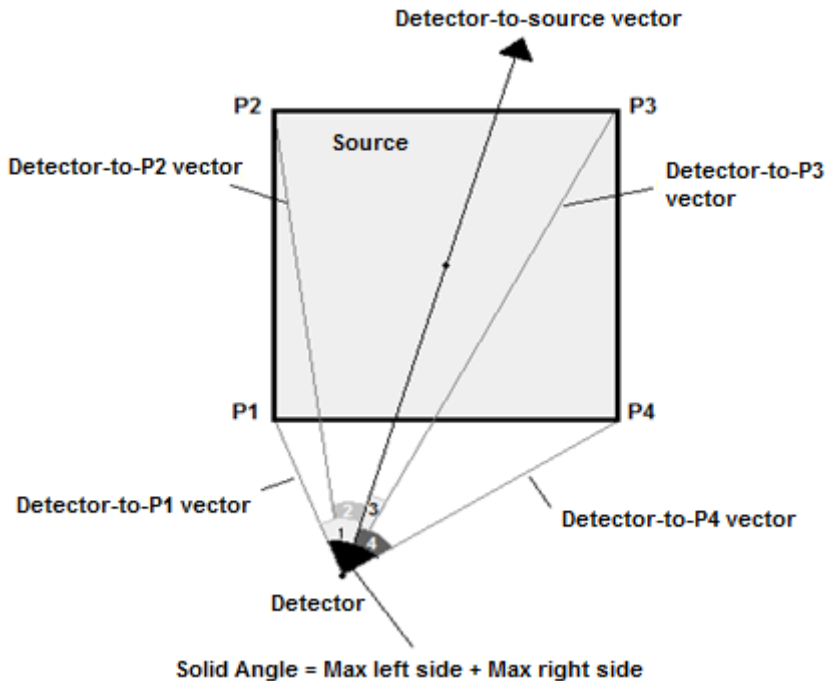
Figure 4-19 2D Simplification of solid angle computation method

That leads onto the second algorithm which creates the new higher resolution mesh. The method is based on the method octrees (a data storing structure) use to divide volume [78]. It takes as a starting point the current mesh. Knowing the position of the vertices of the parallelepiped the length of each side can be easily calculated (width, depth, height). The method then splits in half each side, therefore creating eight new sub-sources out of the original space and giving each an eighth of the activity. In case any of the resulting sub sources' solid angle is still greater than the threshold the sub sources

are subject to a second iteration of the dividing algorithm until the criteria is met or the maximum level of resolution is reached. Note that this method increases the amount of sub sources exponentially with each division. The following figure shows how the original sub source undergoes two iterations of mesh refinement. Also it is worthy to note the fact that newly generated meshes have its points regularly spaced out within the volume of the original source.
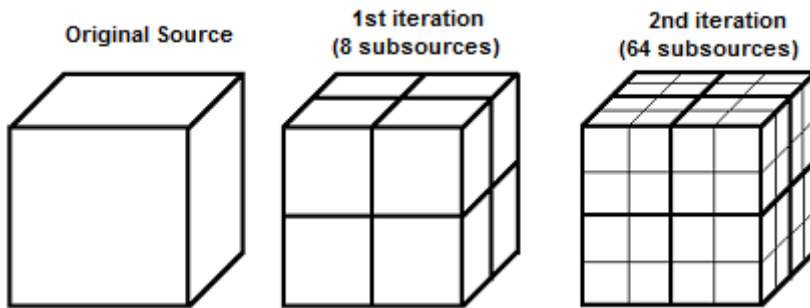
Figure 4-20 Mesh resolution increase by regular splitting all axes

These two methods where implemented in the *model generator* module shown in fig 4-18. As shown by the following pseudo-code snippet.

```
/**** Solid angle driven (regular) Model Generator *****/

Constant Threshold;
Source = GetSource();
Detector = GetDector();
while (sources in group) {
        Vector Det2Source =
        newVector(Detector.pos,Source.pos);
        Vector Det2vertex;

CONTINUES…
```

Figure 4-21 Solid angle driven regular model generator code

```
/********** 1. Calculate solid angle *************/
        Array vertices[8];
        Angle maxleft=0;
        Angle maxright=0;
        for (i=0; i=3; i++) { //check left side vertices
            vertices[i]=Source.GetVertex(i);
            Det2Vertex=newVector(Detector.pos,vertices[i]);

if (GetAngle(Det2Source,Det2vertex) > maxleft)
    maxleft= GetAngle(Det2Source,Det2vertex);
}
for (i=3; i=7; i++) { //check right side vertices
  vertices[i]=Source.GetVertex(i);
  Det2Vertex=newVector(Detector.pos,vertices[i]);
    if (GetAngle(Det2Source,Det2vertex) > maxright)
        maxright= GetAngle(Det2Source,Det2vertex);
    }
        Angle Solidangle = maxleft+maxright;
/*************** 2. Test Solid angle *************/
        If (SolidAngle > Threshold) {
 /************ 3. Generate new model ************/
        New_act=Source.activity/8;
        New_size=Source.size/2;
        New_pos=Source.pos;
        for (all sources) {
          for (i=0;i=7;i++) {
            // place of new sub-source
            disp=calcdisp(i,source_pos)
                newsource[i]   =   new   source(new_act,
                new_size, newpos+disp)
                add2group(newsource[i],sources)
          }
        }
        Break;
```

4.5 Fourth version: Octree non-regular Multi PK (Shielding & Build up)

4.5.1 Rationale of non-regular division

The introduction of the Multi PK paradigm in the previous version of the prototype solved accuracy problems related to the short distance/large source volume case. But this comes at the expense of increasing the computational cost of the PK computation.

Increasing the resolution of a regular mesh can lead to a very high amount of points, since it had been established that the point count is proportional to the computational effort, high resolution mesh translates into a heavy computational cost. This could be a problem for a VR based application such as the one being developed.

It would be convenient for the purposes of this application to have a less computationally intensive growth. This version of the prototype presents a different dividing strategy based on non-regular octree division.

The idea behind this concept is that not all areas of the source volume are equally significant towards the dose rate computation, and therefore if it would be possible to increase the resolution where it is most important keeping the rest of the volume with a low resolution, a significant reduction in computational cost could be achieved with very little accuracy lost.

To determine which areas of the source volume should be divided and which ones not, the proposed method relies on evaluating the solid angle of all the sub-sources and only divide those which are above the threshold and not the whole original source. This produces an irregular model with different levels of resolution. The following figure shows an example of non-regular division compared to the previous regular one (rhombus indicates detector position).
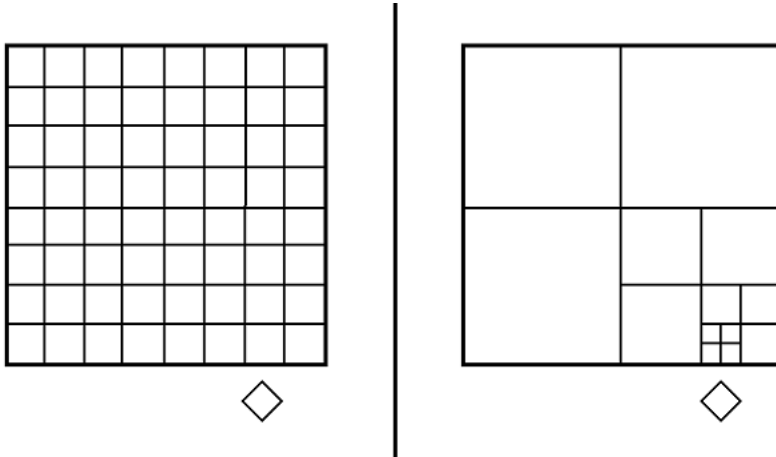
Figure 4-22 Regular vs. non-regular division in 2D

4.5.2   Algorithmic description

The main difference between the regular and non-regular versions of the prototype is in the model generation algorithm. While the method applied is essentially the same, in the regular version the octree based division procedure is applied to the group formed by all the sub-sources, while in the non-regular version only those sub-sources whose solid angle is above the threshold are divided.

The implementation of this change requires that the solid angle test is performed to all the sources (unlike the previous version, where it sufficed to perform solid angle calculations only until one result was above the threshold). On the other hand, the division here is performed only on the above-threshold-sources while in the regular method it is applied to all sources.

The following piece of pseudo-code illustrates the implemented non-regular division.

```
/***Solid angle driven (non-regular) Model Generator ***/

Constant Threshold;
Detector = GetDector();
for (all sources) {
    Source = GetSource();
    Vector Det2Source = newVectr(Detector.pos,Source.pos);
    Vector Det2vertex;

/************** 1. Calculate solid angle ************/
    Array vertices[8];
    Angle maxleft=0;
    Angle maxright=0;
    for (i=0; i=3; i++) { //check left side vertices
        vertices[i]=Source.GetVertex(i);
        Det2Vertex=newVector(Detector.pos,vertices[i]);
        if (GetAngle(Det2Source,Det2vertex) > maxleft)
            maxleft= GetAngle(Det2Source,Det2vertex);
    }
    for (i=3; i=7; i++) { //check right side vertices
        vertices[i]=Source.GetVertex(i);
        Det2Vertex=newVector(Detector.pos,vertices[i]);
            if (GetAngle(Det2Source,Det2vertex) > maxright)
                maxright= GetAngle(Det2Source,Det2vertex);
            }
        Angle Solidangle = maxleft+maxright;

/************** 2. Test Solid angle ***************/
        If (SolidAngle > Threshold) {
CONTINUES …
```

Figure 4-23 Solid angle driven non-regular model generator code

```
…CONTINUED

/*********** 3. Generate new model *************/

        New_act=Source.activity/8;
        New_size=Source.size/2;
        New_pos=Source.pos;
        for (i=0;i=7;i++) {
                // position of new sub-source
                disp=calcdisp(i,source_pos);
                newsource[i] = new source
                (new_act,new_size,new_pos+disp);
                add2group(newsource[i],sources) ;
                }
        }
}
/********************************************/
```

4.6 Fifth version: KD tree non-regular Multi PK (Shielding & Build up)

4.6.1 Rationale of KD tree version

The previous non-regular version aimed at reducing the computational cost of the simulation by reducing the number of sub-sources generated. This was successful, and a large reduction was achieved with respect to the original regular division.

Nevertheless the octree inspired division method still generates a minimum of eight sub-sources per each father source. Therefore the aim of this version was to analyse if there was still room for improvement in this area without losing out on the accuracy front, experimenting with a method that provides a slower growth of sub-source points.

For this aim a different family of trees inspired the division method, the K-dimensional (KD) trees [79]. These were tested in place of the

Octree derived method, the key characteristic of the KD-tree division method is that it can provide increase steps of just one sub source as opposed to the one to eight increase of sub-sources of the previous octree method.

4.6.2 KD-tree division method

K-Dimensional trees (KD-trees) are a type of binary space partitioning tree that were created with the aim of having a fast data structure for common data handling tasks such as searching, insertion and deletion. They use a so called splitting rule to divide one group of data into two in a certain manner.

The developed algorithm imitates the procedure in which KD-trees split data but applied to a volume (the source). The way the splitting works is governed by the splitting rule of which there are several kinds. Some of these like Friedman's [80] or Maneewongvatana's [81] aim at dealing with clustered data or other kinds on inconveniently sorted data. This is not the case at stake since data points do not exist a priori and they must be distributed uniformly.

Consequently the Standard splitting rule originally devised by Bentley [79] is used. This rule uses a plane of infinite dimensions called hyper plane which is placed in the centre of the axis of reference, splitting the volume in two halves.

The axis of reference is determined by the longest side of the parallelepiped volume being divided. In case one or more sides are of equal length, the method sequentially choses a side following a sequential pattern (in this case X->Y->Z) so that the originated sub-sources have a regular shape were all sides are of a similar length. This is important because otherwise sub-sources would be generated where the ratio of one of the sides with respect to the others would be very large, forming "pole" shaped volumes which are a poor representation of the source volume.

The following figure shows how the method works on a simplified 2D area, two iterations of the method are represented. The first iteration splits the original volume in two, since the source shape is a perfect square and both sides are of equal length the selection of the splitting side is decided according to where the detector is placed with respect to the source. On the other hand, the second iteration splits the highest solid angle previously generated sub-source by its longest side. In two iterations only three sub-sources are generated as opposed to the minimum of eight sub-sources the octree method would generate.
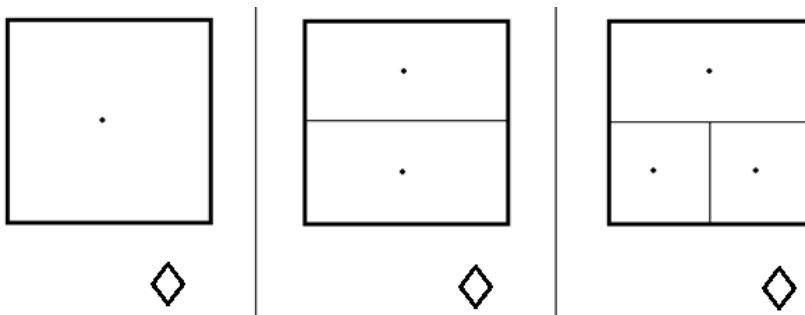
Figure 4-24 The KD-tree volume splitting method in 2D

4.6.3 Algorithmic description of the KD-tree division method

The first step of the KD-tree based splitting algorithm is to select the axis of reference of the source. Unlike in the original version from Bentley, this implementation defines the axis of reference as the one which forms the smallest angle with the source-detector vector. This guarantees that the division takes into account from which direction the source is approached generating more coherent results than a static cyclic rotation which starts with a predefined axis of reference.

The following figure illustrates an example of the described method to select the reference axis, restricted to the 2D plane.
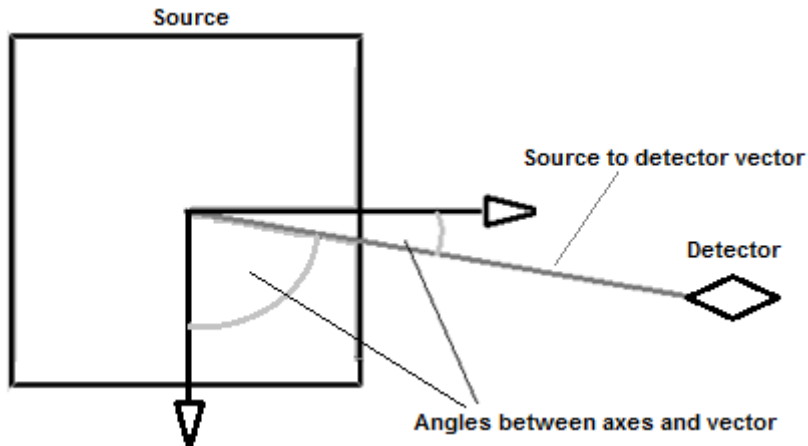
Figure 4-25 The KD-tree reference axis selection method in 2D

Once the initial reference axis has been chosen, the algorithm starts a cyclic order of division axis (X->Y->Z) for the following iterations.

If the algorithm were to ignore the initial orientation of the detector and divide the source volume according to the sequential method it would always start dividing the same axis first. This would generate a situation where for a same given distance of the detector to the source centre a different dose rate level would be obtained. The following figure shows this situation simplified to 2D.
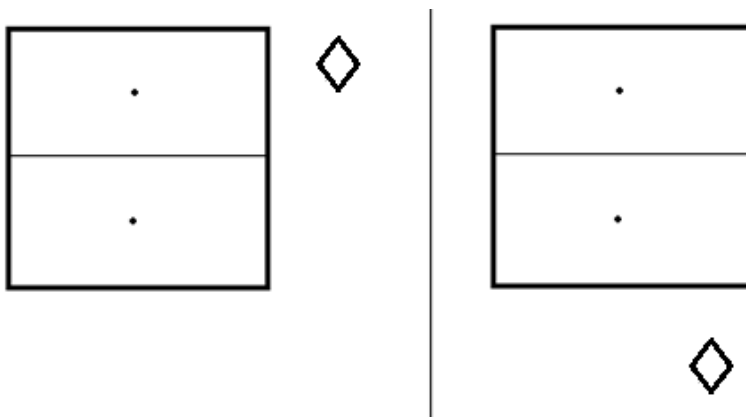
Figure 4-26 Same distance to source, different dose rate

In the example in Fig 4-26 the same division has been applied to both identical sources due to the static rotation of division axis. This causes the right case to have a sub-source point much closer to the detector than the left case, causing a higher dose rate in that case. In reality both cases should receive the same dose rate since the distance of the detector to the source is equivalent.

This problem does not occur with the octree-based division because of the symmetrical properties of that division where all sides are divided in every iteration of the algorithm.

The following piece of pseudo-code illustrates the KD model version implemented. The division axis order selection is implemented within the getRefAxis function. The main differences with the octree-based method are the assignment of activity (half of the father's activity is assigned to the new source since only two sub-sources are created instead of 8) and the updating of the reference axis of division for the next iteration of the KD division which is a new attribute necessary for the sources when using this division method.

```
/****Solid angle driven (KD-style) Model Generator ****/

Constant Threshold;
Detector = GetDector();
for (all sources) {
   Source = GetSource();
   Vector Det2Source =
   newVector(Detector.pos,Source.pos);
   Vector Det2vertex;
/************ 1. Calculate solid angle *************/
   Array vertices[8];
   Angle maxleft=0;
   Angle maxright=0;
   for (i=0; i=3; i++) { //check left side vertices
         vertices[i]=Source.GetVertex(i);
```

```
            Det2Vertex=newVector(Detector.pos,vertices[i]);
            if (GetAngle(Det2Source,Det2vertex) > maxleft)
                maxleft=
    GetAngle(Det2Source,Det2vertex);
                }
    for (i=3; i=7; i++) { //check right side vertices
      vertices[i]=Source.GetVertex(i);
      Det2Vertex=newVector(Detector.pos,vertices[i]);
            if (GetAngle(Det2Source,Det2vertex) > maxright)
                maxright=
    GetAngle(Det2Source,Det2vertex);
            }
    Angle Solidangle = maxleft+maxright;
    /************ 2. Test Solid angle ****************/
    If (SolidAngle > Threshold) {
     /********* 3. Generate new KD model ***********/
    If (refAxis == NULL)
    //Get or set the reference Axis if original source
            RefAxis = getRefAxis(Source,Detector);
    New_act=Source.activity/2; //half the activity
    New_size=Source.size/2; //half the volume
    New_pos1=Source.pos+refAxis/2; //first subsource
    New_pos2=Source.pos-refAxis/2; // 2nd subsource
    Sub1=createNewSource(new_act,new_size,newpos1);
    Sub2=createNewSource(new_act,new_size,newpos2);
    UpdateRefAxis(Sub1);
        UpdateRefAxis(Sub2);
        Add2group(sub1,sources);
        Add2group(sub2,sources);
        DeleteFromGroup(source,sources);
        }
}
```

Figure 4-27 Solid angle driven KD regular model generator

4.7 Sixth version: Multi shape Multi PK (Shielding & Build up)

4.7.1 Rationale of Multi shape version

All the methods shown in this chapter so far have considered the source to be a parallelepiped shaped volume. This assumption is based on the fact that this is actually a very common source shape which can occur in real life cases. Nevertheless it is obviously possible that other shapes might arise, particularly spheres and cylinders are shapes of interest as they are common source objects in the fields of nuclear security and safeguards.

The previously shown methods can be applied to these other kind of shapes, but considering their parallelepiped-like point distribution generation they are bound to induce accuracy errors which can be intolerable given our aim of realistically simulating a hand held gamma detector performance.

Particularly a concerning problem is that points defining sub source centres can be placed outside the volume of the original source shape as the division algorithm continues to increase the resolution, this is shown in the next figure where the octree based division method is applied to a sphere (represented as a circle in 2D), after the second iteration some of the generated points in the outer regions of the volume are actually outside the original source volume.

This poor representation of the boundaries of the sources can lead to over estimation dose calculation errors in measurements near those points.
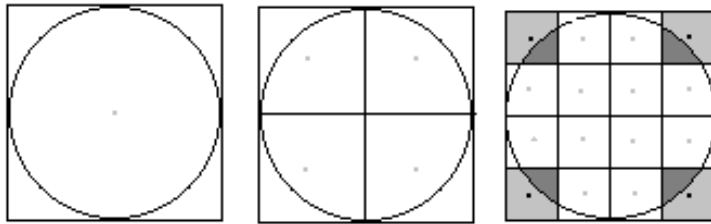
In order to overcome this shape limitation, hereby a method is proposed to adequately represent all sorts of shapes. Starting from the parallelepiped representation the points lying outside the original volume can be trimmed off using a finite element boundary representation based method.

4.7.2 Finite element boundary representation concept

The concept of finite element boundary representation is to represent volumes of solids by their physical limits [82]. In the particular case of dosimetric simulation the aim is to represent sources of multiple forms accurately.

The aim is to represent the solid by a finite element cellular decomposition of its boundary. This provides a flexible method to represent all sorts of volume shapes, the accuracy of the representation can be increased by simply increasing the resolution of the unit cell (sub-source).

Taking as an example the previous figure of the sphere, the finite element boundary representation would cut off the corner points to better approximate the real figure (in that level of resolution) as shown by the following figure.

Original Parallelepiped representation   Finite Element Boundary Representation
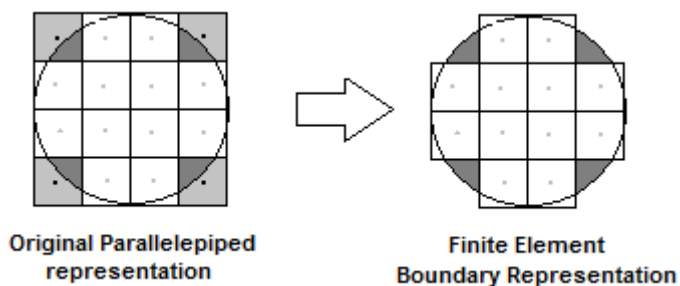
Figure 4-29 Finite element boundary representation of a sphere

The main drawback of this method is that it applies the algorithm on the whole volume of the radiation source, this increases the computational effort on the system, which is not a wanted characteristic in VR based applications. Nevertheless thanks to the computational cost reduction strategies implemented in the previous points it can be successfully applied to a real time simulation case, as the results of its testing will show in the next chapter of the thesis.

4.7.3 Boundary representation methodological challenges

The idea is to take as an input the list of sub-sources generated by one of the previous methods and then trim down all the sources whose central point is outside the original source volume, this strategy requires addressing two issues.

In first place, how to check if the central point of a sub-source is inside or outside the original source, and second, how to re-assign the deleted activity so that the trimmed point mesh has the same total activity as the original source and the distribution of activity is homogeneous in the trimmed mesh.

The proposed solution to deal with the first issue (finding out which points are outside the source) is to trace a vector from the centre point of the sub-source to the point being evaluated and checking for an intersection with the surface of the original volume. If there is none, the point is inside the volume, if there is one intersection, the

112

point must be outside the source. This test will suffice for spheres and cylinders which are the volumes under consideration. For other more irregular shapes it can happen that there is more than one intersection. In this case we will distinguish between even and odd number of intersections, the even numbers will represent points inside and the odd outside. The following figure illustrates the intersection test concept.
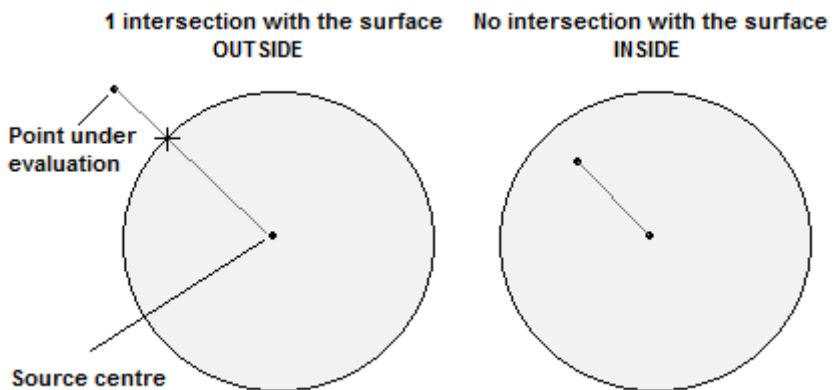
Figure 4-30 Intersection test for points in or out of volume

The second part of the method involves the deletion of the outlying sub-sources (those whose central point is out of the original volume) and the rearranging of the activity attribute value of the remaining sub-sources to account for the loss of the outer ones.

The way this is done is by dividing the original source's total activity by the smallest sub source volume and then assigning to each sub-source the unit activity multiplied by the size factor of the sub source (if there are different sized sub-sources i.e. the non-regular division case).

4.7.4 Algorithmic description of the finite element boundary representation post-processing

The algorithm implemented for this method consists of two parts explained in the previous point and applied to the generated model of sub sources. Each sub-source will be considered inside if its barycentre is inside the original volume source and outside otherwise, the rest of the sub-source volume is not taken into account for this purpose.

The underlying software development kit provides a useful function which evaluates the intersection between a 3D object's surface (the polygons which define it) and a vector, so this will be used within a loop which will test every sub source point by checking the intersection of a vector whose origin is the centre of the original source and its ending is at the point under evaluation. Each sub source found outside the source volume will be deleted from the list of sub sources.

The second part of algorithm starts by calculating the minimal unit activity, this is the activity corresponding to the smallest size sub-source created. The rest of sub-sources will be multiples of this, to facilitate this calculation in the implementation of the source definition a new attribute will be added to define the level of division of the sub-source, which will be used as the multiplying factor.

Once the unit activity value is known, the algorithm will perform a loop where it assigns to each remaining sub-source the activity value multiplied by its size factor. The following piece of pseudo-code illustrates the finite element based boundary representation post-process trimming algorithm.

```
/************   Post-process trimming   **************/

source OSource = getSource(Original_source);
group subsources;
group remaining;

/************* 1. Delete outer-points ***************/

for (i=0; i<subsources.getSize(); i++){
    source tempsou = subsources[i];
    vector tempvec = CreateVector(Osource.pos,tempsou.pos)
    if (testIntersect(tempvec,OSource) == TRUE)
            remaining.add(tempsou);
    }
deleteGroup(subsources);

/************* 2. Re-assign activity value**************/

float minact = OSource.activity/remaining[n].activity;
for (i=0;i<remaining.getSize();i++){
        remaining[i].setAttributeValue(activity,minact*factor);

/********************************************/
```

Figure 4-31 Post-process trimming pseudo code.

4.8 Seventh version: Multiple sources

4.8.1 Rationale of Multi source version

Up to now only the simulation of one source per scenario has been considered. This limits the application to situations where it is necessary to simulate only one source. In the real world of nuclear safeguards and security, situations where there are multiple sources present can occur. For these situations it would be necessary to compute the total dose rate created by the addition of the individual sources present in the scenario. An example of such a scenario could be simulating a series of nuclear waste low radioactivity containers in a storage facility.

The following figure shows the scheme described in the previous paragraph, for readability purposes the shielding, build up and source division iconography from previous schemes is not included in this diagram although it is present in the simulation.
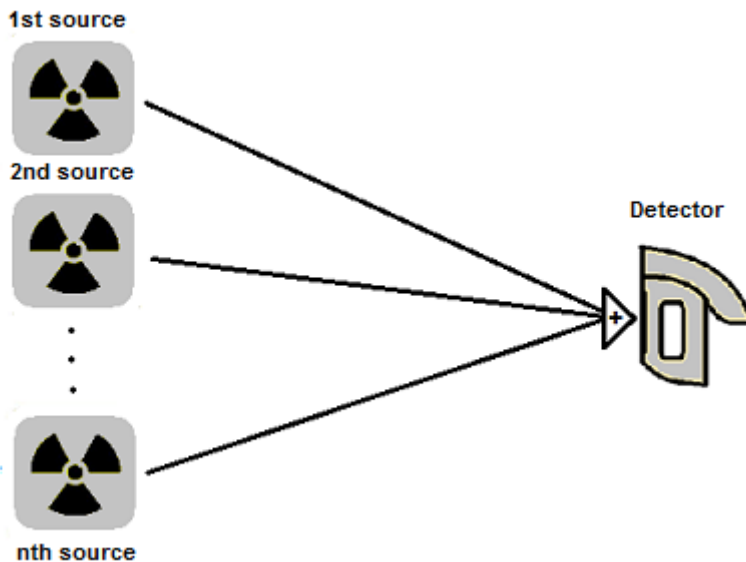
Figure 4-32 Multiple source computation scheme

4.8.2　Software architecture of the solution

From the software architecture point of view most of the functionality created for the multi-point kernel can be reused, since essentially multiple points are multiple sources. The difference is that now those sources could not all be of the same type. Therefore data input parameters which were constant because only one original source was considered now must be variable.

Another possible difference is that if the finite element boundary representation technique presented in the previous point of the chapter is used, then this must also be modified to account for a variable original source instead of a constant one.

To handle this variable, sources will be stored in a group and each source of the group processed individually in a loop like if it were the previous single source case and then the individual source dose rates will be added up to obtain the total dose rate generated by the whole group of sources.

Including this concept into the formula for multi PK shown in equation 4-3 the following expression is obtained.

<div align="right">Equation 4-4</div>

$$D^{eq}(d) = \sum_{k=1}^{k=\#sources} \left(\sum_{j=1}^{j=m} \frac{C\, A_j\ \sum_{i=1}^{i=n} B_i E_i\, P_i\, e^{-(\mu_i\, t_j)_{shield}} \left(\frac{\mu}{\rho}\right)_i^{air}}{4\pi d_j^{\,2}} \right)_k$$

The difference with equation 4-3 is the inclusion of an outer summation loop. The iterating variable 'k' tracks the number of sources being processed. The rest of the expression remains unchanged.

4.8.3 Algorithm description

The modifications in terms of algorithms affect the model generator code shown in fig. 4-21. Now an outer loop is introduced, iterating through all the original sources in the scenario and then performing the multi PK in the same way as previous versions.

```
/***Solid angle driven Model Generator (Multi-source) **/

Constant Threshold;
Detector = GetDetector();
// loop for original sources
for (i=0; i<number of original sources); i++) {
        Source = GetSource(i);  //No longer a constant
        // loop for sub-sources
        for (j=0; j<number of sub-sources; j++)
/****** 1. Calculate solid angle of subsource (j) ********/
                        (unchanged)
/******** 2. Test Solid angle of subsource (j) *********/
                        (unchanged)
/***** 3. Generate new model of subsource (j)   *******/
                        (unchanged)
        }
}
/****************** END ******************/
```

Figure 4-33 Pseudo code for multi source version.

4.9 Complementary development

The functionality presented in this part of the chapter corresponds to the auxiliary code which is necessary to run the prototype but does not constitute a part of the core dosimetry methodology development.

Figure 4-2 at the beginning of the chapter showed the two sub-modules which made part of the Dosimetry module, the dosimetry one was already explained with detail and now it is turn for the *2D Display manager* to be described. This sub-module takes care of the rendering of the virtual display and the functions which provide its data (see display image in Fig 3-4).

This sub module consists of five functions:

- *Search Direction*: This function implements a feature of a real dosimeter interface (model radFINDER™) devised to help the user locate the source. It indicates the direction in which the source lies with respect to where the detector is. This is achieved by increasing or decreasing the size of two horizontal bars accordingly, indicating the angle to the source as a percentage. The measuring range goes from -90º (0 %) to 90º (100 %). When the source is straight ahead, both bars will be at 50 % of their maximum size.

- *Doserate Reading*: This simple function takes as an input the dose rate value calculated by the PK dose rate computation function and displays it on the screen of the virtual dosimeter display. By default the selected measuring unit is µSv/h, but the user can switch to mRem (as used by many real instruments) which is more common in other countries.

- *Waterfall Chart:* This function generates a waterfall chart with the dose rate values received, that is a visual indication of the magnitude of the last few dose readings represented by vertical bars. This tool can help the user to locate the source, as the magnitude will be directly proportional to the distance for a given source (disregarding different attenuation properties). An increasing set of bars indicates an approach to the source, while decreasing bars means the user is moving away. The chart records the last ten dose rate values, which are sent by the *Doserate Reading* function. With each new dose rate value update, the bars are shifted leftwards on the screen, the oldest

measurement is deleted, and the newest is placed on the rightmost position of the chart.

- *Battery Indicator:* This is a simple function which calculates the amount of battery charge left. It consists of a countdown clock and a conversion of the remaining time as a percentage of the total battery life. The clock duration is set to the detector manufacturer's specifications of the expected battery charge duration.

- *Font Creation*: This auxiliary function generates font type replicas of those used in the real detector display and makes them available to the previously described functions which need to make use of them for the output of data. Unlike the previous functions which are updated periodically each iteration, this one is only active at the beginning of the execution.

The way these functions interact in terms of data flow is summed up by the following data flow diagram.
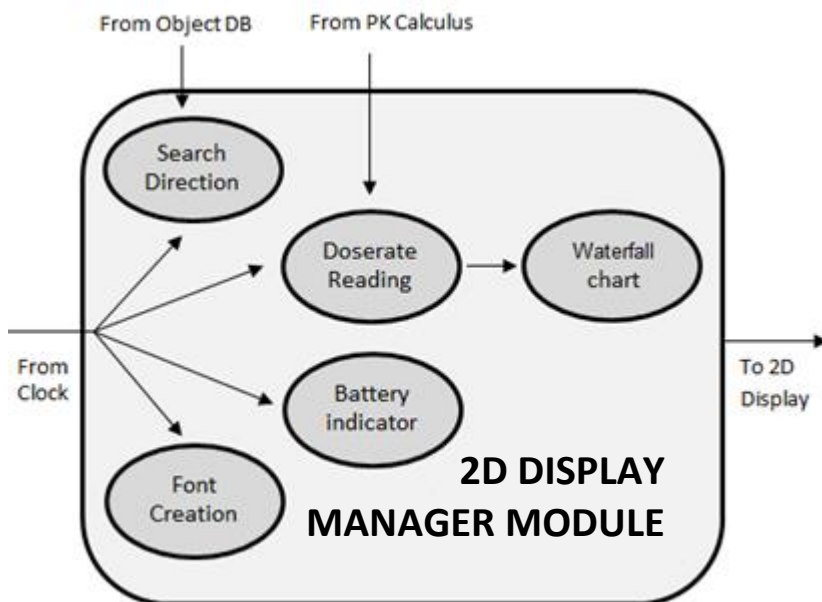
Figure 4-34 Detector Display management DFD

This last point ends this chapter of the thesis dedicated to the developed methodologies. The next chapter will cover the testing performed to evaluate these methods and the results obtained.

5 Testing and Results

In the previous chapters of this thesis many theoretical methods and strategies have been shown. Naturally the following step is to prove their validity, which is the objective of this chapter. In order to do this, the implemented methods were subject to a series of tests, obtaining results which were used to qualify their performance by comparison.

The tests can be classified into two main categories; first the testing against other software codes and secondly the testing against the results obtained from measuring with a real hand held radiation detector.

The chapter is structured in the following manner:

- First, the chapter will focus on the comparison against other computer codes, the results obtained from the developed prototype will be compared against the results of other computer software which will be used as a benchmark of accuracy. Different versions will be tested, the first three (v1, v2, v3) focus on increasing the accuracy while the next two (v4 and v5) focus on computational effort reduction.
- The second part of the chapter will compare the results of the developed prototype with the readings obtained from a real hand held device such as the ones the prototype tries to simulate. Again the same versions will be tested for accuracy in first place and secondly computational cost will be addressed.
- Finally the versions of the prototype which deal with other secondary limitations of the software such as multiple shapes (version 6) and multiple sources (version 7) are tested at the end comparing against computer simulation results.

5.1 Test 1: Simulated Cs-137 source

5.1.1 Experiment setup

The simulated gamma radiation source used is the isotope Caesium Cs-137, this particular source was chosen because it is a very common source in this field and was subject of testing experiments in relevant computer simulation experiments [83]. The source volume is a cube with 20 cm sides containing a homogeneous dilution of Cs-137 in water. The total activity of the source was 43.53 GBq. Only the 662 KeV energy line is considered with a yield of 84.6 %. For this first test the volumetric sources are irrelevant as the source is considered to be a point in space with no volume or shape.

The objective of the test was to compute the equivalent dose rate at different points, varying the distance between the source and detector. Starting 5m away and approaching to the source up to a distance of 15cm. The following figure illustrates what the real life test would be like.
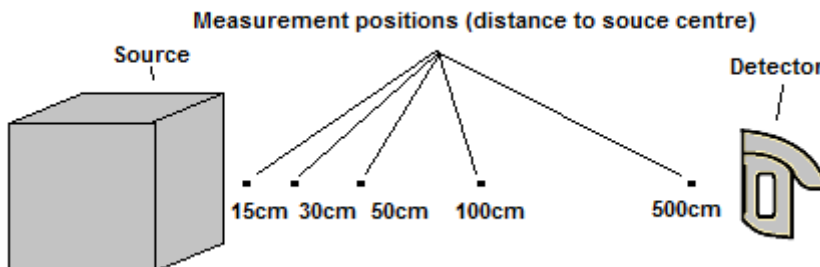
Figure 5-1Test 1 scheme

The particular points chosen correspond to those for whom dose rate data was available from the benchmark software codes, they allow for a comparison of dose rates of different levels of magnitude.

The detector's detecting element volume and shape are also not taken into account in any of the tests performed for this thesis work

and always a single point in space is considered. The volume of the source will be considered or not, depending on the version of the prototype tested.

5.1.2 Benchmark software codes

Several radiation transport software codes were used for testing purposes of the different prototype versions implemented. These were:

1. NUCLEONICA [84] Dosimetry & Shielding: This simple online tool developed by the European Commission's Joint Research Centre was chosen as a representative of the Mono Point Kernel codes. It was chosen because information about its implementation is available (the data tables, types of interpolation etc.) therefore it was possible to compare its results to our prototype using the same data inputs. This tool could calculate the shielding and buildup effects of a shield if required but not the self-absorption of the source.

2. CIDEC [83] is an example of a multi PK code for dose rate calculations capable of dealing with multiple types of shield. Developed by the Centro de Investigaciones Energéticas, Medioambientales y Tecnológicas, it was chosen as a representative of modern codes since its development is quite recent and results data for the chosen test configuration was available.

3. Microshield [85], developed by Grove Engineering is another multi PK, it is a well-known commercial software for dose rate computations. It was chosen because it is a common code used widely in the nuclear and medicine fields and also because there were available results data for the case under evaluation.

4. MCNP 4C2 [86]: This software program for general radiation transport problems belongs to the family of the Monte Carlo codes. This code (and other similar ones) has been used as benchmark for accuracy given the fact that they can provide very accurate calculations (given enough time and computational resources). It has been used for this purpose in this thesis.

5.1.3   V1: Mono PK

The aim of this first test was to test the correctness of the implemented Mono PK code in its first version by comparing it against another PK code (Nucleonica) which uses the same library of PK tables and therefore should produce very similar results.

Given the limitations of the simplest mono PK codes such as the ones being tested in this case, the actual simulation makes several assumptions such as considering the source a point in space without any volume or shape and therefore disregarding the interaction with matter, ignoring the interaction with the cube of water shown in the previous figure. The following figure shows what the mono PK codes being tested actually are doing.
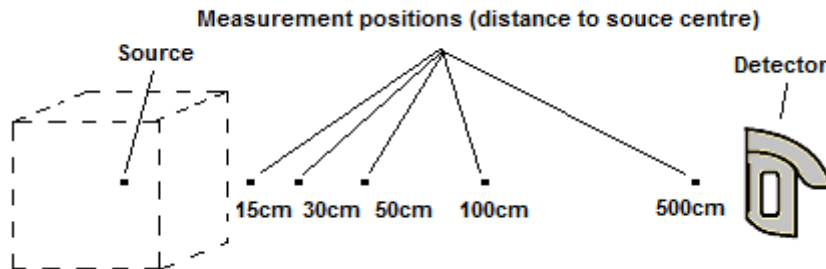
Figure 5-2 Mono PK simulation for Test 1 scheme

For benchmarking purposes a simulation of the test was performed with a Monte Carlo code (MCNP v4) aiming for a high accuracy, therefore using a large amount of simulated particles (10 million).

The following table shows the results obtained for the previously described test with both Nucleonica, the first prototype version (mono PK no shielding, no build up) and the Monte Carlo benchmark code MCNP, along with the deviation of the results of the mono PK methods with respect to the benchmark code.

Distance (cm)	Equivalent Dose rate in air and deviation to MCNP (mSv/h)				
	Proto V1 (mono PK)	Deviation	Nucleonica (mono PK)	Deviation	MCNP
500	0.13	+23	0.14	+29	0.10
100	3.26	+19	3.53	+25	2.63
50	13.03	+15	14.12	+22	11.1
30	36.18	+9	39.22	+16	32.8
15	144.74	+3	156.88	+10	141

Table 5-5-1 Test 1: Dose rate comparison of Prototype V1 vs. Nucleonica code

As expected the dose rate increases exponentially as the distance is reduced, which is the correct behaviour. The mono PK codes follow relatively closely the benchmark code despite working only with a single "particle" instead of tracking the life of millions of particles like the Monte Carlo does, thus providing a huge computational advantage. It can be appreciated that at far distances for some instances the deviation exceeds the accuracy requirement limits set (marked red). A possible explanation for the over estimation of dose rate is the over simplification of the problem setup which ignores the attenuation of the matter. Therefore the following test will use a more detailed version of the PK computation.

The difference between the two mono PK codes can be attributed to the different precision of the data table figures and the interpolation methods.

It can also be seen that the mono PK codes overestimate the dose rate, giving always higher dose rates than the Monte Carlo benchmark for every distance tested. This can be appreciated better in the following graph.
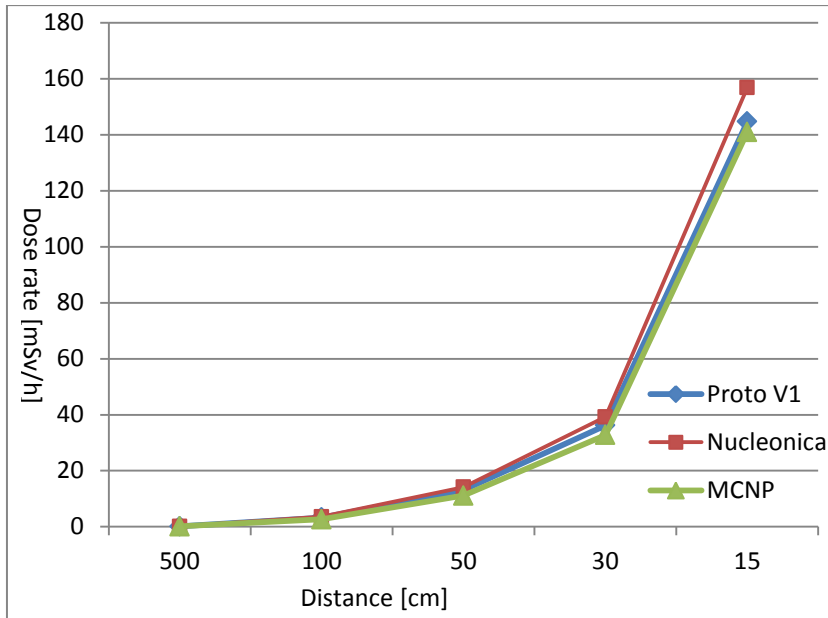
Figure 5-3 Test 1, mono PK codes (without S&BUp) vs. benchmark

5.1.4 V2: Mono PK with Shielding & Build up

The second test aimed at evaluating the implementation of the shielding and buildup effects. As explained in previous chapters this are, an attenuation of the radiation due to the interaction of radiation with matter (shielding) and a buildup of radiation from a non-direct origin (buildup) respectively. In terms of implementation, this physical effect is simulated by introducing two factors in the PK computation formula; ($e^{-(\mu_i\,t)_{shield}}$) which accounts for the shielding and *B* which accounts for the buildup, shown in equation 4-2.

This second test follows the procedure of the first test, using the same simulated source and the same distance steps. The difference lays in the fact that now the self-attenuation and build-up of the source cube is taken into account. This effect is approximated by assuming the radiation travels through half of the distance of cube length through water as shown by the following diagram.
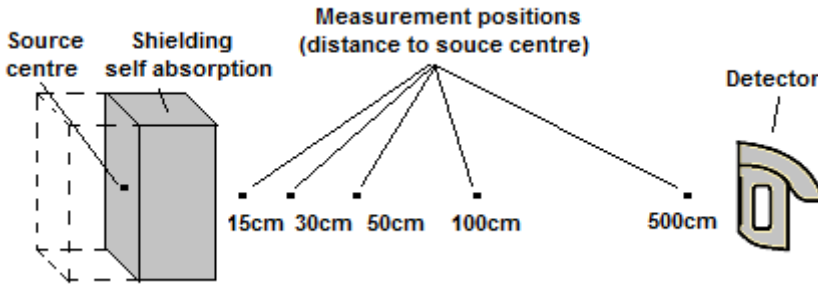
The following table shows the results obtained for the test with the second prototype version (mono PK with shielding and build up) compared to the first version (mono PK without these factors) and the Monte Carlo Benchmark code, alongside with the deviation to the latter.

Distance (cm)	Equivalent Dose rate in air and deviation to MCNP (mSv/h)				
	Proto V1 (mono PK)	Deviation	Proto V2 (mono PK)	Deviation	MCNP
500	0.13	+23	0.11	+9	0.10
100	3.26	+19	2.89	+9	2.63
50	13.03	+15	11.55	+4	11.1
30	36.18	+9	32.09	-2	32.8
15	144.74	+3	128.38	-10	141

Table 5-5-2 Test 2: Dose rate comparison of Prototype V2 vs. V1 and MCNP benchmark code

The introduction of the shielding and buildup factors in the equation has resulted in a general decrease of dose rate compared to the first simpler version of the prototype. Though still not as low as the benchmark code for most cases, the results are now closer. It can be inferred that the newly implemented factors were a step in the right direction in terms of accuracy.
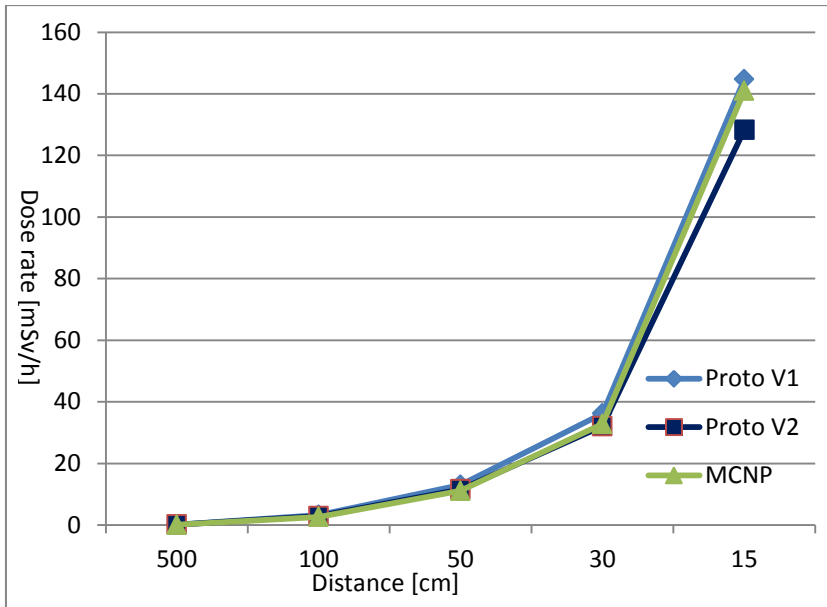
Figure 5-5 Test 2, mono PK with & without S&BUp vs. benchmark

The previous graph shows visually the information of table 5-2, here it is easier to appreciate how the second version of the prototype (V2) represents an improvement (for the case tested) with respect to the first version (V1).

Nevertheless it can be noted that for the closest distance the deviation has increased, on the graph it can be seen that there is a trend where the mono PK code starts under estimating the dose rate as the distance is decreased. This behaviour can be attributed to the error created by using a single point to represent the whole source.

The most significant improvement of the 2nd version of the prototype is that now all the dose rate results are within the requirement limits in terms of accuracy. Nevertheless the growing deviation trend at close distances highlights the limitations of mono PK codes, reducing this negative effect was the motivation for the V3 multi PK version.

5.1.5 V3: Multi PK with Shielding and Build up

The aim of the third test is to evaluate the performance of the third version of the prototype (V3) which features a variable multi PK algorithm using the Octree based division method. The following figure illustrates the scheme of the test for the regular multi PK method where the original source is divided into a regular mesh of points, which split the original volume into a series of sub sources if a certain solid angle threshold is reached. Like in previous tests, five distance points are taken into considerations following a straight line trajectory. Starting from a distance of 5 meters and progressively approaching the detector to the sources in order to reduce the distance in each measurement with respect to the previous.
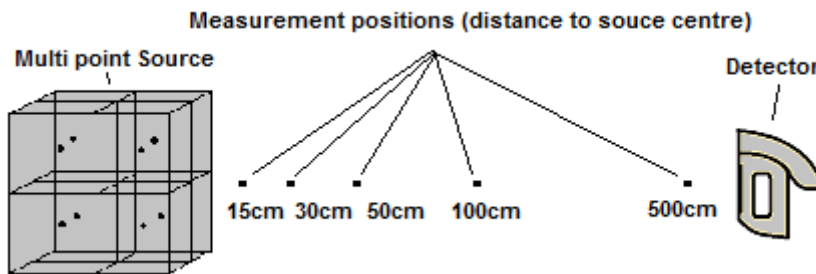
Figure 5-6 Multi PK with shielding simulation for Test 3 scheme

In order to test its overall performance, three characteristics will be analysed, first the dose rate accuracy compared to other multi PK codes (this will show if the multi PK has been correctly implemented), secondly the accuracy with respect to the previous mono PK V2 version (this will highlight the expected improvement if it exists) and finally the computational effort of the solution for this particular case.

Starting with the comparison with other multi PK codes, the results for the equivalent dose rate computation of the Cs-137 case are shown in the following table alongside the deviations to the MCNP benchmark code results.

Position (X,Y,Z) (cm)	Equivalent Dose rate in air & deviation to MCNP (mSv/h)						
	Proto V3 (regular multi PK)	Dev %	CIDEC	Dev %	Micro-shield	Dev %	MCNP
(500,0,0)	0.11	+9	0.11	+9	0.11	+9	0.10
(100,0,0)	2.89	+9	2.89	+9	2.91	+11	2.63
(50,0,0)	11.55	+4	11.80	+6	11.85	+7	11.1
(30,0,0)	33.21	+1	33.74	+3	33.84	+3	32.8
(15,0,0)	138.6	-2	140.5	-0.4	140.4	-0.4	141

Table 5-5-3 Test 3.1: Dose rate comparison of Prototype V3 vs. other Multi PK codes with MCNP as benchmark code

The results shown in the previous table show that the behaviour of the three multi PK codes is very similar with deviations among them of less than 3% in the worst case, and therefore the implementation developed is a valid representative of multi PK codes. With respect to the MCNP benchmark the deviation data show that all of them would be sufficient in terms of accuracy for our purpose.

The advantage of the developed prototype with respect to the CIDEC and Microshield codes is that it automatically choses its point mesh density always trying to minimize the computational cost and manages to perform the first three calculations using only a single point therefore being much less burdensome than the other codes' fixed mesh.

The following part of the test will compare the performance of the V3 with respect to the previous V2 mono PK code, the purpose is to establish how much (if any) improvement has been achieved with the use the newly developed methodology and if it was actually necessary for this particular case.

To study the effect of the geometry of the volume the following test will consider three different approaching trajectories to the source in addition to the frontal one done so far. In the new trajectories the source will be approached from an edge and from a vertex.

Henceforth these cases will be named, frontal, edge and vertex respectively. The following figure illustrates the three lines of approach tested and the points where the virtual detector will be placed.
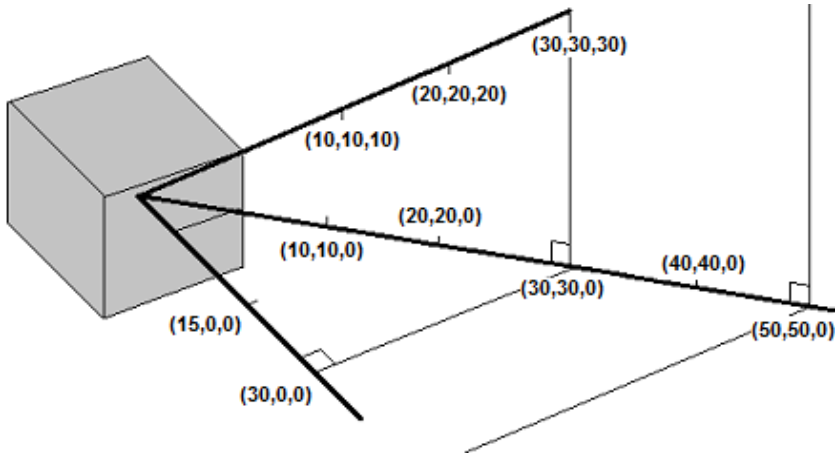
Figure 5-7 Multi PK with shielding simulation positions

The following tables shows the dose rate results for the three testing positions for the variable multi PK version of the prototype compared to the previous mono PK version alongside the deviation with respect to MCNP.

Position (X,Y,Z) (cm)	Equivalent Dose rate in air and deviation to MCNP (mSv/h)				
	Proto V2 (mono PK)	Deviation %	Proto V3 (regular multi PK)	Deviation %	MCNP
(500,0,0)	0.11	+9	0.11	+9	0.10
(100,0,0)	2.89	+9	2.89	+9	2.63
(50,0,0)	11.55	+4	11.55	+4	11.1
(30,0,0)	32.09	-2	33.21	+1	32.8
(15,0,0)	128.38	-10	138.6	-2	141

Table 5-5-4 Test 3A: Dose rate comparison of Prototype V3 vs. V2 and MCNP benchmark code for frontal line

Position (X,Y,Z) (cm)	Equivalent Dose rate in air and deviation to MCNP (mSv/h)				
	Proto V2 (mono PK)	Deviation %	Proto V3 (regular multi PK)	Deviation %	MCNP
(50,50,0)	5.30	-4	5.30	-4	5.49
(40,40,0)	8.29	-4	8.29	-4	8.65
(30,30,0)	14.73	-6	14.73	-6	15.61
(20,20,0)	33.15	-9	36.63	+1	36.29
(10,10,0)	132.6	-34	178.5	+1	177.6

Table 5-5-5 Test 3A: Dose rate comparison of Prototype V3 vs. V2 and MCNP benchmark code for edge line

Position (X,Y,Z) (cm)	Equivalent Dose rate in air and deviation to MCNP (mSv/h)				
	Proto V2 (mono PK)	Deviation %	Proto V3 (regular multi PK)	Deviation %	MCNP
(50,50,50)	3.24	-13	3.24	-13	3.74
(40,40,40)	5.03	-13	5.03	-13	5.84
(30,30,30)	8.99	-13	8.99	-13	10.36
(20,20,20)	20.22	-13	20.22	-13	23.26
(10,10,10)	80.87	-24	102.78	+2	100.4

Table 5-5-6 Test 3A: Dose rate comparison of Prototype V3 vs. V2 and MCNP benchmark code for vertex line

As expected the results show that the newer prototype V3 with multi PK represents an improvement in terms of accuracy with respect to the V2 mono PK version. Particularly where mono PK falters most (at short distances) multi PK provides a much improved solution.

The behaviour varies slightly depending on the approaching line, as the orientation of the geometrical source has an effect on the shielding distances. The furthest away computations with the V3 multi PK version generate the same results as the mono PK V2 version due to the fact the solid angle has not reached the threshold for switching to a higher resolution yet. The following graphs show

the information in a visual manner to better identify the trends in the simulation results.
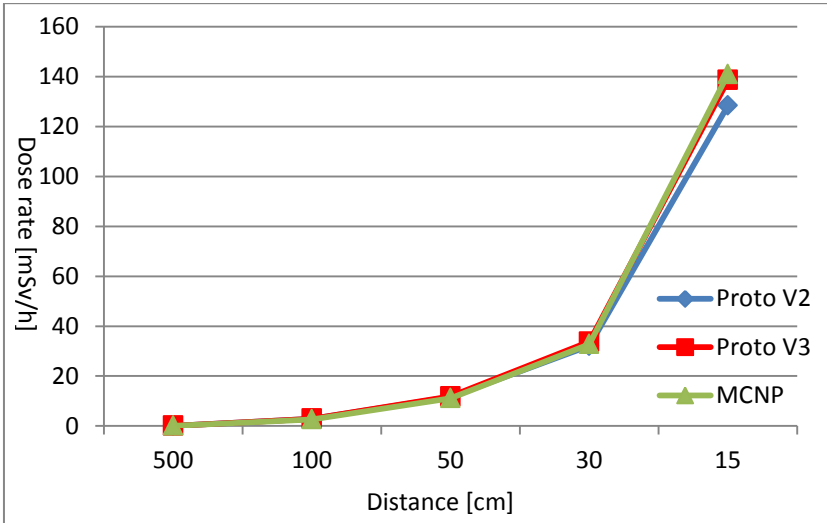
Figure 5-8 Test 3, V3 vs. V2 and benchmark, frontal case
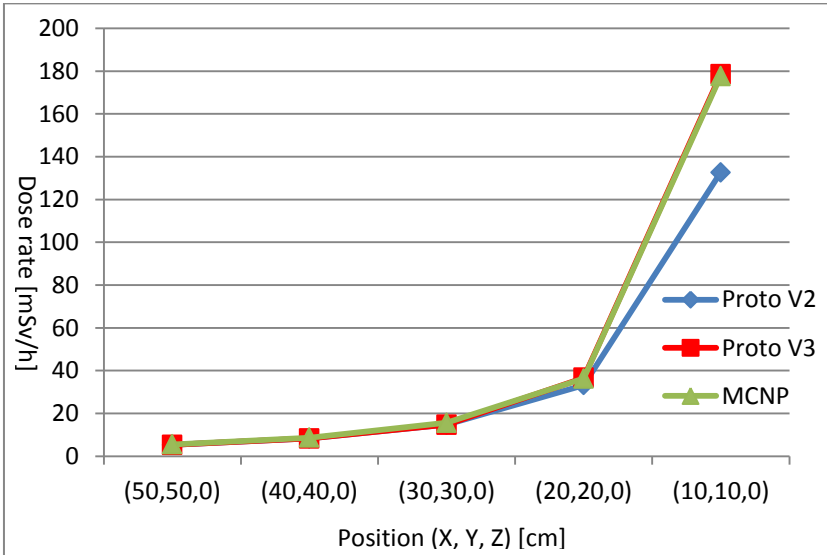
Figure 5-9 Test 3, V3 vs. V2 and benchmark, edge case
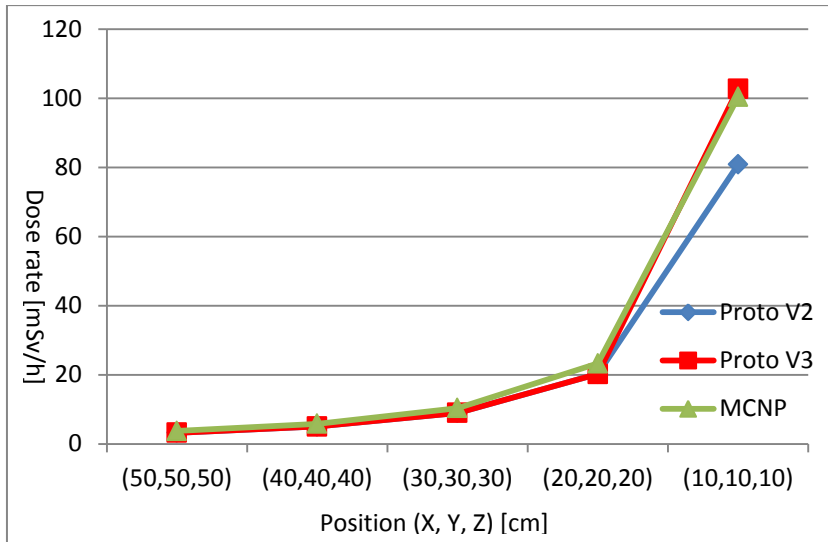
Figure 5-10 Test 3, V3 vs. V2 and benchmark, vertex case

As it can be clearly appreciated on the previous figures, the weakest point of the mono PK algorithm which was the accuracy deviation at short distances has been notably improved, the underestimating tendency of the mono PK code is solved by the multi PK code.

Furthermore it can be seen than the deviation of the mono PK code seems to be worsened by the edge and vertex line approaches, this is due to the fact the self-shielding distance is maximized in these conditions in comparison to the frontal line of approach which reduces the self-shield distance to the minimum. Therefore we can assume any other angle approach for the mono PK will produce a deviation within those two limits.

On the previous tables it can be seen that the worsening in the edge and vertex cases for the closest distance hinted in the graphs actually does not comply with the accuracy requirements, making the V2 insufficient for those cases while on the opposite side the V3 performs extremely well for those near cases.

Nevertheless, the improvement of the accuracy of the dose rate calculation of the V3 version comes at an expense, the increase of computational cost, this leads to the last point of this test: analysing the effect of the new algorithm on computational cost. To achieve this the number of points in each generated mesh will be compared to the points generated by a fixed mesh such as the ones used by other PK codes.

Position (X,Y,Z) (cm)	Number of points in mesh		
	Proto V2 (mono PK)	Proto V3 (multi PK)	Fixed 64 (multi PK)
(500,0,0)	1	1	64
(100,0,0)	1	1	64
(50,0,0)	1	1	64
(30,0,0)	1	8	64
(15,0,0)	1	64	64
Average mesh points	1	15	64

Table 5-5-7 Computational cost comparison between mono PK, variable PK and fixed 64 PK for Cs-137 source case.

The results for the other two approaching lines are the same in terms of computational cost so they will be omitted to avoid redundancy.

The objective of introducing the fixed 64 point mesh is to illustrate the behaviour of already existing codes which do not vary their mesh automatically in real time (e.g. Microshield, CIDEC) like the developed prototype V3 does. 64 points is the maximum resolution the V3 version reached for this case.

The average mesh points gives an idea of the computational cost difference during a common dosimetry exercise where the measuring distances are expected to be heterogeneously spread due to the fact that the users tend to move around the scenario rather than taking measurements from a single point.

The following graph shows the computational cost of the V3 prototype version compared against the mono PK version (V2) and a

fixed mesh with a 64 point kernel at different distances from the source.
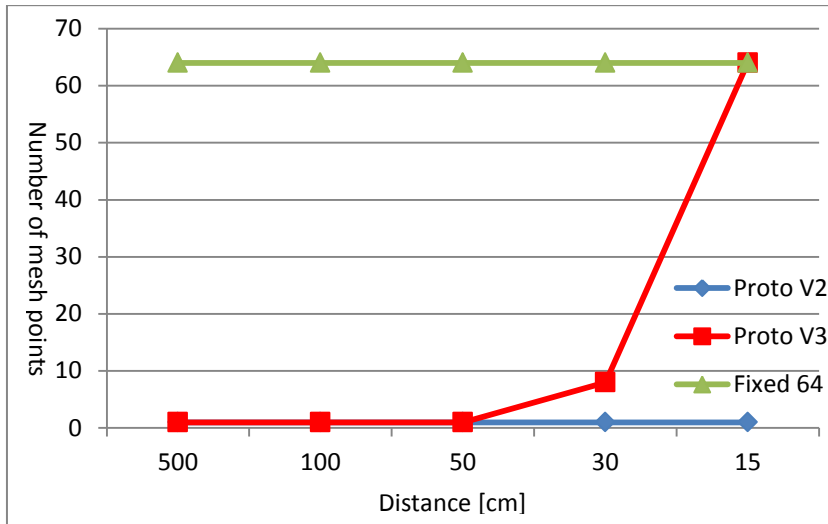
Figure 5-11 Mesh points of V3 vs. mono PK and fixed mesh

On the previous graph one positive result and one negative trend can be appreciated. The positive result is that the automatic variable algorithm manages to use low point meshes in most cases saving a significant amount of computer effort compared to the fixed meshes which are normally used in existing software codes. The negative trend is that the V3 prototype's algorithm increases mesh resolution in an exponential manner, each step multiplies by eight the previous mesh point density.

This rapid growth of mesh points could be a problem considering the real-time requirement of a virtual reality based application because the mesh point number is directly proportional to the computational effort. In order to assess the relevance of this result, the simulation of the V3 prototype is timed on a standard office computer such as the ones where possibly a release version of this prototype application might be run. The recorded times can be seen on the following table.

Position (X,Y,Z) (cm)	Execution time (ms)		
	Proto V2 (mono PK)	Proto V3 (multi PK)	Fixed 64 (multi PK)
(500,0,0)	8	8	285
(100,0,0)	9	8	281
(50,0,0)	8	8	282
(30,0,0)	8	33	288
(15,0,0)	9	287	284
Average computation time	8.4	65.8	284

Table 5-5-8 Timing comparison: mono PK vs. variable PK and fixed multi PK simulations.

The technical characteristics of the hardware and software used are: Intel Xeon © E5640 central processing unit clocked at 2.67GHz, usable memory 3.49 GB of RAM, NVIDIA Quadro FX 3800 graphics card, 32bit Windows 7 operating system, Virtools 5.0 software development kit.

All the timed tests found on this document have been obtained with the same computer under similar workload conditions.

The results show that there is proportionality between the number of mesh points and execution time; the single PK operations take on average 8ms. This includes two parts, first there is a period dedicated to tasks not related to the PK computation which takes about 3ms to 5ms depending on the load of tasks of the computer on that moment. Secondly on average each point kernel operation takes a further 4ms. Given the time limit set for this task (1s) all the distances tested meet the time limit requirement. Nevertheless only one more level of point mesh density could be applied without incurring in a violation of the time limit requirement.

5.1.6 V4: Multi PK non regular

The objective of the fourth version of the prototype was to reduce the computational cost burden of the V3 version keeping a degree of accuracy within the requirements established. This algorithm uses the concept of non-regular division which leads to source volumes divided in different levels of resolution according to the importance each of area of the source has towards the PK computation as explained in the previous chapter. The following figure shows an example of a source after being divided with the non-regular method.
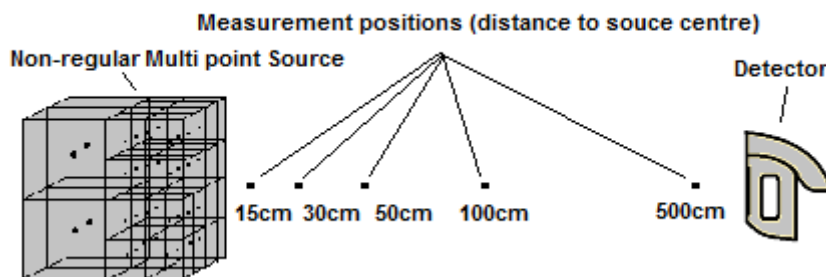
Figure 5-12 Example of a non-regularly divided source volume

To evaluate its performance, the V4 version underwent the following tests; first a comparison with the V3 code dose rate results in order to evaluate if the accuracy is still acceptable despite the reduction in number of mesh points, and second a comparison of the computational cost to find out if the expected gain in this requirement was actually obtained. This computational cost was again estimated by recorded the execution time of the prototypes on the testing computer.

Therefore in first place the dose rate data is computed. The following tables show the results for the dose rate computation of the previous V3 and new V4 and their deviations with respect to the benchmark code.

Position (X,Y,Z) (cm)	Equivalent Dose rate in air and deviation to MCNP (mSv/h)				
	V3 (regular multi PK)	Deviation %	V4 (non-regular multi PK)	Deviation %	MCNP
(500,0,0)	0.11	+9	0.11	+9	0.10
(100,0,0)	2.89	+9	2.89	+9	2.63
(50,0,0)	11.55	+4	11.55	+4	11.1
(30,0,0)	33.21	+1	33.21	+1	32.8
(15,0,0)	138.6	-2	138.2	-2	141

Table 5-5-9 Test 4A: Dose rate comparison of Prototype V4 vs. V3 and MCNP benchmark code for frontal line

Position (X,Y,Z) (cm)	Equivalent Dose rate in air and deviation to MCNP (mSv/h)				
	V3 (regular multi PK)	Deviation %	V4 (non-regular multi PK)	Deviation %	MCNP
(50,50,0)	5.30	-4	5.30	-4	5.49
(40,40,0)	8.29	-4	8.29	-4	8.65
(30,30,0)	14.73	-6	14.73	-6	15.61
(20,20,0)	36.63	+1	36.63	+1	36.29
(10,10,0)	178.5	+1	176.9	-1	177.6

Table 5-5-10 Test 4A: Dose rate comparison of Prototype V4 vs. V3 and MCNP benchmark code for edge line

Position (X,Y,Z) (cm)	Equivalent Dose rate in air and deviation to MCNP (mSv/h)				
	V3 (regular multi PK)	Deviation %	V4 (non-regular multi PK)	Deviation %	MCNP
(50,50,50)	3.24	-13	3.24	-13	3.74
(40,40,40)	5.03	-13	5.03	-13	5.84
(30,30,30)	8.99	-13	8.99	-13	10.36
(20,20,20)	20.22	-13	20.22	-13	23.26
(10,10,10)	102.78	+2	102.78	+2	100.4

Table 5-5-11 Test 4A: Dose rate comparison of Prototype V4 vs. V3 and MCNP benchmark code for vertex line

It can be appreciated that the initial far away distances tested obtain the same result both with V3 and V4, this is because the first level of division yields the same 8 point mesh in both cases, it is not until the second level of division starts that a difference appears between both methods.

This can be seen in closest distance computation for the first two subcases, where there is a small difference between both cases. In the third case (vertex approach) there is no difference between both cases at any point due to the algorithm only reaching the first level of division.

The deviation results show that the new non-regular algorithm did not affect negatively the accuracy of the computation; in fact it presents a fractional improvement in the tested case. The objective of remaining within the requirement limits for accuracy is largely satisfied.

Considering the magnitude of the variation, graphs related to the previous tables are omitted, since the only provide redundant information and the difference could not be appreciated visually by the reader.

The second part of the V4 testing related to computational cost follows; discovering if the non-regular division provides a noticeable improvement in terms of computational cost with respect to the previous regularly divided mesh algorithm (V3). For this purpose the number of points generated for the frontal and edge cases will be studied.

The following two tables sum up the number of mesh points generated in each of these cases. The vertex case is omitted from the results because it rendered the exact same meshes with both the V3 and V4 versions and therefore any information it provides is redundant to that previously obtained in the testing of those versions.

Position (X,Y,Z) (cm)	Number of points in mesh		
	V3 (regular multi PK)	V4 (non-regular multi PK)	Fixed 64 (multi PK)
(500,0,0)	1	1	64
(100,0,0)	1	1	64
(50,0,0)	1	1	64
(30,0,0)	8	8	64
(15,0,0)	64	36	64
Average mesh points	15	9.4	64

Table 5-5-12 Mesh points for variable regular PK, variable non-regular and fixed 64 PK for Cs-137 source front case

Position (X,Y,Z) (cm)	Number of points in mesh		
	V3 (regular multi PK)	V4 (non-regular multi PK)	Fixed 64 (multi PK)
(50,50,0)	1	1	64
(40,40,0)	1	1	64
(30,30,0)	1	1	64
(20,20,0)	8	8	64
(10,10,0)	64	22	64
Average mesh points	15	6.6	64

Table 5-5-13 Mesh points for variable regular PK, variable non-regular and fixed 64 PK for Cs-137 source edge case

As expected, the non-regular division manages to reduce the amount of points generated by dividing only the closest sub-sources. This particular case does not deepen into very high point meshes due to the small size of the original size, meaning at most distances tested the algorithm retains the mono PK source model, but in the two instances where the V4 algorithm makes a difference with respect to the V3 regular division, a 44% and 66% reduction of points is achieved respectively.

To better comprehend the new trend of point mesh density increase, the previous information from tables 5-12 and 5-13 is shown in graphical form in the following two figures.
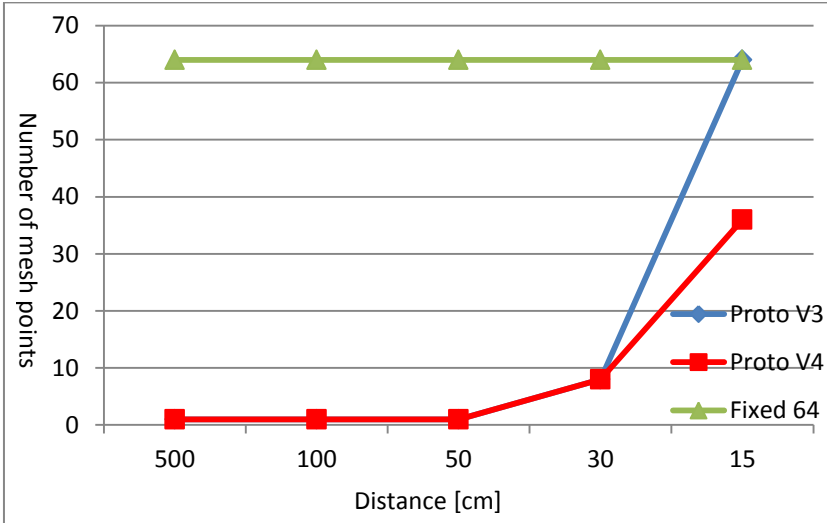
Figure 5-13 Mesh points of V4 vs. V3 & fixed mesh, frontal case
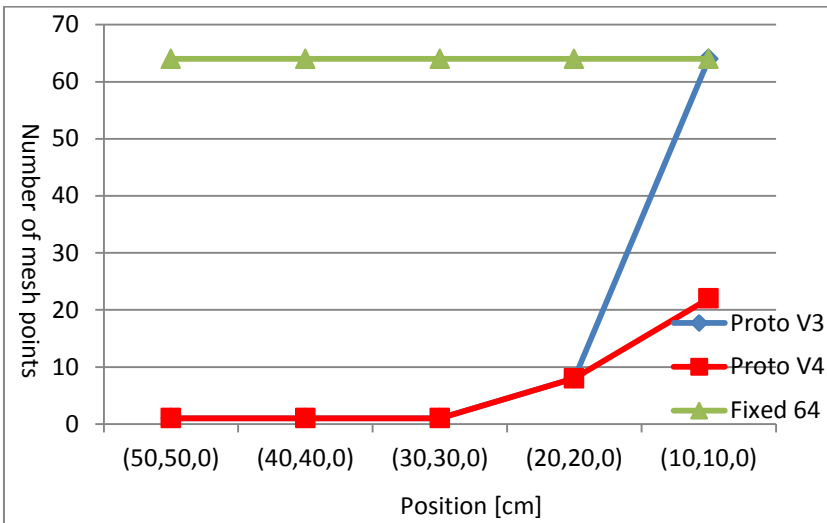
Figure 5-14 Mesh points of V4 vs. V3 & fixed mesh, edge case

The behaviour of the V4 algorithm mimics the V3 for the first four measurements (due to the solid angle not increasing enough to oblige the algorithm to increase the point mesh density), but the subsequent measurement is clearly much lower than the exponential growth shown by the V3 prototype. Depending on the approaching path taken, V4 shows a behaviour which ranges from halving the V3 growth in the worst (frontal) case, to an almost linear increase in the edge case (best case).

To understand the meaning of this result in practical terms (running the algorithm in the VR prototype), the execution time for the test was measured in the same way as it had been done for the previous version.

The following two tables show the execution time for the two relevant cases (frontal, edge) of the V4 (non-regular multi PK) version alongside the execution time of the V3 (regular multi PK) and Fixed mesh (64 points). These execution times for the V3 and the fixed 64 point mesh versions are taken from the previous section of testing results since they are the same exact case for both simulations and no variation is to be expected by rerunning the same code under the same conditions.

Position (X,Y,Z) (cm)	Execution time (ms)		
	V3 (regular multi PK)	V4 (non-regular multi PK)	Fixed 64 (multi PK)
(500,0,0)	8	8	285
(100,0,0)	8	7	281
(50,0,0)	8	8	282
(30,0,0)	33	32	288
(15,0,0)	287	133	284
Average computation time	65.8	37.6	284

Table 5-5-14 Timing comparison: V3 vs. V4 and fixed multi PK simulations for frontal case.

Position (X,Y,Z) (cm)	Execution time (ms)		
	V3 (regular multi PK)	V4 (non-regular multi PK)	Fixed 64 (multi PK)
(50,50,0)	8	8	285
(40,40,0)	8	8	281
(30,30,0)	8	8	282
(20,20,0)	33	34	288
(10,10,0)	287	91	284
Average computation time	65.8	29.8	284

Table 5-5-15 Timing comparison: V3 vs. V4 and fixed multi PK simulations for edge case.

The timing results show that the V4 provides a 50% and 66% reduction in average execution time for frontal and edge cases respectively with respect to the V3 version. What is most important, the specific instances which benefit from the improvement are the slowest ones (closest distance) which are the ones prone to violate the time limit requirement. Nevertheless it must be stated the V3 was sufficient for this case, which was quite favourable in terms of dimensions.

5.1.7   V5: Multi PK non regular KD

The aim of the KD tree approach to source volume division is to improve the computational efficiency of the dose rate computation by reducing the number of points generated in each division step. The method used up until now in V3 and V4 versions is based in octrees, it splits each sub-source into eight sources, the KD-tree version divides each source in two. This way only one point is added to the mesh in each step. This method is still a non-regular multi PK computation including shielding and buildup.

The following figure shows an example of a source after being split twice with the KD tree method.
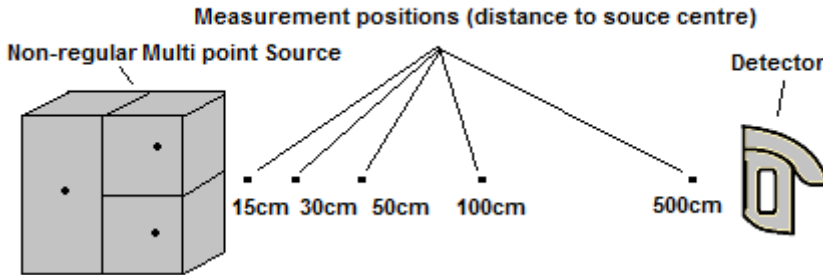
Figure 5-15 KD simulation for Test 1 scheme

The test is structured in the same way as the two previous versions, first the dose rate accuracy of the new model will be tested to guarantee that the requirement is met and secondly the computational cost will be analysed via mesh point count analysis and execution time comparison in order to assess the improvement achieved in this parameter.

The following tables show the results for the computed equivalent dose rate using the new V5 algorithm (KD tree based volume division algorithm) and the comparison to the previous version 4 (Octree based volume division algorithm), alongside their deviations to the MCNP benchmark code results expressed as a percentage difference with the benchmark code.

Position (X,Y,Z) (cm)	Equivalent Dose rate in air and deviation to MCNP (mSv/h)				
	V4 proto	Deviation %	V5 proto	Deviation %	MCNP
(500,0,0)	0.11	+9	0.11	+9	0.10
(100,0,0)	2.89	+9	2.89	+9	2.63
(50,0,0)	11.55	+4	11.55	+4	11.1
(30,0,0)	33.21	+1	34.65	+6	32.8
(15,0,0)	138.2	-2	140.1	-1	141

Table 5-5-16 Dose rate of Prototype V4, V5 and real detector readings for frontal line.

Position (X,Y,Z) (cm)	Equivalent Dose rate in air and deviation to MCNP (mSv/h)				
	V4 proto	Deviation %	V5 proto	Deviation %	MCNP
(50,50,0)	5.30	-4	5.30	-4	5.49
(40,40,0)	8.29	-4	8.29	-4	8.65
(30,30,0)	14.73	-6	14.73	-6	15.61
(20,20,0)	36.63	+1	36.88	+2	36.29
(10,10,0)	176.9	-1	164.3	-7	177.6

Table 5-5-17 Dose rate of Prototypes V4, V5 and real detector readings for edge line.

Position (X,Y,Z) (cm)	Equivalent Dose rate in air and deviation to MCNP (mSv/h)				
	V4	Deviation %	V5	Deviation %	MCNP
(50,50,50)	3.24	-13	3.24	-13	3.74
(40,40,40)	5.03	-13	5.03	-13	5.84
(30,30,30)	8.99	-13	8.99	-13	10.36
(20,20,20)	20.22	-13	20.22	-13	23.26
(10,10,10)	102.78	+2	87.44	-13	100.4

Table 5-5-18 Dose rate of Prototype V4, V5 and real detector readings for vertex line.

The results obtained show two distinct trends. First, the three furthest away distances in each case do not reach the solid angle limit where the source is divided, therefore the mono PK representation remains and the results are the same for both V5 and V4. The closest distances require a division of the original source and here is where the two volume dividing methods generate different results.

The results of the accuracy analysis show that the new V5 version produces an increase of the deviation of the dose rate calculation. For the frontal case, the average increase is less than 1%, while the maximum deviation remains unchanged. For the edge case, the

average deviation rises by 1.4% up to an average of 4.6% with an individual maximum of 7%. For the vertex approach (worst case), the average deviation is increased by 2.2% up to 13%. All these deviation values are still within the limits set in the requirements. Therefore the V5 version, albeit less accurate than the V4, is still an adequate solution in terms of dose rate accuracy.

To better illustrate the rate of growth of the two different versions compared, the dose rate data is converted to graphical form and shown in the following figures.
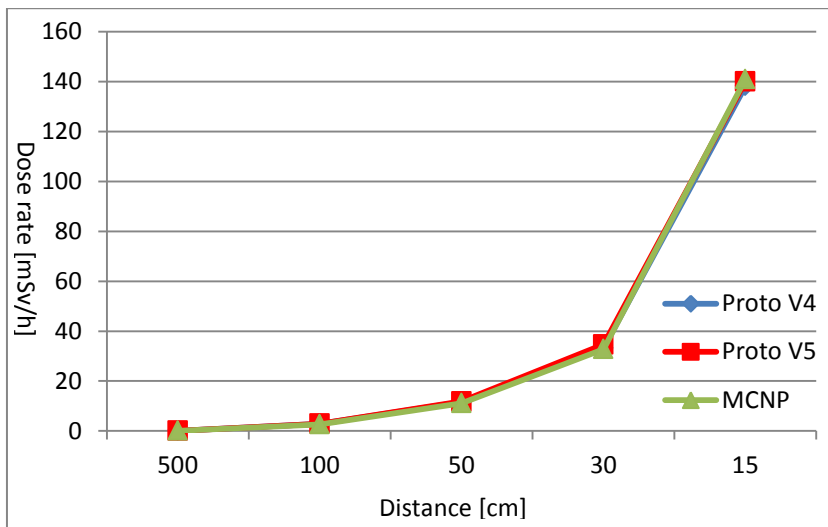
Figure 5-16 Dose rate V4 vs. V5 & benchmark, front case

The new version of the prototype overestimates the dose rate slightly more than the previous V4 for the 30cm instance but offers a more accurate result for the 15cm instance. In both instances the V5 provides a higher dose rate output than the V4.

In any case the difference is barely noticeable by the reader because the deviation always stays below the 10% mark in all the distances tested.
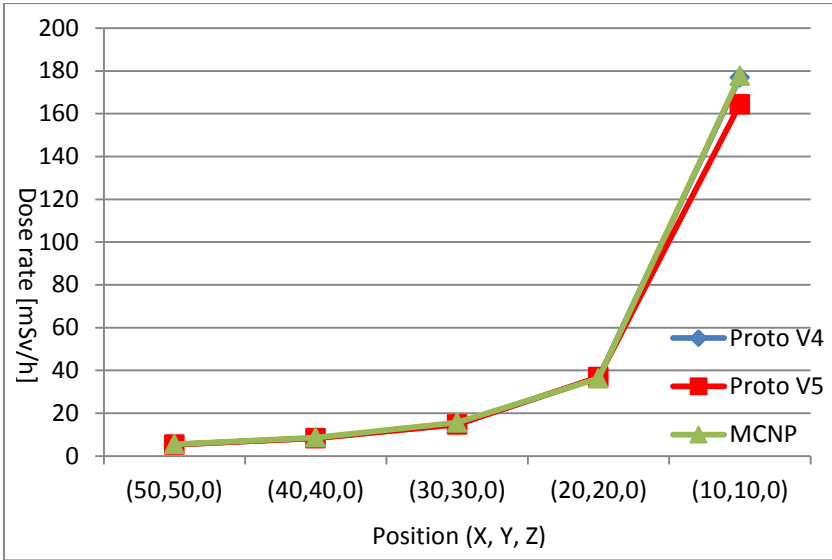
Figure 5-17 Dose rate V4 vs. V5 & benchmark, edge case
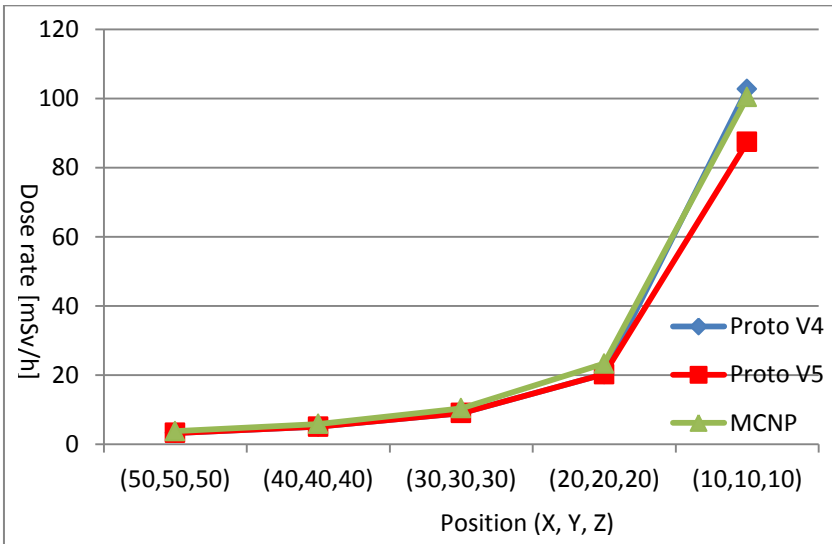
Figure 5-18 Dose rate V4 vs. V5 & benchmark, vertex case

Unlike the frontal case the edge and vertex approaching lines do generate a larger deviation to the benchmark code in the V5 version.

It both cases there is a noticeable underestimation of the dose rate at the closest distance.

The key point is how large this deviation is, because in order to be a valid solution for the purpose of this thesis, the deviation must remain within the limits established in the requirements.

The next element to analyse is the computational cost of the new algorithm. This will indicate if the loss of accuracy is justifiable. As with previous tests in this chapter the number of mesh points generated by the V5 algorithm for each case will be compared to the previous V4 version.

The following tables show the mesh point count for each of the instances tested in all three approaching lines.

Position (X,Y,Z) (cm)	Number of points in mesh		
	V4	V5	Fixed regular
(500,0,0)	1	1	36
(100,0,0)	1	1	36
(50,0,0)	1	1	36
(30,0,0)	8	3	36
(15,0,0)	36	36	36
Average mesh points	9.4	8.4	36

Table 5-5-19 Mesh point count of V4, V5 and fixed mesh for Cs-137 source, front case

Position (X,Y,Z) (cm)	Number of points in mesh		
	V4	V5	Fixed regular
(50,50,0)	1	1	36
(40,40,0)	1	1	36
(30,30,0)	1	1	36
(20,20,0)	8	4	36
(10,10,0)	22	15	36
Average mesh points	6.6	4.4	36

Table 5-5-20 Mesh point count of V4, V5 and fixed mesh for Cs-137 source, edge case

Position (X,Y,Z) (cm)	Number of points in mesh		
	V4	V5	Fixed regular
(50,50,50)	1	1	36
(40,40,40)	1	1	36
(30,30,30)	1	1	36
(20,20,20)	1	1	36
(10,10,10)	15	5	36
Average mesh points	3.8	1.8	36

Table 5-5-21 Mesh point count of V4, V5 and fixed mesh for Cs-137 source, vertex case

The results of the previous tables indicate that the new V5 does actually provide a reduction in terms of point mesh density with respect to V4. On average the improvement is between 1% and 2.2% depending on the approaching line taken. In all the instances except one (where the result is equal) there is a reduction of points. The maximum individual reduction occurs in the closest instance of the vertex line approach, where a reduction of 66% occurs with respect to the previous version.

The fixed regular mesh of 36 points indicates the level of point density that would have been necessary to match the total points of the highest point count instance of the variable versions tested. It shows how much computational effort is being wasted compared to the newest V5 version which has in its worst case an average point count under 10.

The figures on the following page show the information of the previous tables in line graphs to better illustrate the gains of the V5 algorithm.
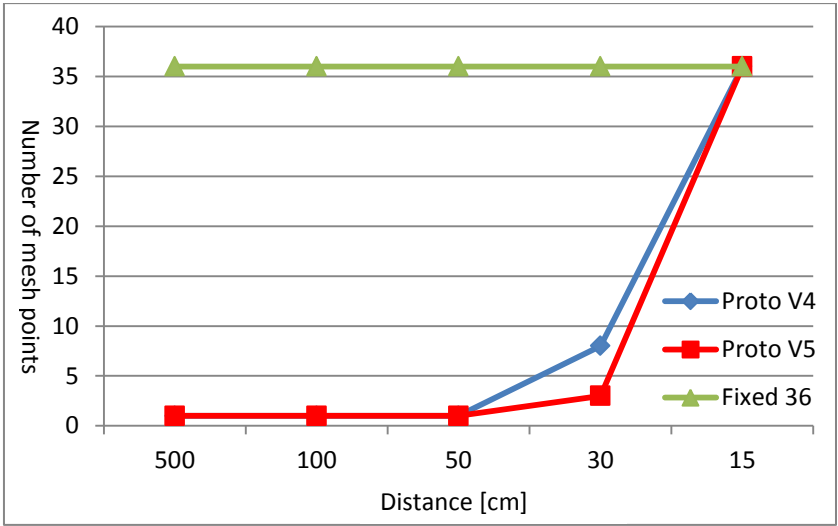
Figure 5-19 Mesh points of V5 vs. V4 for frontal case
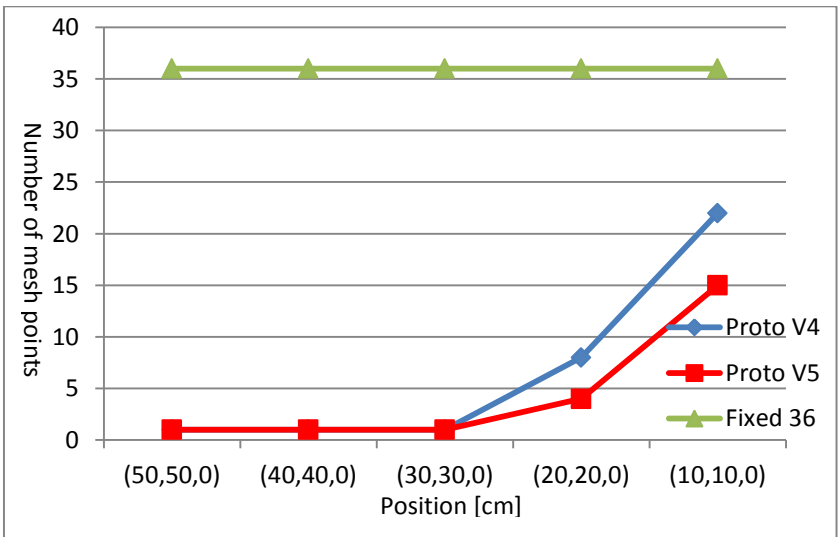
Figure 5-20 Mesh points of V5 vs. V4 for edge case

153
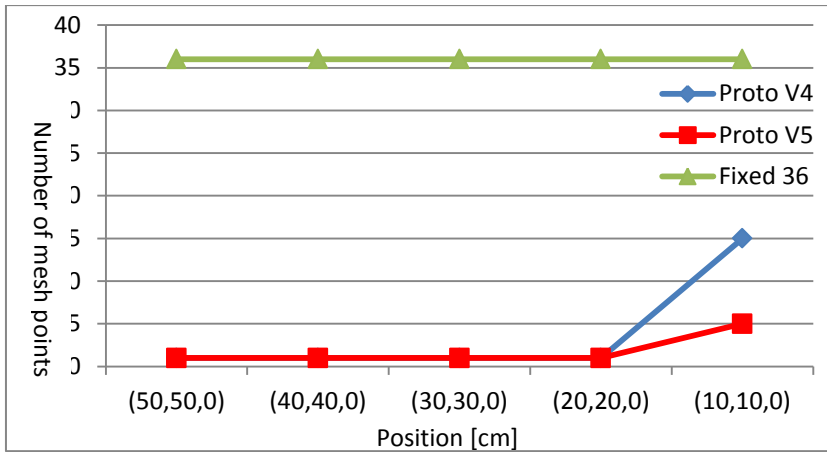
Figure 5-21 Mesh points of V5 vs. V4 for vertex case

The trends observed in the previous graphs show that V5 rate of growth is similar to that of V4 just at a lower level, though this cannot be generalized, since the frontal case shows that both algorithms may reach the same growth on particular instances. Considering the best result was obtained for the vertex case, it seems to indicate the less perpendicular approaches to the source's surfaces obtain better results with the V5 version.

Finally the V5 version prototype is run in the same machine used for testing the previous tests and its execution time is measured. This is shown in the following tables.

Position (X,Y,Z) (cm)	Execution time (ms)		
	V4	V5	Fixed 36
(500,0,0)	8	8	135
(100,0,0)	7	8	135
(50,0,0)	8	8	135
(30,0,0)	32	21	135
(15,0,0)	133	138	135
Average computation time	37.6	36.6	135

Table 5-5-22 Timing comparison: V4 vs. V5 and fixed multi PK simulations for frontal case.

Position (X,Y,Z) (cm)	Execution time (ms)		
	V4	V5	Fixed 36
(50,50,0)	8	8	135
(40,40,0)	8	9	135
(30,30,0)	8	8	135
(20,20,0)	34	19	135
(10,10,0)	91	75	135
Average computation time	29.8	23.8	135

Table 5-5-23 Timing comparison: V4 vs. V5 and fixed multi PK simulations for edge case.

Position (X,Y,Z) (cm)	Execution time (ms)		
	V4	V5	Fixed 36
(50,50,0)	8	8	135
(40,40,0)	7	7	135
(30,30,0)	8	7	135
(20,20,0)	8	8	135
(10,10,0)	78	28	135
Average computation time	21.8	11.6	135

Table 5-5-24 Timing comparison: V4 vs. V5 and fixed multi PK simulations for vertex case.

The results of the time measurements are a reflection of the point mesh count analysis, providing a directly proportional result. It is meaningful to point out that in the best case scenario (vertex approaching line) the V5 is on average over ten times faster than a conventional regular fixed mesh. That said, the difference with the V4 is much less noticeable. For the front case there is barely any advantage (worst case), and for the edge and vertex cases there is an improvement of 20% and 47% respectively.

Considering the real time limitation, both the V4 and V5 are well under the limit and represent valid options for this testing source, with the V5 being slightly quicker and the V4 slightly more accurate.

5.2   Test 2: Real K-40 source

5.2.1   Experiment setup

To complement the computer simulations performed in the previous test with a simulated Cs-137 source, a second test was devised using a real source (K-40) and a real detector.

In this test the dose rate generated by the K-40 in a stack of potassium chloride (KCl) sacks will be measured. This source is chosen as a test case because it is a common cause of false alarms at radiation portals at international border crossings.

In order to setup the test for the VR simulation, the activity of the source, the density and the geometry need to be defined.

The manufacturer of the product guarantees that over 95 % of the material is KCl, therefore we assume the whole mass of 750 kg to be KCl. Using the data mass numbers, isotopic abundance and activity of K-40, the activity of the source is computed to be 12.54 MBq.

To define the geometry of the source, the stack was measured and represented as a 110cm long, 110cm wide and 60cm tall parallelepiped. From this measurement, the volume (110*110*60 = 726 000 cm^3) was inferred and, given the mass stated by the manufacturer, the density was found to be (1.033g/cm3).

The original PK database did not include mixtures of elements so it was updated with a new table for KCl mass attenuation coefficient, where all values are estimated as an average of the existing K and Cl table values. The 1460 keV energy line was considered with a yield of 10.72 %

Background radiation was subtracted from the measurements taken with the survey meter – all the data in the tables are without background, as in this prototype the aim is to evaluate the method.

Similarly to the previous simulated Cs-137 source, a series of measurement positions were established which approached the source from different angles. The following figure illustrates the testing scheme for this source. The vertex line from the previous source test is substituted by the above approach line. This was done because considering this source is not a cube like the Cs-137 it would be more relevant to compare the effect of different area sides of the parallelepiped source.
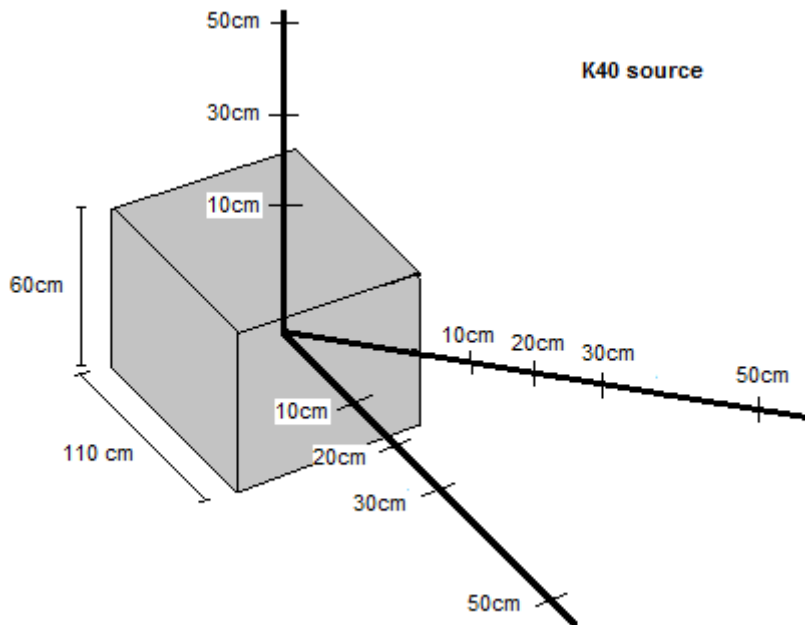
Figure 5-22 Multi PK simulation positions, K-40 source

5.2.2   Real hand held radiation detector (survey meter)

A real survey meter such as the ones this work tries to simulate was used for taking readings of the real radiation source. The chosen

detector is a model Victoreen 451P [87] from the manufacturer Fluke Biomedical. The main relevant characteristics of this portable device are:

- Accuracy: 10% maximum deviation of reading in 90% of the measuring range, which is well in line with the recommendations set by the IAEA for accuracy of handheld survey meters (up to 20% deviation permitted). The accuracy for the remaining 10% of the measuring range, which corresponds to the 0 to 0.5 µSv/h is not specified by the manufacturer. This factor determines which kind of calculation will be used in the simulation in order to achieve an accuracy which is in line with that of the real device.

- Response time: The response time varies depending on the dose range being measured, the higher the dose the lower the response time. For the lowest range (0 to 0.5 µSv/h) the device has a response time of five seconds. In the best case response time lowers up to 1.8 seconds. This determines the method to simulate radiation transport and limits the resolution of the source representation.

- Operating range: The device offers five different measuring ranges to suit sources of different radiating magnitudes, starting from the 0 to 0.5 µSv/h and successively increasing the top limit by one order of magnitude in each range, therefore having a 0 to 50mSv/h limit in its largest range.

- Radiation detected: The device can detect gamma radiation above 25keV. This value is higher than the minimum energy value of the PK energy tables used in the calculation, therefore the PK computation will not incur in extrapolation error. This device also detects beta radiation above 1MeV, which is not relevant to the thesis objectives.

- Warm up time: Real detectors require a warm-up time, this feature is not replicated in the simulation to speed up the work but it could be easily implemented if the training procedure required it so.

5.2.3   V1: Mono PK

As with the previous source (simulated Cs-137) the test will start with comparison of the simplest version of the prototype V1 against the benchmark, the difference being now the benchmark is the real measurements taken with the real detector. This way the results are sustained by two different means which will give more weight to the validity of the results and conclusion. The scheme for the test is the same and can be seen in fig 5-2.

The following table shows the results obtained for first prototype version (mono PK no shielding, no build up) and the Victoreen 451p readings, along with the deviation of the results of the mono PK method with respect to the benchmark data. Only a frontal measurement is taken since there direction of measurement does not affect the V1 version because it ignores the geometry of the source.

Distance (cm)	Equivalent Dose rate in air and deviation (μSv/h)		
	Proto V1 (mono PK)	Deviation %	Vic 451P detector
50	0.21	+133	0.09
30	0.32	+88	0.17
20	0.41	+78	0.23
10	0.55	+49	0.37

Table 5-5-25 Test 2: Dose rate comparison of Prototype V1 vs. V2 ad real detector readings

The results obtained for this case follow the same trend as for the Cs-137 case, but are significantly worse, the reason being the activity of the source is in this case much lower and the volume of the source bigger. The computed dose rates are all well over the detector results.

The deviation is clearly over the required limit for all the instances measured, ranging from 49% up to 133%, meaning the V1 version is not a valid tool for this case by a large margin. It can be appreciated a

trend were the deviation is reduced as the distance is reduced but nevertheless it is never sufficient.

5.2.4 V2: Mono PK with Shielding & Build up

Following the same logic as in the first test, due to the unacceptable degree of accuracy of the V1 prototype, the V2 version is brought forward to try to compensate the limitations of the V1 version. Figure 5-4 illustrates the testing scheme used.

The illustrate the difference between the performance of two versions, the following table shows the results obtained for first prototype version (mono PK no shielding, no build up), alongside the second version and the Victoreen 451p readings, along with the deviation of the results of the mono PK method with respect to the benchmark data.

Distance (cm)	Equivalent Dose rate in air and deviation (µSv/h)				
	Proto V1 (mono PK)	Dev %	Proto V2 (mono PK)	Dev %	Vic 451P detector
50	0.21	+133	0.049	-46	0.09
30	0.32	+88	0.075	-67	0.17
20	0.41	+78	0.095	-59	0.23
10	0.55	+49	0.127	-66	0.37

Table 5-5-26 Test 2: Dose rate comparison of Prototype V1 vs. V2 ad real detector readings

The results obtained by the V2 are the complete opposite to the V1, that is, a systematic underestimation of the dose rate compared to the real readings obtained. Unlike the V1 there is no visible trend in increase or reduction of the deviation depending on the distance.

The deviation of the V2 version is generally better than for the V1 case (all instances but one show a reduction) but it is still way over the limit set in the requirements, with dose rates that halve the values of the real detector.

The following graph shows the dose rate data of the V1, V2 and real detector data. It can be appreciated that the patterns of both prototypes diverge from the real data, hinting that the results will still be unacceptable in other distances measured, therefore this solutions are not valid for the purpose of the work.
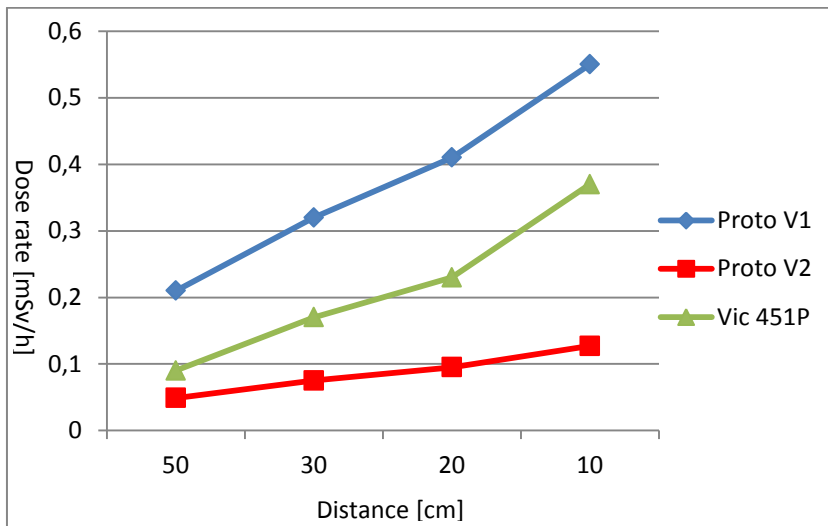
Figure 5-23 Test 2, V1 vs. V2 and benchmark

5.2.5 V3: Multi PK with Shielding and Build up

Having tested the first two versions of the prototype (V1 and V2) with poor results in terms of accuracy, the third (V3) multi point version is now tested. This multi PK code greatly improved the accuracy of the dose rate computation in the first case and it is expected to do so in this case too. As in the case of the Cs-137 source, the computational cost of the version will be tested too.

The results will be shown alongside with the previous V2 results so that the improvement can be clearly appreciated. The following three tables show the equivalent dose rate computed for the different distances set for V2 and V3 version alongside their deviation with respect to the real detector.

161

Distance (cm)	Equivalent Dose rate in air and deviation (µSv/h)				
	Proto V2 (mono PK)	Dev %	Proto V3 (regular multi PK)	Dev %	Vic 451P detector
50	0.049	-46	0.095	+6	0.09
30	0.075	-67	0.187	+10	0.17
20	0.095	-59	0.265	+15	0.23
10	0.127	-66	0.388*	+5	0.37

Table 5-5-27 Test 2: Dose rate comparison of Prototype V2 vs. V3 and real detector readings for frontal line

Distance (cm)	Equivalent Dose rate in air and deviation (µSv/h)				
	Proto V2 (mono PK)	Dev %	Proto V3 (regular multi PK)	Dev %	Vic 451P detector
50	0.194	+7	0.184	+2	0.18
30	0.346	+38	0.29	+16	0.25
10	0.778	+62	0.497*	+4	0.48

Table 5-5-28 Test 2: Dose rate comparison of Prototype V2 vs. V3 and real detector readings for above line

*The limit of sub-sources is reached, results provided for the largest mesh supported by the simulation software. The full mesh should have contained 4096 points.

Distance (cm)	Equivalent Dose rate in air and deviation (µSv/h)				
	Proto V2 (mono PK)	Deviation %	Proto V3 (regular multi PK)	Deviation %	Vic 451P detector
50	0.014	-77	0.042	-30	0.06
30	0.019	-89	0.092	-8	0.1
20	0.024	-79	0.117	-16	0.14
10	0.029	-85	0.185	-3	0.19

Table 5-5-29 Test 2: Dose rate comparison of Prototype V2 vs. V3 and real detector readings for edge line

As seen in the previous point, the mono PK version seems to deviate noticeably with respect to the benchmark figures. The non-cubical

shape of the source seems to generate both positive and negative deviations depending on the approaching side for the mono PK code. The information can be seen visually below in the following graphs.
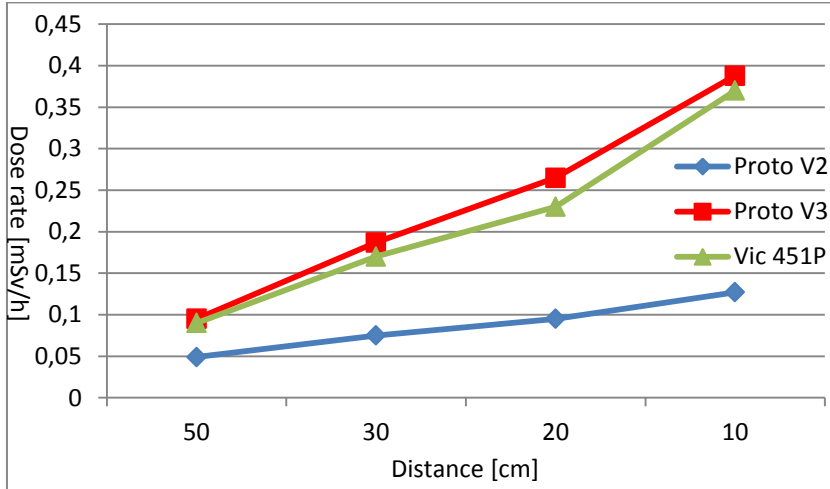
Figure 5-24 Test 2, V3 vs. V2 & benchmark, frontal case
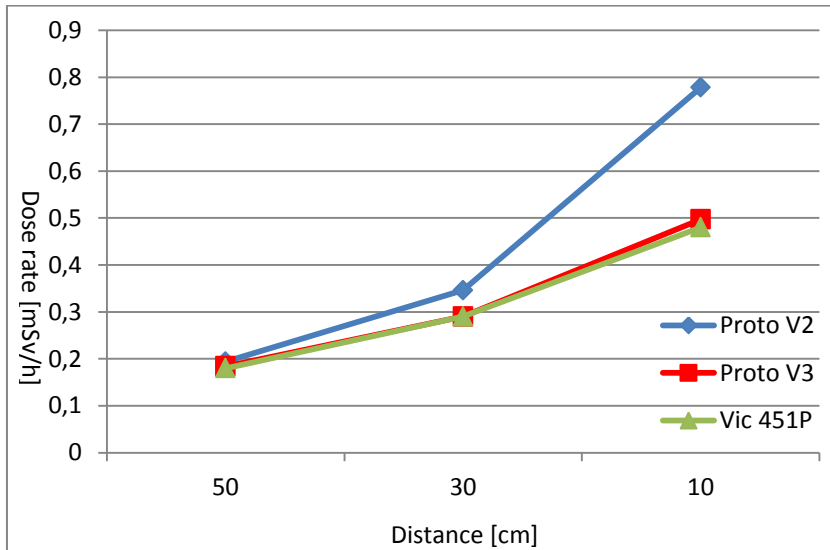
Figure 5-25 Test 2, V3 vs. V2 & benchmark, above case
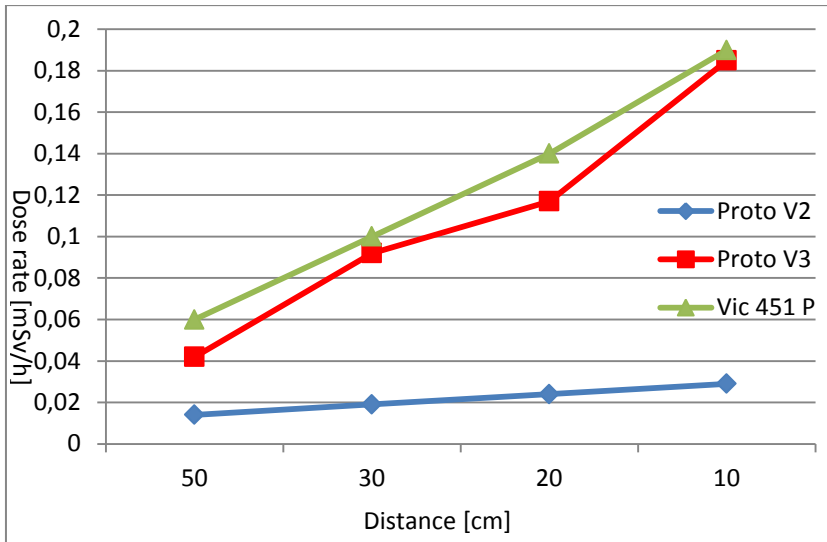
Figure 5-26 Test 2, V3 vs. V2 & benchmark, edge case

Observing the trends shown in the previous graphs, it can be deduced that the mono PK is very sensible to non-cubical source shapes, resulting in large deviations both over and under the benchmark readings. These deviations increase with the proximity to the source. On the contrary the V3 regular multi point kernel follows the results of the benchmark much more accurately, particularly for the frontal and above subcases. The edge case shows a less curvilinear line due to the constant mesh change.

The deviation results differ greatly for the mono PK and multi PK codes. In this test the mono PK fails to reach the accuracy limits set for the great majority of cases. Particularly the edge case which represents the worst case scenario for the mono PK (because the self-shielding distance is at its maximum) offers a result well under the benchmark.

On the contrary the multi PK code follows the benchmark data much more closely with average deviations well within the established limit for all three approaching lines. There is no clear trend in increase or decrease of deviation in the multi PK case due to the different point

meshes the algorithm has chosen for the different distances, but considering the compliance with the limits the calibration can be considered adequate.

The worst individual result (-30% deviation) for the furthest away point in the edge case is slightly over the limits, considering the dose rate at this point is lower than the background radiation generated dose it does not compromise the validity of the result.

The next step in the evaluation of performance of the V3 prototype for this test case is to analyse the computational cost of the case. As in the previous case the number of sub source points of the mesh will be evaluated for the frontal case.

Distance (cm)	Number of points in mesh		
	Proto V2 (mono PK)	Proto V3 (multi PK)	Fixed (multi PK)
50	1	8	4096
30	1	64	4096
20	1	512	4096
10	1	4096	4096
Average mesh points	1	1170	4096

Table 5-5-30 Computational cost comparison between mono PK, variable PK and fixed multi PK for K-40 source case.

For this case a fixed regular mesh of 4096 points has been used to illustrate the computational cost of a non-variable code which matches the maximum resolution reached by the V3 variable code in this experiment.

The results show a rapid growth in number of points for the V3 multi PK algorithm, to better study this trend, the data is shown on graphical form in the following figure.
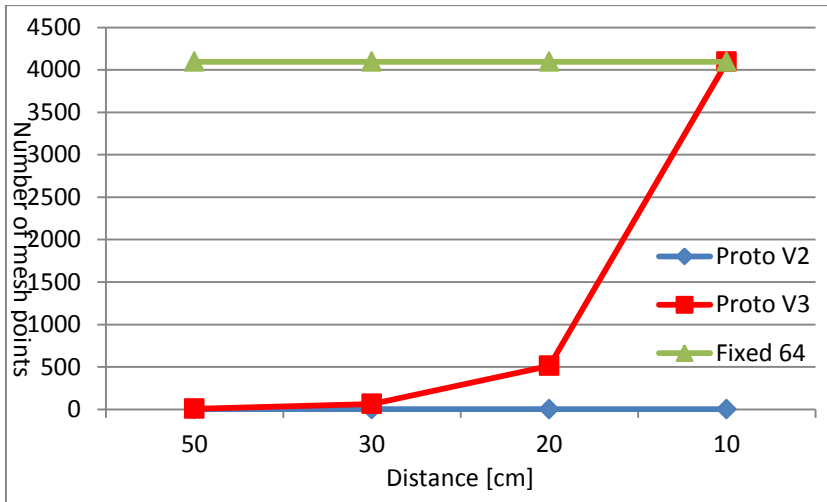
It can be appreciated from the graph that the mesh density grows exponentially, exactly as seen in the previous testing case. Albeit this time given the similar distances but larger source volume, a larger number of mesh points is generated by the V3 algorithm. Once again it is proven that the variable method saves a lot of computational effort compared to fixed mesh of the maximum resolution when far from the source.

The question which arises is if this reduction is enough to comply with the speed limitations imposed by the VR paradigm. In order to answer this question the execution time of the simulation for the frontal case is recorded. The next table shows the results obtained.

To be noted that due to the limitations of the hardware used, it was not possible to do the simulation of the necessary amount of sub sources (4096) for the cases marked with a '*' on the table, therefore this value is extrapolated using as a base the previous step (512) execution time.

Distance (cm)	Execution time (ms)		
	Proto V2 (mono PK)	Proto V3 (multi PK)	Fixed 4096 multi PK
50	4	18	10784*
30	4	158	10784*
20	5	1348	10784*
10	4	10784*	10784*
Average computation time	4.25	3077	10784*

Table 5-5-31 Timing comparison between mono PK, variable PK and fixed multi PK simulations for K-40 Source case

The results obtained show that fixed mesh of 4096 points will not meet the time limitations imposed. On the opposite end mono PK V2 version is the quickest solution but as previously proved it does not meet the accuracy requirements. The variable algorithm developed allows for a valid execution time in most situations tested but at the closest distance it falters largely, requiring 10s to perform the dose rate computation while the real detector might take as little as 1.8s.

5.2.6   V4: Multi PK non regular

As in the previous section the testing consists of two parts, first the accuracy of the V4 algorithm will be compared against the previous V3 version and a benchmark and secondly the computational cost.

The same testing distances and approaching trajectories as in the previous K-40 testing are used for this test. See figure 5-12 for a reminder of the testing positions. Also the same benchmark results will be used, these are the readings obtained by a real hand-held gamma radiation detector.

The following tables show the computed equivalent dose rate obtained for this test alongside the deviation to the MCNP benchmark.

Distance (cm)	Equivalent Dose rate in air and deviation (μSv/h)				
	Proto V3 (regular)	Deviation %	Proto V4 (non-regular)	Deviation %	Vic 451P detector
50	0.095	+6	0.095	+5	0.09
30	0.187	+10	0.185	+9	0.17
20	0.265	+15	0.254	+9	0.23
10	0.388*	+5	0.367	-1	0.37

Table 5-5-32 Dose rate of Prototype V3, V4 and real detector readings for frontal line.

Distance (cm)	Equivalent Dose rate in air and deviation (μSv/h)				
	Proto V3 (regular)	Deviation %	Proto V4 (regular)	Deviation %	Vic 451P detector
50	0.184	+2	0.184	+2	0.18
30	0.29	+16	0.289	+13	0.25
10	0.497*	+4	0.484	+1	0.48

Table 5-5-33 Dose rate of Prototype V3, V4 and real detector readings for above line.

*The limit of sub-sources is reached, results provided for the largest mesh supported by the simulation software. The full mesh should have contained 4096 points.

Distance (cm)	Equivalent Dose rate in air and deviation (μSv/h)				
	Proto V3	Deviation %	Proto V4	Deviation %	Vic 451P detector
50	0.042	-30	0.042	-30	0.06
30	0.092	-8	0.085	-15	0.1
20	0.117	-16	0.109	-22	0.14
10	0.185	-3	0.166	-13	0.19

Table 5-5-34 Dose rate of Prototype V3, V4 and real detector readings for edge line.

The objective with the new V4 non-regular method was to remain within the accuracy limits set for the task, it was expected that reducing the number of sources would worsen the accuracy of the computation with respect to the V3 version.

The results show that actually in many instances, the accuracy of the dose rate computation was improved by the V4 version despite working with a smaller number of points to represent the source. The improvement appears on the frontal and above approaching lines, while the edge line suffers a small worsening.

Taking a look at the average deviations from the previous tables, it can be seen that the accuracy has not been compromised to a degree that makes the new V4 algorithm unfit for the requirements set. In fact an improvement has been noted for the front and above cases and only in the edge case a small (5.7%) extra deviation occurs. This is mainly due to the furthest away instance which is anyway the same for both V3 and V4 which at that point still run a mono PK representation of the source. A specific fine tuning of the solid angle threshold could alleviate this.

In order to better examine the meaning of the dose rate computations obtained, and spot trends which might be hard to visualize in the tabulated data, the following figures show the information in graphical form.
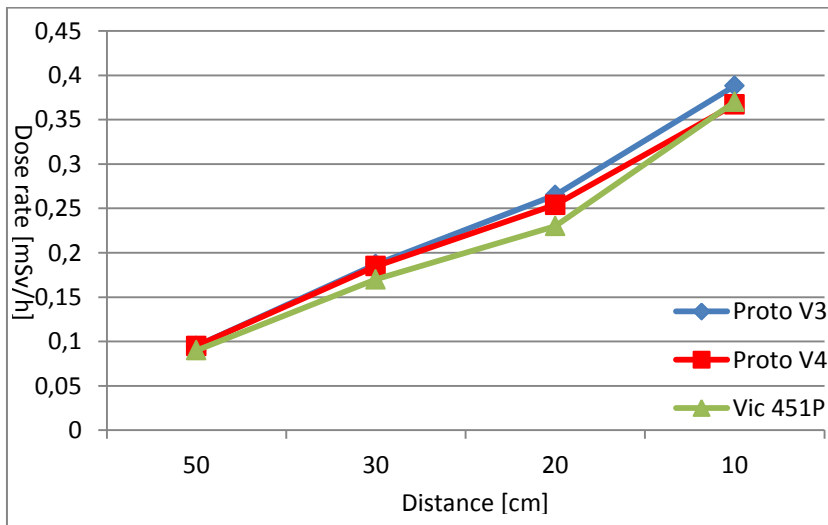
Figure 5-28 Dose rate of V3, V4 & real detector, frontal case
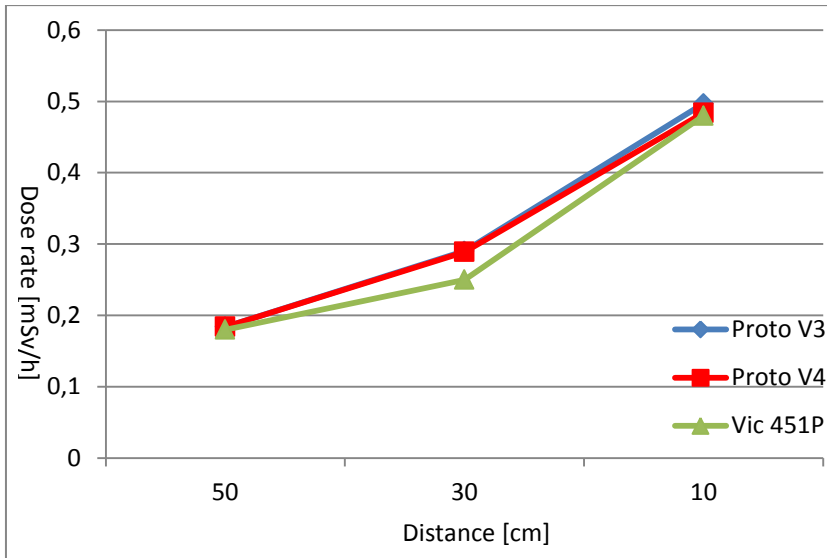
Figure 5-29 Dose rate of V3, V4 & real detector, above case
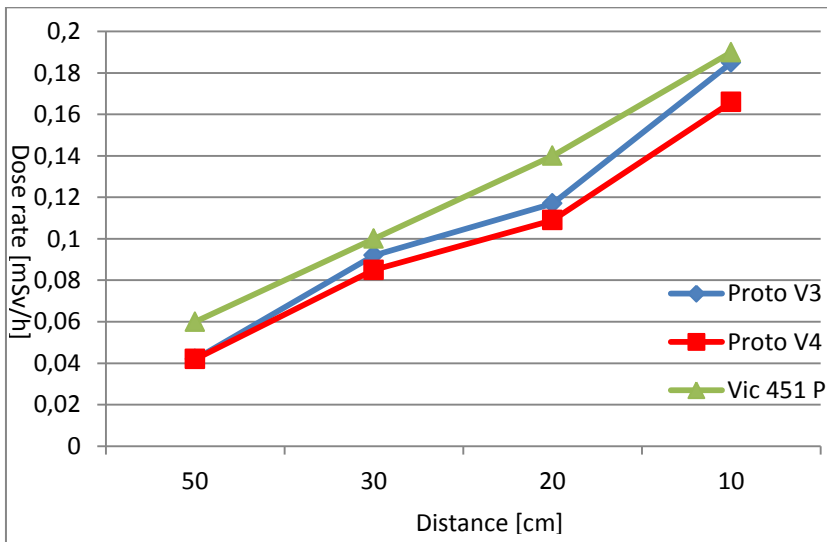
Figure 5-30 Dose rate of V3, V4 & real detector, edge case

From the previous graph it can be deduced that the new V4 follows the same trend as the V3, the simulation follows the real readings closely and distance or approaching line do not seem to be a factor in

the results. In terms of accuracy it represents a minor improvement for the frontal and above cases and tends to underestimate the dose rate for the edge case slightly.

Now that it has been established that from the accuracy point of view, V4 is still an acceptable choice it follows that the computational cost of the new algorithm is analysed. The same procedures as before are used. The following tables show the point mesh density generated by the V4 algorithm for each testing instance.

Distance (cm)	Number of points in mesh		
	Proto V3	Proto V4	Fixed (multi PK)
50	8	8	4096
30	64	36	4096
20	512	64	4096
10	4096	120	4096
Average mesh points	1170	57	4096

Table 5-5-35 Mesh point of V3, V4 and fixed multi PK for K-40 source, front case.

Distance (cm)	Number of points in mesh		
	Proto V3	Proto V4	Fixed (multi PK)
50	64	36	4096
30	64	36	4096
10	4096	148	4096
Average mesh points	1408	73.3	4096

Table 5-5-36 Mesh point of V3, V4 and fixed multi PK for K-40 source, above case.

Distance (cm)	Number of points in mesh		
	Proto V3	Proto V4	Fixed (multi PK)
50	8	8	512
30	64	22	512
20	64	22	512
10	512	50	512
Average mesh points	162	25.5	512

Table 5-5-37 Mesh point of V3, V4 and fixed multi PK for K-40 source, edge case.

It can be appreciated that the V4 represents a very noticeable improvement with respect to the V3 in all the approaching lines tested, reducing the number of point by an order of magnitude in the closest distance instances. For the front and edge cases the first instance obtains the same result with both algorithms due to the fact the first level of mesh division is always one to eight sub-sources in any case. The edge case shows a lower growth than the front and above cases, the reason for this behaviour is that an approach from the edge line keeps more areas of the volume further away than a perpendicular line approach (frontal or above), these represent the worst case scenario for the V3 algorithm (and any other solid angle triggered method).

To provide further insight into the computational cost evolution of this algorithm, the information from the previous tables is converted into graphs in order to better distinguish growth trends. The following three figures show the graphs for these three cases of the K-40 source test.
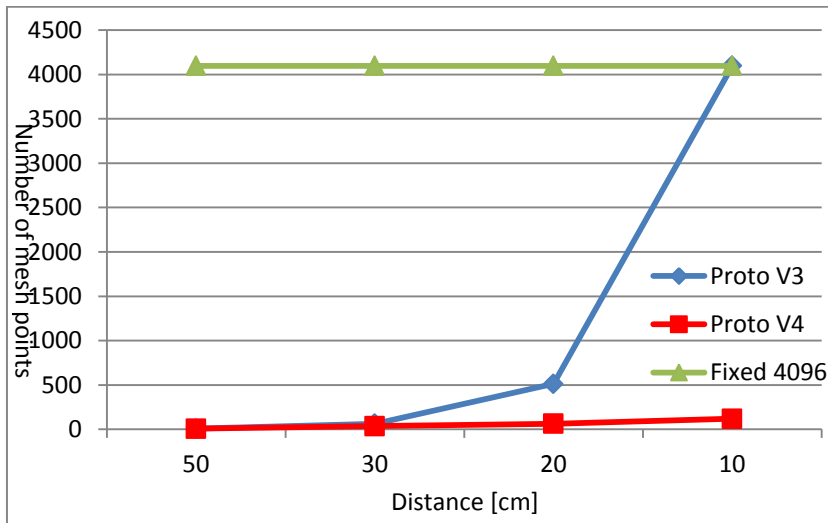
Figure 5-31 Mesh points of V4 vs. V3 & fixed mesh, frontal case
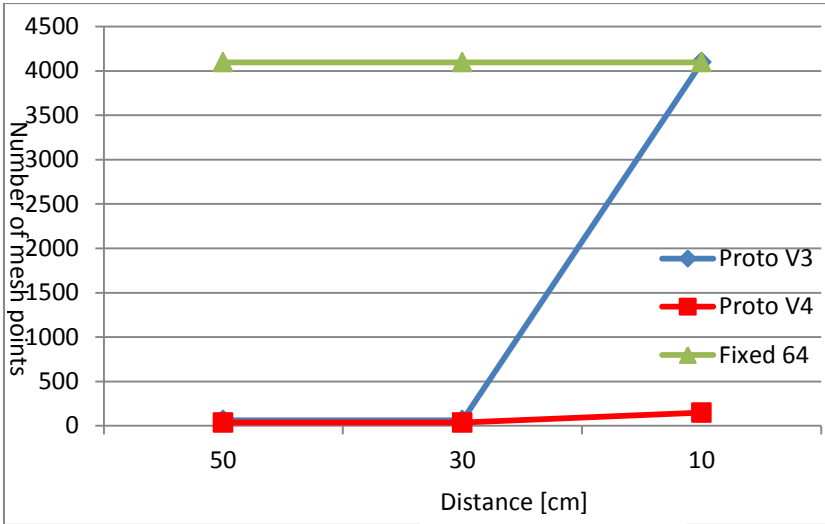
Figure 5-32 Mesh points of V4 vs. V3 & fixed mesh, above case
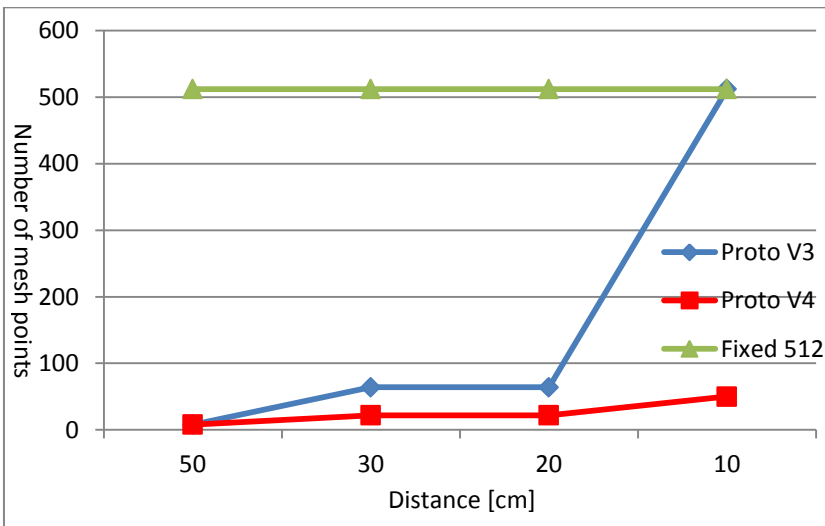
Figure 5-33 Mesh points of V4 vs. V3 & fixed mesh, edge case

In the previous graphs it can be noted that the curves of the V4 algorithm represent an almost linear growth, providing a large reduction in terms of mesh points compared to the exponential growth of V3 curves. The approaching line does not seem to have a noticeable effect on the relative behaviour of the V4 with respect to

V3, the difference between V3 and V4 remains similar in the distinct approaches.

Finally to provide the reader with an idea of how this method translates to real life, the implemented simulation is run and its execution time recorded for all the previous instances as it has been done with the V3 testing.

The following graphs show the execution times for the three approaching line cases for the V4 version (non-regular multi PK) of the algorithm alongside its predeceasing algorithm and the fixed mesh (4096 points) method.

Distance (cm)	Execution time (ms)		
	Proto V3	Proto V4	Fixed 4096 multi PK
50	18	18	10784*
30	158	84	10784*
20	1348	166	10784*
10	10784*	358	10784*
Average computation time	3077	156.5	10784*

Table 5-5-38 Execution time of V3 vs V4 for K-40 Source, frontal case.

Distance (cm)	Execution time (ms)		
	Proto V3	Proto V4	Fixed 4096 multi PK
50	158	86	10784*
30	152	84	10784*
10	10784*	388	10784*
Average computation time	3698*	186	10784*

Table 5-5-39 Execution time of V3 vs V4 for K-40 Source, above case.

Distance (cm)	Execution time (ms)		
	Proto V3	Proto V4	Fixed 512 multi PK
50	18	18	1348
30	156	50	1348
20	158	52	1348
10	1356	122	1348
Average computation time	422	60.5	1348

Table 5-5-40 Execution time of V3 vs V4 for K-40 Source, edge case.

*The limitations of the machine and hardware used did not allow for the simulation of the necessary amount of sub sources (4096), therefore this value is extrapolated using as a base the previous step (512) execution time.

The execution time results confirm the expected gains announced by the previous analysis of the point mesh densities. On average the frontal and above cases execution times are reduced by a factor of 20, the edge case improves almost tenfold.

There is a massive execution time reduction for particular instances of the frontal and above cases, the closest distance instance shows an improvement by a factor of 30. The edge case also shows a large improvement with an execution time over 10 times quicker than the previous V3 algorithm. These instances are important because it is where V3 fails to meet the timing limitations specified in the requirements, therefore making V4 a necessary and valid improvement.

These results confirm that the target of V4 which was to obtain a reduction of computational complexity without compromising the accuracy, has been achieved.

5.2.7   V5: Multi PK non regular KD

As with previous versions of the prototype, a test is performed on this new version of the prototype. To be consistent with the work done, the exact same testing procedure is performed.

Therefore in first place the dose rate computation for this case is evaluated. The following tables show these results alongside the deviation to the benchmark detector readings.

Distance (cm)	Equivalent Dose rate in air and deviation (µSv/h)				
	Proto V4	Deviation %	Proto V5	Deviation %	Vic 451P detector
50	0.095	+5	0.095	+6	0.09
30	0.185	+9	0.187	+10	0.17
20	0.254	+9	0.259	+13	0.23
10	0.367	-1	0.372	+1	0.37

Table 5-5-41 Dose rate of Prototype V4, V5 and real detector readings for frontal line.

Distance (cm)	Equivalent Dose rate in air and deviation (µSv/h)				
	Proto V4	Deviation %	Proto V5	Deviation %	Vic 451P detector
50	0.184	+2	0.179	-1	0.18
30	0.289	+13	0.271	+8	0.25
10	0.484	+1	0.459	-4	0.48

Table 5-5-42 Dose rate of Prototype V4, V5 and real detector readings for above line.

Distance (cm)	Equivalent Dose rate in air and deviation (µSv/h)				
	Proto V4	Deviation %	Proto V5	Deviation %	Vic 451P detector
50	0.042	-30	0.038	-37	0.06
30	0.085	-15	0.078	-22	0.1
20	0.109	-22	0.106	-24	0.14
10	0.166	-13	0.165	-13	0.19

Table 5-5-43 Dose rate of Prototype V4, V5 and real detector readings for edge line.

The results indicate that the V5 is maybe more sensible to the area of the sides of the source volume than the V4, since it provides higher dose rate values than the V4 in the frontal test (smaller surface area) and lower in the above test (larger surface area). With respect to the benchmark, the V5 provides less deviation than the V4 in particular cases, generally at closer distances but there are some exceptions so a general rule cannot be inferred.

The average deviation of the V5 increases slightly with respect to the V4. 1.5% for the frontal case and 4% for the edge case, for the above case it is reduced by 1%. The highest average deviation (24%) is just under the 25% limit established; therefore it is a valid solution in general. There is one instance which is above the limit, (37%) but given that for such low doses the real detector does not guarantee the accuracy limit itself it does not compromise the validity of the software tool.

To try to discern the behaviour of the V5 prototype in this test case the previous dose rate data is converted to a graphical format shown in the following figures.
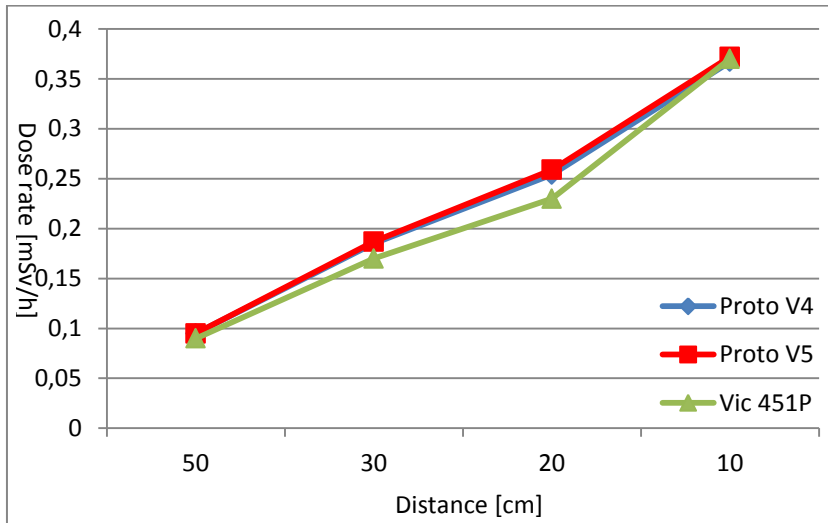
Figure 5-34 Dose rate V4, V5 & real detector, frontal case
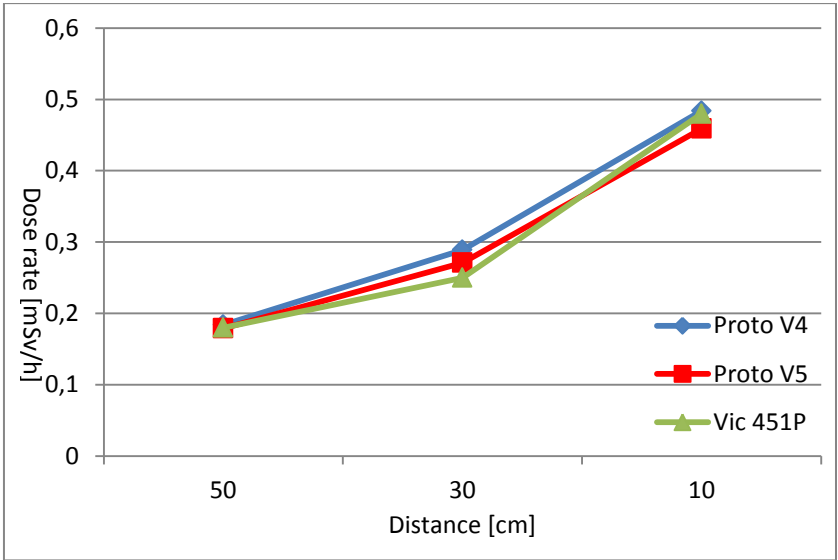
Figure 5-35 Dose rate V4, V5 & real detector, above case
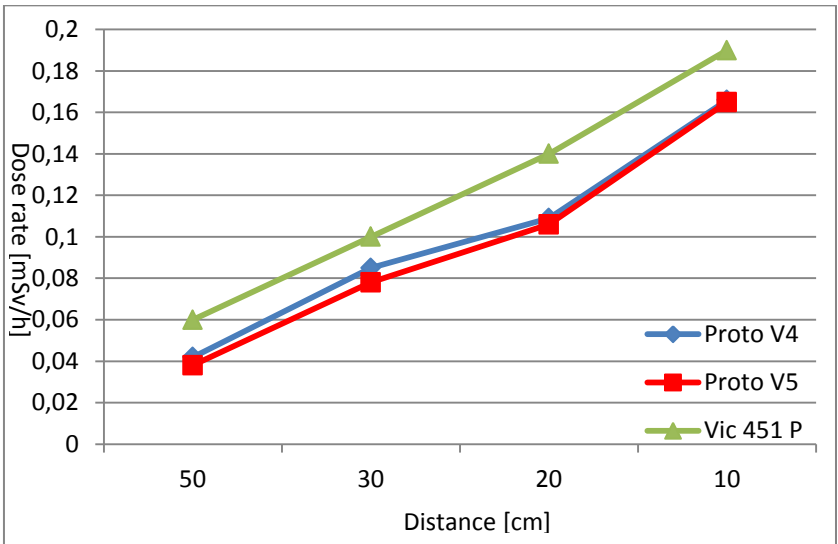
Figure 5-36 Dose rate V4, V5 & real detector, edge case

From the graphs it can be deduced that the V5 has a similar behaviour to the V4 version, in terms of deviation with respect to the benchmark, both underestimate or overestimate in the same cases,

with the individual exception of the closest point in the above testing line where the V4 result overestimates and the V5 underestimates.

The V5 (like the V4) tends to converge to the results of the benchmark as distance is reduced (and consequently number of points in the mesh increased). It is necessary though to quantify the dose rate performance in order to consider the V5 a valid option, at least in terms of accuracy.

The next step in the evaluation of the version is to analyse the computational cost of the algorithm. In first place the number of sub source points generated by this method will be analysed. The following tables show the mesh points generated in each instance of the testing for all three approaching lines compared to the previous V4 version and to a regular mesh.

Distance (cm)	Number of points in mesh		
	Proto V4	Proto V5	Fixed (multi PK)
50	8	6	512
30	36	18	512
20	64	26	512
10	120	52	512
Average mesh points	57	25.5	512

Table 5-5-44 Number of points for V4, V5 and fixed multi PK for K-40 source, front case.

Distance (cm)	Number of points in mesh		
	Proto V4	Proto V5	Fixed (multi PK)
50	36	12	512
30	36	20	512
10	148	60	512
Average mesh points	73.3	30.6	512

Table 5-5-45 Number of points for V4, V5 and fixed multi PK for K-40 source, above case.

Distance (cm)	Number of points in mesh		
	Proto V4	Proto V5	Fixed (multi PK)
50	8	4	512
30	22	8	512
20	22	11	512
10	50	25	512
Average mesh points	25.5	12	512

Table 5-5-46 Number of points for V4, V5 and fixed multi PK for K-40 source, edge case.

The results obtained show that on average the new V5 (KD tree based division method) approximately halves the computational cost of the V4 prototype (Octree based division method) for this test case. The line of approach does not seem to be a relevant factor in the mesh density with all three cases showing similar improvement values with respect to V4. The largest reduction corresponds to the above case which is down by 58% followed by the frontal line (55%) and finally the edge case (53%).

With respect to the fixed mesh which represents the highest level of density that the non-regular algorithms reach at their individual maximums, the reduction is almost 20 times less points per mesh even for the less convenient case for V5. In the best case scenario (edge) the new V5 version uses a mesh with 40 times less points than the fixed mesh version.

To better appreciate the rate of growth of the new algorithm (V5) with respect to the previous version (V4) and the fixed mesh, the point mesh data is shown in graphical form in the following figures, containing one line graph for each of the three approaching lines tested.
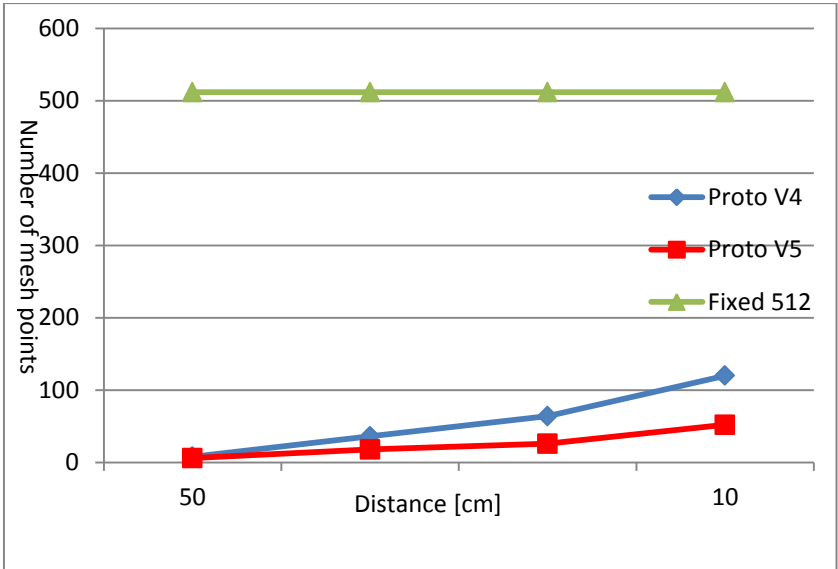
Figure 5-37 Mesh points of V5 vs. V4 & fixed mesh, frontal case
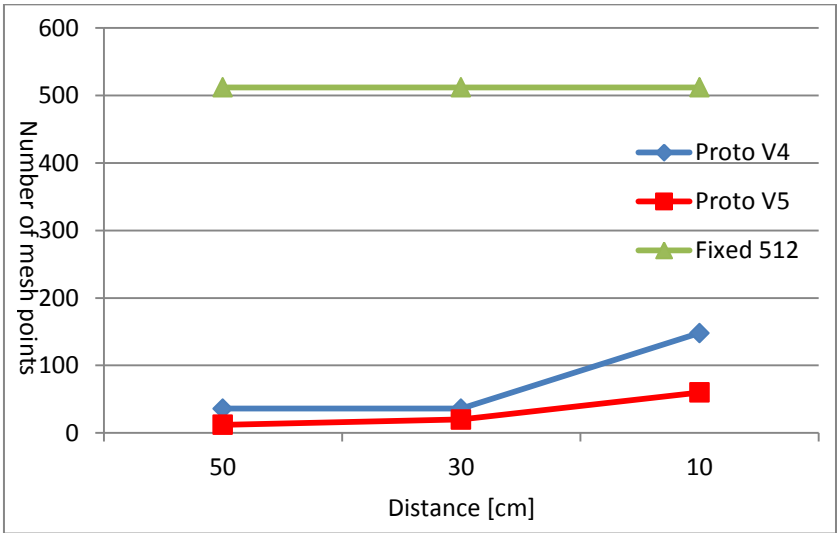
Figure 5-38 Mesh points of V5 vs. V4 & fixed mesh, above case

181
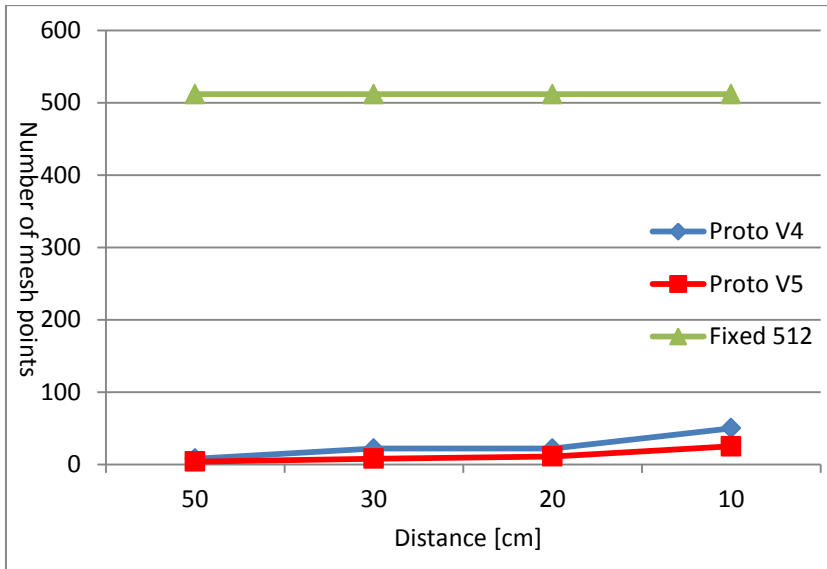
Figure 5-39 Mesh points of V5 vs. V4 & fixed mesh, edge case

A lesser steepness in the growth rate of the V5 algorithm can be appreciated. This trend is consistent throughout the three approach lines and all the individual instances, growing substantially as the distance to the source decreases.

In order to discover if this theoretical advantage translates into a practical advantage, the prototype is run on the testing hardware used for the previous test and the execution time for each instance has been recorded and shown in the following tables alongside the previously recorded execution time of a 512 fixed mesh point (just a reminder to the reader: the magnitude of the fixed mesh density is chosen to equal to the maximum density the tested variable methods reach in the densest part of the volume they generate). Also it is important to notice the fact that for the real hand held radiation detector the minimum acquisition time is 1.8s which can be set as a practical limit for the simulation computation (any simulation which takes longer does not meet the real time requirement of VR based applications).

182

Distance (cm)	Execution time (ms)		
	Proto V4	Proto V5	Fixed 512 multi PK
50	18	15	1348
30	84	47	1348
20	166	73	1348
10	358	147	1348
Average computation time	156.5	70.5	1348

Table 5-5-47 Execution time of V4 vs V5 for K-40 Source, frontal case.

Distance (cm)	Execution time (ms)		
	Proto V4	Proto V5	Fixed 512 multi PK
50	86	34	1348
30	84	56	1348
10	388	171	1348
Average computation time	186	87	1348

Table 5-5-48 Execution time of V4 vs V5 for K-40 Source, above case.

Distance (cm)	Execution time (ms)		
	Proto V4	Proto V5	Fixed 512 multi PK
50	18	15	1348
30	50	26	1348
20	52	34	1348
10	122	71	1348
Average computation time	60.5	36.5	1348

Table 5-5-49 Execution time of V4 vs V5 for K-40 Source, edge case.

The execution times shown in the previous tables show that the reduction seen in the mesh point count converts into a proportional reduction in execution time. Making the new V5 algorithm the quickest valid version of all the developed until now, and an execution time improvement with respect ordinary regular meshes used by existing software of approximately 20 times. The V5 algorithm has met both the accuracy and real time requirements set.

5.3   V6 Prototype: Multi PK + Trimming post process

The aim of this last version of the prototype was to implement a method to deal with source volumes which are not parallelepipeds, because although it is a very common shape, it is not the only one. Therefore a test has been devised where a spherical and cylindrical source are used, which are geometries which can also frequently occur in NS&S.

5.3.1   Limitations of the parallelepiped representation

The first step is to prove that actually the previous methods which represent sources as parallelepipeds are not valid for other kinds of shapes, in this case a sphere of 10cm radius of the same Cs-137 dissolved in water. The test performed will follow the same strategy as the previous, computing the dose rate at different distances from the source as shown by the following figure.
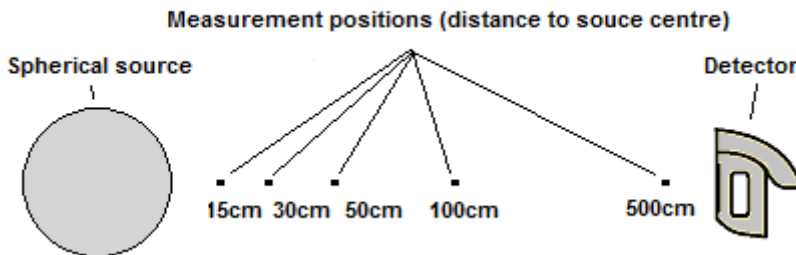
Figure 5-40 Test scheme for spherical source

The following table shows the results produced by applying the V4 (non-regular multi PK) method to a sphere with a radius of 10cm and the same characteristics as the 20cm side cube used previously.

Distance (cm)	Equivalent Dose rate in air Sphere (mSv/h)			
	V4 (frontal)	V4 (edge)	V4 (vertex)	MCNP
500	0.115	0.115	0.116	0.125
100	2.89	2.89	2.92	3.15
50	11.55	11.58	11.62	12.7
30	34.7	34.9	35.13	35.4
15	141.8	174.5	276	143

Table 5-5-50 Dose rate of sphere measured at front, vertex and edge positions.

The results show that although the algorithm behaves well for the frontal position computations it massively overestimates the dose rate at short distances from the edge and vertex approaching lines.
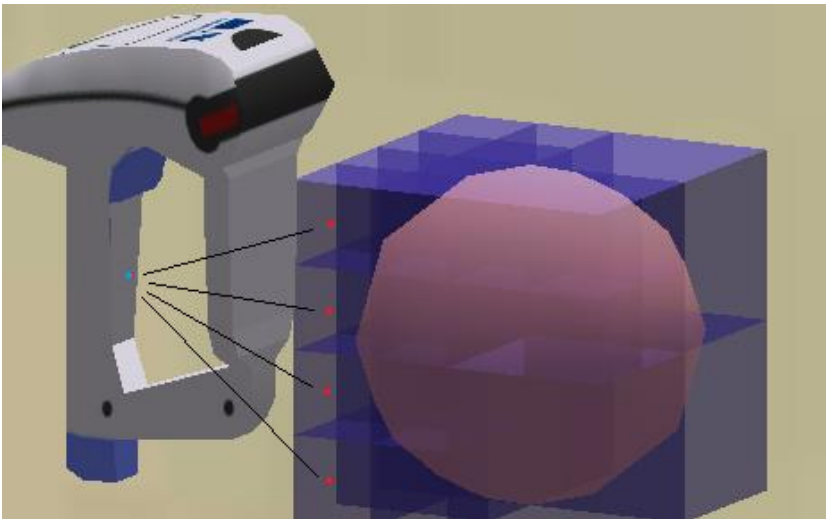
Figure 5-41 Overestimation of sphere as a parallelepiped

This is due to two factors; first the position of the detector is actually "inside" the parallelepiped source generated for the closest edge and vertex cases shortening the distance between the sub-source centres and detection point. Secondly the points outside the sphere are not

affected by the self-attenuation of the water inside the source, increasing the dose rate further. The previous figure illustrates this situation. The red points in the previous figure mark some of the points of the kernel which have been placed outside the sphere volume, reducing the distance to the detector and not undergoing any attenuation due to the matter in the sphere.

This problem leads to an overestimations of 24% (which would be on the limit but tolerable) and 95% (unacceptable for the purpose of this work) for the edge and case closest cases respectively. Furthermore the correct behaviour for a spherical source would be that the position would not affect the dose rate as long as the distance to the detector is the same, which is clearly not the case.

5.3.2   Post-processing of the source representation

Having proved that in order to deal with multi-form sources a new method is needed, the proposed solution is based on a post-processing method based on finite element boundary representation which eliminates the generated sub-sources which fall outside the original source volume and a redistribution of the activity.

The solution tried is to combine the V4 (non-regular multi PK) with the trimming post process. The dose rate results produced by this combination can be seen in the following table.

Distance (cm)	Equivalent Dose rate in air Sphere (mSv/h)		
	V4 (frontal)	V6 (frontal + post process)	MCNP
500	0.115	0.115	0.125
100	2.89	2.89	3.15
50	11.55	11.55	12.7
30	34.7	34.7	35.4
15	141.8	102.6	141

Table 5-5-51 Comparison of V4 vs. V4+post process & MCNP, front case

The result shows that there is no difference in the computations corresponding to distances form 30cm and further. This is due to the fact that the trimming post process does not apply to those situations, as either there is only one single source whose centre point matches the original source's centre, or the generated sub sources centres are all within the original volume of the source. Only at the closest distance there are sub-sources generated whose centre point is outside the original sphere volume and therefore eliminated.

The result for the closest instance is 28% under the benchmark therefore this solution is not valid from the accuracy point of view. This underestimation of the dose rate can be explained by the fact that applying the trimming post process to the model generated by the non-regular division algorithm leads to "shifting the activity of the source backwards". This can be seen in the following figure.

Figure 5-42 Dose rate underestimation due to "activity shifting"

It can be seen in this figure that part of the volume of the sphere in the front (closer to the detector) is disregarded and a large part of void behind the source is counted as part of source volume (purple volume). These large sub-sources on the back have their centre inside the sphere but close to the surface, therefore a large part of the sphere's activity is distributed towards the outside.

5.3.3 Recalibration of the algorithm

To try to alleviate this problem a possible solution is to increase the resolution of the point mesh by lowering the threshold solid angle, this could reduce the areas of void which is accounted as source volume at the back of the source. In order to increase the resolution, the solid angle threshold (currently 60º) will be reduced. Increasing the resolution slows down the process which could be a problem from the real-time performance point of view, but the trimming process reduces the number of points so it partially counteracts this effect.

The algorithm will be re-calibrated and re-tested, altering the solid angle threshold in steps of equal magnitude (5º) in order to obtain a behaviour that suits the requirements; the testing is stopped at the 20º case due to the fact that with that angle the 15cm case results in an execution time (3.7s) unacceptable for the requirements set. The following table contains the dose rate results for the frontal case.

Distance (cm)	Equivalent Dose rate in air Sphere (mSv/h)				
	60º	55º	50º	45º	MCNP
500	0.115	0.115	0.115	0.115	0.125
100	2.89	2.89	2.89	2.89	3.15
50	11.55	11.55	11.55	11.55	12.7
30	34.7	34.7	34.7	34.7	35.4
15	102.6	102.6	102.6	132.9	143
Distance (cm)	Equivalent Dose rate in air Sphere (mSv/h)				
	40º	35º	30º	25º	20º	MCNP
500	0.115	0.115	0.115	0.115	0.115	0.125
100	2.89	2.89	2.89	2.89	2.89	3.15
50	11.55	12.3	12.3	12.3	12.3	12.7
30	34.7	28.98	28.98	34.2	32.5	35.4
15	132.9	128.4	130.8	135.3	138.3	143

Table 5-5-52 V4+post process with different threshold angles compared to MCNP for the frontal line case.

The result show that there is no perfect setup which obtains the best result for all distances and therefore a choice has to be made which satisfies both requirements, aiming at a valid accuracy and speed.

In order to define which threshold angles are valid from the dose rate accuracy point of view, the dose rate deviation to the MCNP benchmark is computed for every case and shown in the following table.

Distance (cm)	Deviation to MCNP benchmark (%)								
	60º	55º	50º	45º	40º	35º	30º	25º	20º
500	8	8	8	8	8	8	8	8	8
100	8	8	8	8	8	8	8	8	8
50	9	9	9	9	9	3	3	3	3
30	2	2	2	2	2	18	18	3	8
15	28	28	28	7	7	10	9	5	3

Table 5-5-53 V4+post process with different threshold angles deviation to MCNP for the frontal line case.

The results show that the first three angles provide an insufficient accuracy for the shortest distance case and therefore are discarded, the trends are not unmistakably clear and although reducing the angle reduces the deviation in many cases, it is not a general always valid rule. Two clear exceptions can be seen in the 35º and 30º cases for the 30cm instance which raises the deviation from the previous (at 40ª) 2% up to 18%.

The second requirement states that the time per dose rate computation must not exceed the reading time of a real detector, for the detector tested this limit is 1.5s. Therefore the execution time of the different options is measured.

The following table shows these values generated by the V6 version of the prototype.

Distance (cm)	Execution time of V6 (ms)								
	60º	55º	50º	45º	40º	35º	30º	25º	20º
500	8	8	8	8	8	8	8	8	8
100	9	8	8	8	8	8	9	8	8
50	8	8	9	8	8	33	32	34	32
30	44	42	42	44	42	98	95	158	238
15	172	178	176	241	240	497	699	1846	3704

Table 5-5-54 Execution time of V5 prototype with different solid angle threshold for frontal case.

The data from the previous table shows that the last two options (25º and 20º) provide results for the shortest distance instance which are not acceptable from the real-time requirement point of view.

This leaves as valid options the angles ranging from 45º down to 30º. Given the fact that the shorter angles do not provide a clear advantage in terms of accuracy, in fact they might worse the result at certain differences, it seems that the best possible choice is the quickest (highest angle) from the valid ones that is the 40 º threshold.

5.3.4   Testing simulated Cs-137 spherical source with recalibrated algorithm

Performing the simulation for all three approaching lines with the algorithm setup with a 40º degree solid angle provides the following results shown in the next table.

Distance (cm)	Equivalent Dose rate in air Sphere (mSv/h)			
	V6 (frontal)	V6 (edge)	V6 (vertex)	MCNP
500	0.115	0.115	0.116	0.125
100	2.89	2.89	2.92	3.15
50	11.55	11.58	12.33	12.7
30	34.7	34.9	31.69	35.4
15	132.9	134.9	134.8	143

Table 5-5-55 Dose rate of sphere measured at front, vertex and edge positions with 40ª threshold.

The results obtained with the newly calibrated V6 version solve the problems generated by the 60º calibration simulation. An increase in the accuracy of the algorithm can be seen and the behaviour of all three approaching lines is very similar, as it should be for a spherical source.

To assess the validity of the dose rate results obtained, the deviation of the V6 simulation results to the MCNP benchmark is calculated and shown on the following table.

Distance (cm)	Deviation to MCNP benchmark %			
	V6 (frontal)	V6 (edge)	V6 (vertex)	MCNP
500	8	8	7	0.125
100	8	8	7	3.15
50	9	9	3	12.7
30	2	1	10	35.4
15	7	6	6	143

Table 5-5-56 Deviation of sphere measured at front, vertex and edge positions with 40ª threshold.

The deviation results from the previous table show that the accuracy of the recalibrated V6 prototype is compliant with the requirements for all instances tested and by quite a significant margin. The previous calibration "shifting" of the activity of the source problem has been successfully corrected.

This can be visually seen in the following figure, showing the detector at the shortest distance instance for the frontal case. Thanks to the newly calibrated algorithm the large areas of void that the representation of the source had misrepresented in fig 5-42 have been greatly reduced and the shape of the new virtual source (marked in blue) is much more similar to the original sphere (marked in pink).
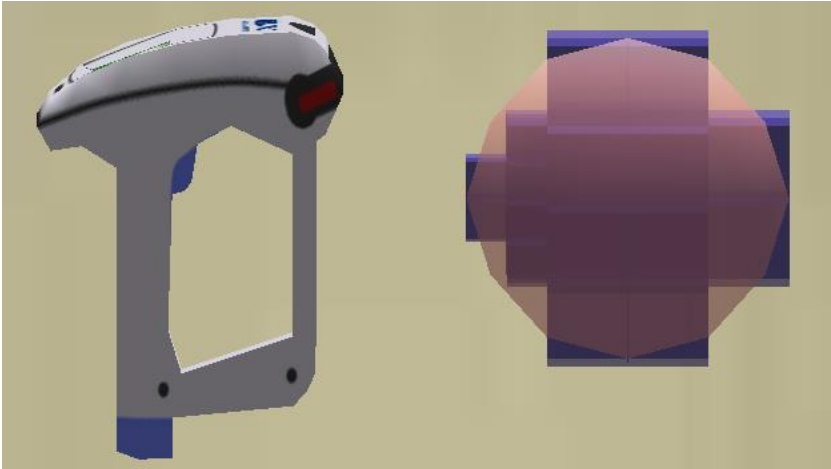
Figure 5-43 Representation source with 40º calibration at 15cm

Now that the accuracy issue has been successfully treated, the next step is to analyse the computational cost of the newly calibrated V6. For this purpose, the number of points (sub-sources) generated to make the mesh for each instance and approaching line will be counted. The following table shows the data.

Distance (cm)	Point mesh density		
	V6 (frontal)	V6 (edge)	V6 (vertex)
500	1	1	1
100	1	1	1
50	1	1	8
30	8	14	11
15	48	66	55

Table 5-5-57 Point mesh density for at front, vertex and edge positions.

The results show a behaviour similar to that of the previously developed algorithms, which increase the number of points steadily as the distance is decreased. The most significant data is the 15cm instance. In this case, the standard V4 calibrated at 60º generates 36 points, if calibrated at 40º it generates 64. The post processing eliminates some of those sub sources reducing the total number of

mesh points to 48. Therefore this V6 represents and intermediate solution between the 40º and 60º standard V4 solutions.

In order to understand if this solution is valid in a practical situation, the V6 prototype calibrated at 40º is run on the testing hardware and the execution time of both the post processing and the main PK computation is measured. The following table shows these results.

Distance (cm)	Execution time (ms)					
	V6 (frontal)		V6 (edge)		V6 (vertex)	
	PK calculus	trimming	PK calculus	trimming	PK calculus	trimming
500	8	4	9	5	9	5
100	9	5	8	6	8	5
50	8	4	9	5	34	4
30	36	4	58	3	44	3
15	210	4	284	5	212	3

Table 5-5-58 Point mesh density for at front, vertex and edge positions.

The results follow the trend set by the point mesh density, with clear increase in execution time associated to distance reduction. The trimming post processing requires a fixed amount of time which never exceeded 5ms which is less than the PK computation time of a single point. Considering the slowest computation required a total of 289ms (284 PK computation plus 5ms for trimming) the V6 performance is well within the established real-time behaviour limit of 1.8s, making it a viable option for the purpose of the task.

5.3.5 Testing simulated Cs-137 cylindrical source with recalibrated algorithm

To further validate the algorithm developed for multiple shapes, a second source geometry is tested. In this case a cylinder of dimensions 88cm high, 60cm diameter is tested. This geometry has been chosen as it is one of the standard sizes for nuclear waste barrels stored in temporal and permanent storage sites and therefore

is a shape which might occur often in nuclear safety and security exercises. The following figure shows the testing scheme performed.
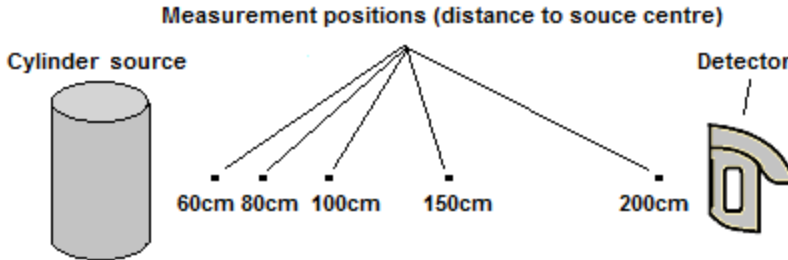
Figure 5-44 Testing scheme for cylindrical source

As in previous tests there will be two parts, first accuracy of the dose rate will be assessed and second the computational cost of the case will be studied. The testing scheme will be the same as used previously with the sphere and the parallelepiped cases, that is computing the dose rate at different distances from the source.

The following table shows the results for the equivalent dose rate computation obtained for the cylindrical source with the prototype and its deviation to the MCNP code.

Position (cm)	Equivalent Dose rate in air Cylinder and deviation (mSv/h)		
	V6 (non-regular + trimming)	deviation	MCNP
(200,0,0)	0.36	+24	0.29
(150,0,0)	0.65	+14	0.57
(100,0,0)	1.6	+9	1.47
(80,0,0)	2.47	-0.4	2.48
(60,0,0)	4.98	+0.2	4.97

Table 5-5-59 Dose rate of cylinder, frontal case with 40º threshold.

The results obtained indicate that generally the accuracy is acceptable although the furthest distance is a borderline case, while

the two closest distances have an extremely good accuracy. The large difference in deviation between the first and second instances is due to the passage from mono PK (at 200cm) to the first level of multi PK. Nevertheless in the first level of multi PK all eight sub sources generated have their central point within the original cylinder volume, so no trimming is applied, which explains the moderate deviation. The next instance involves a further increase in the point mesh resolution and the first appearance of the trimming algorithm managing to lower the deviation under 10%. The last instance involves an even further level of resolution and significant trimming, resulting in an accuracy deviation below 1%.

The trend previously described can be seen in the following graph, notice the convergence of the prototype method with the Monte Carlo benchmark code
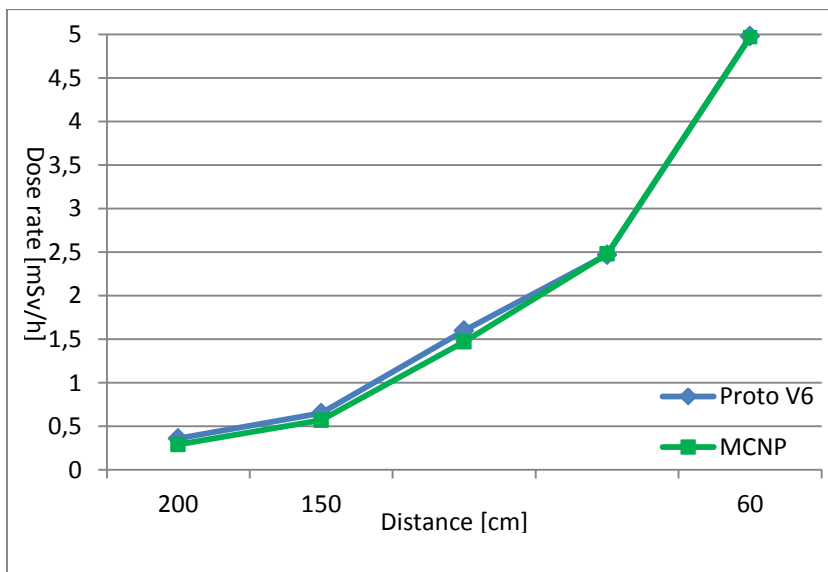
Figure 5-45 Dose rate results for V6 and real detector

Having tested the dose rate accuracy of the method the next task is to analyse the computational cost of the method. For this purpose the point mesh count and execution time will be measured.

First the point mesh density of the generated model will be counted, before the trimming (standard V4 algorithm) and after the trimming (V6). The following table shows this information.

Position (cm)	Point mesh density for cylindrical source		
	V6 (non-regular trimmed)	V4 (non-regular)	Trimmed points
(200,0,0)	1	1	0
(150,0,0)	8	8	0
(100,0,0)	28	36	8
(80,0,0)	28	36	8
(60,0,0)	76	104	28

Table 5-5-60 Point mesh density for cylinder source.

Comparing the new V6 algorithm with trimming to the one it is based on (V4) the V6 reduces the number of points to compute. The reduction is dependent upon the type of shape of the source. In the first and second instances the trimming part of the algorithm is not executed because all the generated points are within the original cylinder volume, it is only at the third instance (1m away) where the first sub-sources are trimmed away to represent the boundary of the cylinder. The fourth instance keeps the same representation, hence no change in the number of points with respect to the third. In the final instance at 60cm distance a further resolution increase is performed and some of the generated points are trimmed off resulting in a 76 point mesh.

The following part of the experiment is to measure the time it takes to compute that 76 point mesh including how much the trimming process took.

The following table shows the timing information of the trimming process, the PK computation and the addition of both for all the distance instances tested.

Position (cm)	Execution time (ms)		
	Trimming	PK computation	Total
(200,0,0)	2	9	11
(150,0,0)	2	33	35
(100,0,0)	8	108	116
(80,0,0)	1	106	107
(60,0,0)	8	304	312

Table 5-5-61 Execution time for cylinder source.

The most significant data from the timing analysis is the fact that the trimming function took in the worst case scenario 8ms to perform its task, therefore it hardly takes a toll on the overall performance and does not represent a menace to the real time requirement. The PK computation part is equivalent to the V4 performance and the total time for the worst case adds up to 312ms which is well below the limit established.

5.4   V7 Prototype: Multiple sources

The objective of this last version of the prototype is to deal with scenarios where multiple sources are present. The application must add up the flux generated by the individual sources to compute the overall dose rate. In essence this is just a summation of the individually generated dose rates.

The experiment performed was to simulate a scenario with three sources and check that each individual source is treated independently and correctly in terms of point mesh resolution and the total dose adds up. The scheme of the simulation is shown in the following figure. Three sources are placed inline 10cm apart from each other, perpendicular to the approach line of the detector, in other words it is the same scheme as the previous test for one cylinder but with two more on the side.
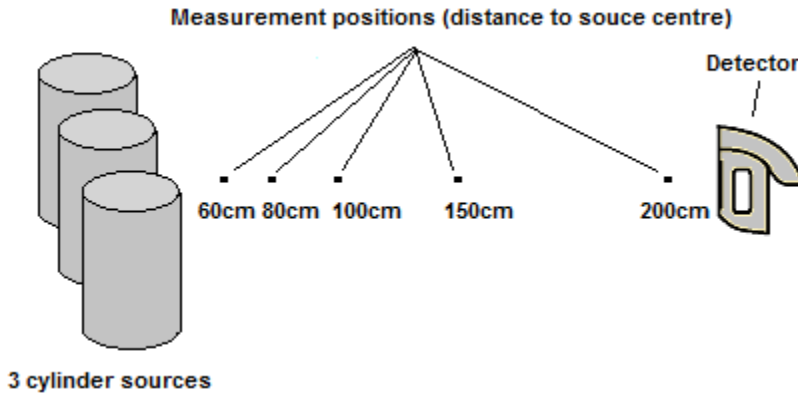
Figure 5-46 Testing scheme for multiple cylindrical sources

The dose rate of each individual source is computed in first place with the V6 algorithm, the results added up and compared to the V7 multi source simulation of the three sources. The following table shows the dose rate results.

Position (cm)	Equivalent Dose rate in air Cylinder and deviation (mSv/h)				
	V6 Cylinder 1	V6 Cylinder 2	V6 Cylinder 3	V6 addition	V7
(200,0,0)	0.36	0.32	0.24	0.92	0.93
(150,0,0)	0.65	0.53	0.35	1.53	1.51
(100,0,0)	1.6	1.31	0.48	3.39	3.4
(80,0,0)	2.47	1.49	0.52	4.48	4.47
(60,0,0)	4.98	1.94	0.53	7.45	7.45

Table 5-5-62 Dose rate of individual and joint sources.

The addition of the three individual doses matches the total dose computed by the V7 algorithm. The negligible differences are due to the rounding up of the figures of the individual doses.

To illustrate what is going on inside the prototype, the following figure shows side by side both the original cylindrical sources (on the

left) and generated representation by the V7 algorithm (on the right). The generated representation shows the points as blue cubes of different size according to the level of resolution they have within the multi PK computation mesh.

It can be noted that the closest cylinder to the detector shows two different levels of resolution (this is due to the non-regular division part of the method), and the finite element boundary representation post processing of the method has trimmed away the points in the outer part of the bounding parallelepiped, making the source resemble a cylinder even if quite crudely at this level of boundary definition.

The second closest source shows signs of higher resolution and trimming only in the side closest to the detector, while the third and furthest source has undergone only one subdivision iteration, but since the centres of all the generated sub-sources lay within the original cylinder volume no trimming has been applied to that source volume.
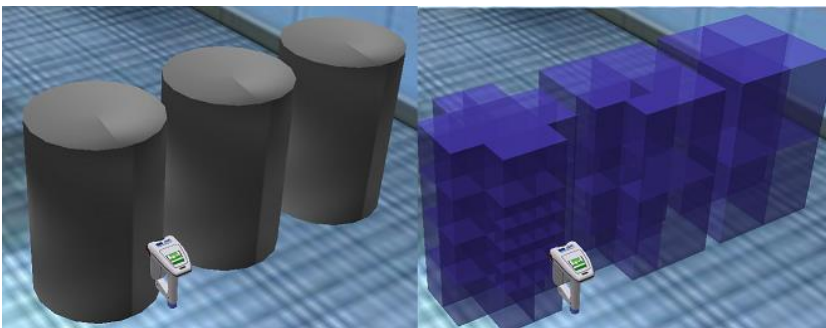
Figure 5-47 Original sources (left), V7 representation (right)

To conclude the analysis of the V7 version (multi source), the execution time of the summation of the individual V6 (single source) simulations will be recorded and compared to the V7 execution time in order to understand if the management of the extra loop affects significantly the execution time of the whole simulation.

Position (cm)	Execution time of V7 compared to V6 (ms)				
	V6 Cylinder 1	V6 Cylinder 2	V6 Cylinder 3	V6 addition	V7
(200,0,0)	12	14	14	40	18
(150,0,0)	46	52	12	110	70
(100,0,0)	164	44	10	218	228
(80,0,0)	162	104	44	310	288
(60,0,0)	424	106	42	572	590

Table 5-5-63 Execution time of V6 addition vs. V7.

From the results from the execution time we can extract two pieces of information, in first place, the V7 is a more efficient manner to achieve the results than the three separate V6 individual simulation due to the fact other computer tasks non-related to the PK-simulation take time no matter what is done. Second due to this overhead time interval, the longer the simulation (more points) the less relevant this overhead is, as the PK computation begins to take over as the most time consuming process in the computer.

Lastly, even for the worst case (590ms), the total execution time for the V7 algorithm is well under the limit set for the time requirement (1.8s for the detector used).

5.5 Testing and Results summary table

Source Simulated	Version	Aim of the test	Benchmark (other reference codes)	Requirements met Accuracy	Requirements met Time
Simulated Cs-137 Dissolved in water 20cm side cube	V1	Assess the feasibility of VR dosimetry app	Monte Carlo (Nucleonica)	No	Yes
	V2	Improve accuracy of V1 prototype	Monte Carlo (V1)	Yes	Yes
	V3	Improve accuracy of V2 prototype	Monte Carlo, (V2, MicroShield, CIDEC)	Yes	Yes
	V4	Improve time of V3 at minimal accuracy cost	Monte Carlo (V3)	Yes	Yes
	V5	Improve time of V4 at minimal accuracy cost	Monte Carlo (V4)	Yes	Yes
Real K40 mixed in KCl 110cm x 60 box	V1	Assess the feasibility of VR dosimetry app	Victoreen 451p survey meter	No	Yes
	V2	Improve accuracy of V1 prototype	Victoreen 451p survey meter	No	Yes
	V3	Improve accuracy of V2 prototype	Victoreen 451p survey meter	Yes	No
	V4	Improve time of V3 at minimal accuracy cost	Victoreen 451p survey meter	Yes	Yes
	V5	Improve time of V4 at minimal accuracy cost	Victoreen 451p survey meter	No*	Yes
Simulated Cs-137 in water 10cm radius sphere	V6	Adapt method to all type of convex shapes.	Monte Carlo	Yes	Yes
Simulated Cs-137 in water 88 x 44 cm radius cylinder	V6	Adapt method to all type of convex shapes.	Monte Carlo	Yes	Yes
	V7	Apply method to multiple sources in a single scenario	Σ V6 individual results	Yes	Yes

6 Conclusions

This work was set out to explore the possibilities of using virtual reality related techniques in the field of nuclear safeguards and security; concretely the aim was to develop an accurate and fast simulator of a gamma radiation detector for virtual training purposes. At the beginning of this thesis, several questions were raised with regards to the feasibility of the task, the main two being: (1) Were the state of the art available gamma radiation transport computation methods capable of meeting the real time demands of Virtual Reality? And (2) was such an application capable of reaching the necessary accuracy for it to be a valid training tool?

In order to answer these questions a working path was established starting from a deep review of the state of the art and from there onwards searching solutions for the problems that existing methods could not solve. For each method devised, a series of evaluation tests were performed to assess if the objectives were met on a prototype application. The results of these tests highlighted limitations of the method, which served as a starting point for the next version's objectives. The next point will take the reader through the conclusions that were drawn from each of these versions.

6.1   Summary of conclusions

A total of seven solutions were elaborated during this thesis, each introduced a method or concept aimed at satisfying the objectives set beforehand. For each solution a new version of the prototype was implemented and tested. The consequent results produced provided the ingredients to make a judgement of the underlying concept introduced, and draw some conclusions summarized next.

6.1.1 V1 Mono PK prototype

The first version of the simulator application featured a mono point kernel gamma radiation transport computation based on the position of a detector and a source within a rich 3D virtual reality environment, providing real-time dose rate results to the user. This prototype was the software cornerstone upon which the subsequent versions built on.

The aim of this version was to demonstrate that such an application was possible which combined virtual reality concepts with real time physics simulation. The novelty of the method resided in the combination of two existing concepts which had not been put together until then. The performance of the prototype under testing proved that indeed it was possible to develop a virtual reality based gamma radiation detector simulator and run it on practical cases such as the one introduced.

Despite achieving its primary goal, some limitations in terms of accuracy of the dose rate computation arose due to the overly simplified method used.

6.1.2 V2 Mono PK with shielding and buildup

The second version of the application was born with the intent of improving the general lack of accuracy which affected its predecessor method without compromising the real time performance obtained. A new more complex PK computation was implemented and the 3D objects definition and PK databases were expanded to add the characteristics necessary to include shielding and buildup effects in the dose rate computation. The results obtained showed a significant improvement in terms of dose rate accuracy, which made the method sufficient for most of the test situations performed.

Nevertheless a limitation appeared in terms of accuracy of the method at short distances, which was above the established limit for a minority of cases.

6.1.3 V3 Multi PK with shielding and buildup

The third version of the prototype had as an objective to tackle the insufficient accuracy at short distances of the mono PK method used in the previous version. The proposed solution was using a multiple PK which could vary the density of its point mesh according to a solid angle check in an automatic manner. This allowed for a fast mono PK computation if possible and a slower multi PK source representation when necessary.

The results proved that all the dose rate accuracy issues of the previous versions were satisfactorily dealt with, it can be concluded that for the average case this method provides a sufficiently accurate dose rate computation for a wide range of possible cases.

On the other hand another kind of problem appeared, this was the lengthy execution time of the method in one of the instances tested (highest point density), which was slower than the reading time of the read detector and therefore affects negatively the realism of the simulation.

6.1.4 V4 Non regular Multi PK with shielding and buildup

The non-regular source representation concept was developed as a solution to deal with the excessive computational burden that regular point meshes can cause in particular cases as evidenced by the testing of the previous version. The idea was to increase the density only in the areas of the original source volume whose dose rate output is more significant to the overall computation, therefore reducing the computational effort but without losing much accuracy.

The testing was very successful, for all testing cases the results complied with both accuracy and time requirements set. This outcome proves within the limits of the testing capabilities that the non-regular solid angle driven multi PK method is a novel and valid solution for a dosimetry application in VR environments.

6.1.5   V5 KD tree based division method for Multi PK

The fifth version of the algorithm explores the use of a division method for the source volume based on KD-tree division methods rather than the octree derived division method used in the previous multi-PK versions. The new KD tree method represents a lighter option from the computational effort point of view but its division can generate less regular sub-sources which might not be as accurate in terms of dose rate computation.

Unlike previous versions this is not the response to a flaw or limitation of the previous method but more of an alternative for the users to prioritise higher accuracy or prioritise faster execution time of the simulation depending on their needs.

The results proved that the V5 version is indeed quicker than the V4 but has a small trade off in terms of dose rate accuracy. Having this option enriches the future user's range of simulation and it represents an interesting solution for low end hardware systems.

6.1.6   V6 Post processed multi PK

The sixth version developed during this thesis had as a main target to explore the possibility of applying any of the developed methods to sources whose volume were not a parallelepiped, since that was how all sources are treated by the previous versions. It is based on a post-processing of the generated mesh where points placed outside the original source volume are eliminated and their activity is redistributed among the inner remaining points.

The testing of this version proved three points; in first place that the representation of a spherical or cylindrical source as a parallelepiped induced accuracy errors beyond the limits set and made the development of this version a necessity for non-parallelepiped cases. Secondly that the proposed method is sufficiently accurate for the case tested and lastly that the extra time required for the post processing does not hinder the real time limitation.

6.1.7 V7 Multiple sources

The last version of the prototype features the possibility to simulate multiple sources in a single scenario, providing the user with the overall equivalent dose rate generated by all sources. This is useful in certain simulation exercises where there are distributed sources like for example a storage site. It is based on the previous V6 method and has its same characteristics and limitations.

The testing of this method was done taking as a benchmark the addition of individual dose rates computed with the previous V6 algorithm. The results showing that the summation was being correctly executed.

6.1.8 Summary of methods

The following table summarizes the characteristics, limitations and performance results of all the developed versions of the prototype.

Version	Shield & Build Up	Division Method	Multiple Source shapes	Multiple sources	Speed Test	Accuracy Test
V1	None	-	No	No	Pass	Fail
V2	Yes Single	-	No	No	Pass	Partial Pass
V3	Yes Single	Regular	No	No	Partial Pass	Pass
V4	Yes Single	Octree Based	No	No	Pass	Pass
V5	Yes Single	KD-tree based	No	No	Pass	Pass
V6	Yes Single	Octree based	Yes	No	Pass	Pass
V7	Yes Single	Octree based	Yes	Yes	Pass	Pass

Table 6-1 Summary of characteristics per version

6.2   Limitations of the work

The work developed has proven to be a flexible tool which could be applied to a wide range of practical applications. Nevertheless there are present some limitations to the prototypes developed. The main ones are:

6.2.1   Inherent PK limitations

The PK method uses a series of data tables. These tables cover a certain energy range, e.g. for attenuation coefficients start at 0.015MeV and reach up to 15 MeV. This limits the energy rays that can be computed by interpolation. For energy lines outside the table ranges, extrapolation is used instead of linear interpolation; this can lead to an error. In practice it is not much of a problem because the real detectors used have a range covered by the tables, e.g. the Victoreen 451P detector used for benchmarking in this work has an energy detection range between 0.023 and 1.3MeV.

6.2.2   Geometrical limitations

The tested geometries correspond to common shapes of real radioactive sources such as parallelepipeds and spheres. The performance of the solid angle driven method presented in this work is suited for these and for any shape whose ratio of length to width and depth is not overly disproportionate. Unrealistic (in practice) shapes such as very thin and long poles might not produce accurate results or lead to very dense untreatable meshes.

6.2.3   Shielding limitations

Only one layer of shielding is implemented in the developed versions, which in practical terms it means a second layer of shielding would not be accounted for in the simulation if it happened to appear in the setup of the problem. Furthermore the data tables for the attenuation coefficients of the shielding elements are limited and only the most common materials are present.

6.2.4   Flux limitations

The detector in reality receives radiation from several possible directions; only direct flux and buildup flux have been taken into account because in most common situations the other flux inputs such as backscattering (radiation bouncing off other obstacles and being directed towards the detector) are so small they can be discarded.

6.3   Future developments

Although the prototype application presented in this thesis meets all of its objectives, it is by no means a perfect solution, and there is room for improvement both in terms of accuracy and speed.

A possible future development to improve the accuracy of the dose rate computation would be to apply a redistribution of the activity of the sub-sources based on the concept of the marching cubes algorithm in order to better represent the sub sources in boundaries of the original source volume. Alternatively the placement of the point in the mesh could be altered instead of activity value.

Another possible development would be to include into the PK computation the backscattering flux, for which an efficient algorithm would have to be devised in order to not jeopardize the real time behaviour of the application.

Also it could be convenient depending on the case to implement a method to deal with multiple shielding obstacles instead of the single obstacle versions developed up to now.

Lastly real time morphing of the source volume could be an interesting future development in order to represent non-solid state radiation sources such as liquids spilling from a tank or gaseous clouds.

6.4   Concluding statement

The main contribution of this work has been the creation of novel efficient methods to represent radiation sources within a virtual reality environment for gamma radiation transport purposes such as dosimetry.

These methods have proven under testing that they are a valid solution for their purpose due to the speed and accuracy they offer, which complies with the requirements for set for a realistic VR based dosimetry application.

Bibliography

[1]   D. Fischer, History of the International Atomic Energy Agency. The First Forty Years., 1997.

[2]   T. Moltó Caracena, D. Brasset, E. Vendrell Vidal and E. Ruiz Morales, "A Design and Simulation Tool for Nuclear Safeguards Surveillance Systems," in *ESARDA 31st annual meeting*, 2009.

[3]   N. Bohr, "On the Constitution of Atoms and Molecules, Part I," *Philosophical Magazine,* no. 26, pp. 1-24, 1913.

[4]   M. Herrero, "The Standard Model," *NATO ASI Series C Mathematical and Physical Sciences-Advanced Study Institute 534,* pp. 1-60, 1999.

[5]   G. F. Knoll, Radiation Detection and Measurement, John Wiley & Sons, Inc., 2010.

[6]   A. Hastings, J. Smith and M. Lucas, Gamma-Ray Detectors.

[7]   I. E. Sutherland, "The Ultimate Display," in *IFIP Congress*, 1965.

[8]   F. P. Brooks Jr., "What's Real About Virtual Reality?," *IEEE Computer Graphics and Applications,* vol. 19, no. 6, pp. 16-27, 1999.

[9]   V. Hayward et al, "Haptic interfaces and devices," *Sensor Review,* vol. 1, no. 24, pp. 16-29, 2004.

[10] J. Cremer, "Driving simulation: challenges for VR technology," *Computer Graphics and Applications, IEEE,* vol. 16, no. 5, pp. 16-20, 1996.

[11] J. Kuhl et al., "The Iowa Driving Simulator: An Immersive Research Environment," *Computer,* vol. 28, no. 7, pp. 35-41, 1995.

[12] B. T. Sullivan and A. P. Soukup, "The NASA 747-400 Flight Simulator: A National Resource for Aviation Safety Research," American Institute of Aeronautics and Astronautics, San Diego, CA, 1996.

[13] R. Zazeckis et al., "New Capabilities of the NTPRO 4000 Full Mission Ship Handling Simulator in the Assessment and Evaluation Processes at Lithuanian Maritime Academy," in *Marine Navigation and Safety of Sea Transportation*, 2009.

[14] I. Klapan et al., "Application of Advanced Virtual Reality and 3D Computer Assisted Technologies in Computer Assisted Surgery and Tele-3D-computer Assisted Surgery in Rhinology," 2011.

[15] C. R. Larsen et al., "Effect of virtual reality training on laparoscopic surgery: randomised controlled trial.," *British Medical Journal,* no. 338, 2009.

[16] D. Opdyke, J. S. Williford and M. North, "Effectiveness of computer-generated (virtual reality) graded exposure in the treatment of acrophobia.," *Am J Psychiatry,* vol. 1, no. 52, 1995.

[17] A. S. Carlin, H. G. Hoffman and a. S. Weghorst, "Virtual reality and tactile augmentation in the treatment of spider phobia: a case report.," *Behaviour research and therapy,* vol. 2, no. 35, pp. 153-158, 1997.

[18] C. Botella et al., "Virtual reality treatment of claustrophobia: a case report," *Behaviour Research and Therapy,* vol. 36, no. 2, pp. 239-246, 1998.

[19] P. S. Dunston et al., "An immersive virtual reality mock-up for design review of hospital patient rooms.," *Collaborative Design in Virtual Environments,* pp. 167-176, 2011.

[20] F. Shao, A. J. Robotham and K. K. Hon, "Development of a 1: 1 Scale True Perception Virtual Reality System for design review in automotive industry.," in *Internation Conference on Manufacturing Research ICMR 2012*, 2012.

[21] S. Stansfield, "Applications of virtual reality to nuclear safeguards," Sandia National Laboratories, Albuquerque, 1998.

[22] K. Michel et al, "An ideal marriage: Projected Virtual Reality & Numerical Models that keep it real," in *INMM Annual meeting*, Tucson, Arizona, 2009.

[23] A. Mól et al, "Virtual Environments simulation for dose assessment in nuclear plants," *Progress in nuclear energy,* no. 51, pp. 382-387, 2009.

[24] Z. Kriz et al, "Unreal III BASED 3-D VIRTUAL MODELS FOR TRAINING AT NUCLEAR POWER PLANTS," in *Proceedings of the 1st International Nuclear and Renewable Energy Conference (INREC10)*, Amman, Jordan, 2010.

[25] F. Vermeersch, "Dose assessment and dose optimization in decommissioning using the VISIPLAN 3D ALARA planning tool.," in *Radiation protection and decomissioning conference ABR/BVS.*, Brussels, 2003.

[26] E. Nystad, A. Drøivoldsmo and A. Sebok, "Use of radiation maps in a virtual training environment for NPP field operators," Halden Work Report HWR-681, Halden, 2002.

[27] M. Scott and M. Kelly, "A Collaborative Environment for Information Driven Safeguards," in *IAEA Symposium on International Safeguards*, Los Alamos, 2010.

[28] B. Hayes, D. Few, K. Michel, D. Determan and K. LeBlanc, "Augmented reality: Don't we all wish we lived in one?," Los Alamos National Laboratory, Los Alamos, 2010.

[29] J. K. Tackentien, C. Owens and R. Brown, "Lessons Learned and Potential Paths Forward in Virtual Reality Developments for the International Atomic Energy Agency.," in *INMM annual meeting 2013*, Palm Desert, 2013..

[30] S. Huang et al., "Roles of Information Technology in Nuclear Criticality Safety Training.," in *American Nuclear Society*, Atlanta, 2013.

[31] T. Moltó Caracena, J. G. M. Gonçalves and S. E. Pickett, "A Virtual Reality based Safeguards Surveillance Training Tool," in *ESARDA 35th annual meeting - Symposium on safeguards and nuclear material management,*, 2013.

[32] T. Moltó Caracena, J. Gonçalves and S. Pickett, "Hands-on training of IAEA Safeguards Surveillance Concepts using a VR based Application," in *Proceedings of INMM 54th Annual Meeting*, Palm Springs, USA, 2013.

[33] T. Caracena, J. Goncalves, P. Peerani and E. Vidal, "A Variable Point Kernel Dosimetry Method for Virtual Reality Simulation Applications in Nuclear Safeguards and Security," *IEEE Transactions on Nuclear Science,* vol. 60, no. 5, 2013.

[34] U. S. Metropolis N., "The monte carlo method.," *Journal of the American statistical association,* vol. 44, no. 247 , pp. 335-341, 1949.

[35] L. Carteret al., "Monte Carlo Code Development in Los Alamos," Los Alamos NM, USA., 1975.

[36] R. Brun, F. Bruyant and M. Marie., "GEANT Detector Description and Simulation Tool, CERN Program Library Long Writeup W5013," Geneve, 1995.

[37] S. Agostinelli et al., "GEANT4—a simulation toolkit.," *Nuclear instruments and methods in physics research section A: Accelerators, Spectrometers, Detectors and Associated Equipment,* vol. 506, no. 3, pp. 250-303, 2003.

[38] J. Baro et al., "PENELOPE: an algorithm for Monte Carlo simulation of the penetration and energy loss of electrons and positrons in matter.," *Nuclear Instruments and Methods in Physics Research Section B: Beam Interactions with Materials and Atoms,* vol. 100, no. 1, pp. 31-46, 1995.

[39] A. Ferrari et al, "Fluka.," CERN-library, Geneve, 2005.

[40] J. P. Both et al., "A survey of TRIPOLI-4.," in *Proceedings of International Conference on Radiation Shielding.*, 1994.

[41] H. Hirayama et al., "The EGS5 code system.," United States. Department of Energy, 2005.

[42] P. Andreo, "Monte Carlo techniques in medical radiation physics.," *Physics in Medicine and Biology 36.7 (): 861.,* vol. 36, no. 7, pp. 861-909, 1991.

[43] P. A. Mazzali and L. Lucy, "The application of Monte Carlo methods to the synthesis of early-time supernovae spectra.," *Astronomy and Astrophysics,* no. 279, pp. 447-456, 1993.

[44] T. Booth, K. Kelley and S. McCready, "Monte Carlo Variance Reduction Using Nested Dxtran Spheres," in *PSD-2008 conference proceedings, also Nuclear Technology*, 2009.

[45] C. Solomon, A. Sood, T. Booth and J. Shultis, "An Sn Approach to Predicting Monte Carlo Cost with Weight Dependent Variance Reduction," *Trans. Am. Nuc. Soc,* no. 103, 2010.

[46] H. G. Hughes, "Variance Reduction with Pulse-Height Tallies in MCNP," in *Workshop on Uncertainty Assessment in Computational Dosimetry*, Bologna, Italy, 2007.

[47] A. Assad et al., "A new approximating Formula for Calculating Gamma-ray Buildup Factors in Multilayer Shields," *Nuclear Science and Engineering,* no. 132, pp. 203-216, 1999.

[48] Y. Wu, "CAD-based interface programs for fusion neutron transport simulation.," *Fusion Engineering and Design,* vol. 7, no. 84, pp. 1987-1992, 2009.

[49] I. M. Prokhorets, S. I. Prokhorets, M. A. Khazhmuradov, E. V. Rudychev and D. V. Fedorchenko, "Point-Kernel method for radiation fields simulation.," *PROBLEM OF ATOMIC SCIENCE AND TECHNOLOGY, Series: Nuclear Physics Investigation,* no. 48, pp. 106-109, 2007.

[50] G. A. Warren, L. E. Smith, M. Cooper and W. Kaye, "Evaluation framework for search instruments.," in *Nuclear Science Symposium Conference Record, 2005 IEEE*, 2005.

[51] Y. Li, L. Lu, A. Ding, H. Hu, Q. Zeng, S. Zheng and Y. & Wu, "Benchmarking of MCAM 4.0 with the ITER 3D model.," *Fusion Engineering and Design,* no. 82, pp. 2861-2866., 2007.

[52] S. Chandrasekhar, Radiative transfer, Courier Dover Publications, 1960.

[53] B. G. Carlson and K. D. Lathrop, Transport Theory–The Method of Discrete Ordinates, New York: Gordon & Breach, 1968.

[54] W. A. Rhoades and R. L. Childs, "The TORT three-dimensional discrete ordinates neutron/photon transport code.," No. ORNL-6268., Oak Ridge National Lab., TN (USA), 1987.

[55] W. Rhoades and M. Emmett, "DOS - The Discrete Ordinates System," ORNL/TM-8362, 1982.

[56] J. Engle and W. Ward, "A USERS MANUAL FOR ANISN: A ONE DIMENSIONAL DISCRETE ORDINATES TRANSPORT CODE WITH ANISOTROPIC SCATTERING. No. K--1693.," ORNL, Oak Ridge, Tenn., 1967.

[57] N. M. Greene and L. M. Petrie., "XSDRNPM-S: A One-Dimensional Discrete-Ordinates Code for Transport Analysis.," ORNL, Oak Ridge, 1983.

[58] D. G. Cacuci, Handbook of Nuclear Engineering, Springer, 2010.

[59] Y. Chen, "Coupled Monte Carlo-discrete ordinates computational scheme for three-dimensional shielding calculations of large and complex nuclear facilities," Wissenschaftliche Berichte FZKA, Karlsruhe , 2005.

[60] Kalugin M.A., "Simulation of the Radiation Fields from Ionizing Radiation Sources inside the Containment in an Accident," Physics of Atomic Nuclei, vol. 73, no. 13, pp. 2198-2202, 2010.

[61] American Nuclear Society, Gamma-ray attenuation coefficients and buildup factors for engineering materials, La Grange Park, Illinois, USA: American Nuclear Society, 1991.

[62] C. Eisenhauer and G. L. Simmons, "Point isotropic gamma-ray buildup factors in concrete.," *Trans. Amer. Nucl. Soc.,* vol. 16, pp. 358-360, 1973.

[63] A. Chilton, "Optimized Taylor parameters for concrete buildup factor data.," *Nucl. Sci. Eng.,* no. 64, pp. 799-800, 1977.

[64] A. Chilton, "Tschebycheff-fitted Berger coefficients for Eisenhauer-Simmons gamma-ray buildup factors in ordinary concrete.," *Nucl. Sci. Eng.,* no. 69, pp. 436-438, 1979.

[65] Y. Harima, Y. Sakamoto, S. Tanaka and M. Kawai, "Validity of the geometric-progression formula in approximating gamma-ray buildup factors.," *Nucl. Sci. Eng.,* vol. 1, no. 94, pp. 24-35, 1986.

[66] L. Smith et al., "Coupling Deterministic and Monte Carlo Transport Methods for the Simulation of Gamma-Ray Spectroscopy Scenarios," *IEEE Transactions on Nuclear Science,* vol. 55, no. 5, 2008.

[67] M. B. Emmett, C. E. Burgart and T. J. Hoffman., "DOMINO, a general purpose code for coupling discrete ordinates and Monte Carlo radiation transport calculations.," No. ORNL--4853. Oak Ridge National Lab., Oak Ridge, 1973.

[68] F. R. Mynatt, "A User's Manual for DOT, A Two-Dimensional Discrete Ordinates Transport Code with Anisotropic Scattering.," K-1694, Union Carbide Corporation, Oak Ridge, 1967.

[69] E. Straker et al., "The MORSE code - A Multigroup Neutron and Gamma-ray Monte Carlo Transport Code.," ORNL-4585, Oak Ridge, 1970.

[70] J. Wagner and A. Haghighat, "Automated Variance Reduction of Monte Carlo Shielding," *Nuclear Science and Engineering,* no. 128, pp. 186-208, 1997.

[71] D. Systemes, "3DVIA Virtools," Dassault Systèmes, [Online]. Available: http://www.virtools.com. [Accessed 2013].

[72] T. Moltó Caracena, J. G. Gonçalves, E. Vendrell Vidal and P. Peerani, "Virtual Reality based simulator for Dose Rate calculations in Nuclear Safeguards and Security," in *ESARDA Symposium*, Budapest, 2011.

[73] J. G. Gonçalves, T. Moltó Caracena, V. Sequeira and E. Vendrell Vidal, "Virtual Reality based System for Nuclear Safeguards Applications," in *IAEA Symposium*, Vienna, 2010.

[74] T. Moltó Caracena, J. Goncalves, P. Peerani and E. Vendrell Vidal, "Real time Radiation Detection Simulator for Nuclear Security Training," in *Joint Virtual Reality Conference of Euro VR – EGVE – VEC*, Stuttgart, 2010.

[75] W. Stevens, G. Myers and L. Constantine, "Structured Design," *IBM Systems Journal,* vol. 2, no. 13, pp. 115-139, 1974.

[76] G. Software, "Microshield 9.XX," Lynchburg, VA 24503 USA, 2013.

[77] J. Galy and J. Magill, "WEB-BASED DOSIMETRY AND SHIELDING CALCULATIONS IN NUCLEONICA," ITU European Commission, Karlsruhe.

[78] H. H. Chen and T. S. Huang., "A survey of construction and manipulation of octrees.," *Computer Vision, Graphics, and Image Processing,* vol. 43, no. 3, pp. 409-431, 1988.

[79] J. L. Bentley, "Multidimensional binary search trees used for associative searching.," *Communications of the ACM,* vol. 18, no. 9, pp. 509-517, 1975.

[80] J. J. Friedman, J. L. Bentley and R. A. Finkel, "An algorithm for finding best matches in logarithmic expected time," *ACM Trans. Mathematical Software,* vol. 3, pp. 209-226, 1977.

[81] S. Maneewongvatana and D. M. Mount., "It's okay to be skinny, if your friends are fat," 1999.

[82] A. A. G. Requicha and H. Voelcker, "Boolean operations in solid modeling: Boundary evaluation and merging algorithms," *Proceedings of the IEEE,* vol. 73, no. 1, pp. pp.30,44, 1985.

[83] Ó. Vela, E. de Burgos and J. M. Pérez, "Dose rate assessment in complex geometries.," *Nuclear Science, IEEE Transactions on,* vol. 53, no. 1, pp. 304-311, 2006.

[84] J. Magill et al, "NUCLEONICA: a nuclear science portal.," *ENS News,* no. 17, 2007.

[85] C. A. Negin, "MICROSHIELD-a microcomputer program for analyzing dose rate and gamma shielding.," *Transactions of the American Nuclear Society,* vol. 53, pp. 421-422, 1986.

[86] R. A. Forster, L. J. Cox, R. F. Barrett, T. E. Booth, J. F. Briesmeister, F. B. Brown and A. Sood, "MCNP™ version 5.," *Nuclear Instruments and Methods in Physics Research Section B: Beam Interactions with Materials and Atoms,* no. 213, pp. 82-86., 2004.

[87] Fluke Corporation, Victoreen 451P & 451P-DE-SI Ion chamber survey meter Operators Manual, Cleveland, Ohio, USA, 2005.

[88] T. Moltó Caracena, J. G. Gonçalves, P. Peerani and E. Vendrell Vidal, "Virtual Reality based Simulator for Dose Rate Calculations in Nuclear Safeguards and Security," in *ESARDA Symposium*, Budapest, 2011.

[89] G. Janssens-Maenhout, Nuclear Safeguards and Non-Proliferation, Office for Official Publications of the European Communities, 2008.

Appendix A

This appendix specifies the list of publications related to the work performed during this PhD, along with a brief description and their relation to the thesis.

A Design and Simulation Tool for Nuclear Safeguards Surveillance Systems

T. Molto Caracena, D. Brasset, E. Vendrell Vidal, E. Ruiz Morales, J.G.M. Gonçalves

Published in Proceedings of ESARDA - 31st Annual Meeting - Symposium on Nuclear Material Management, 2009.

This is the first article published by the author in the context of virtual reality based applications in the field of nuclear safeguards and security; it describes a possible training application for future IAEA inspectors where they can learn how to set up surveillance systems in nuclear material storage sites.

This work introduced already some of the concepts treated in this thesis such as virtual scenarios for training and task specification (chapters 3.3 and 3.4). The developed prototype of this thesis is based on these concepts.

Virtual reality based system for nuclear safeguards applications

J. Gonçalves, T. Moltó Caracena, V. Sequeira, and E. Vendrell Vidal

Poster presented and paper published in proceedings of IAEA Symposium on International Safeguards, 2010.

This article and it respective poster presented two prototype applications, one of them being the genesis of this PhD, a virtual reality based application prototype featuring a virtual radiation

detector (several actually) within a scenario which represented a customs border control area.

At this stage there was no simulation of the physical processes underlying radiation transport, the inverse of the distance to the source was displayed on screen as explained in section 3.5 of this document. This way the behaviour of dose rate reducing with distance is mimicked. Nothing more elaborated was included because the purpose was to illustrate the possibility of this kind of training application to the audience and explore this and other ways in which virtual reality techniques could be of interest in the field of Nuclear safeguards and security.

Real-time Radiation Detection Simulator for Nuclear Security Training

T. Moltó Caracena, J. G. M. Gonçalves, P. Peerani, E. Vendrell Vidal
Poster presented and paper published in proceedings of Joint Virtual Reality Conference of Euro VR – EGVE – VEC, Stuttgart 2010.

In this conference a poster and its explaining article were presented, unlike the previous one which featured a broad demonstrational approach on VR for Nuclear Safeguards, this one was exclusively focused on the virtual radiation detector simulation application. Further interactivity behaviour with objects was included and most importantly the first attempt to provide a dose rate value was presented.

This version, explained in chapter 3.6 of the thesis used a dose rate mapping of the scenario generated offline with a MC simulation and then a value was linearly interpolated from the closest points to the detector on the map. The resulting prototype allowed for the first time to have a real dose rate value albeit with some limitations in terms of interactivity.

Virtual Reality based Simulator for Dose Rate Calculations in Nuclear Safeguards and Security

T. Moltó Caracena, J. G. M. Gonçalves, P. Peerani, E. Vendrell Vidal

Article published in Proceedings of ESARDA 33rd annual meeting - Symposium on safeguards and nuclear material management, 2011.

This article describes in detail the Point Kernel method which is used for the first time in the radiation detector simulation application, this corresponds to the versions of the prototype explained in the thesis chapters 4.2 and 4.3, without and with Build up respectively.

The importance of the this version is that for the first time the prototype application showed it could cope with both the accuracy and real time restrictions imposed by the problem.

Also the definition of the training task to be simulated was introduced which is important for the application to be a valuable and useful tool in real training sessions.

Free form source representation for a VR dosimetry training application

T. Moltó Caracena, J.G.M. Gonçalves, P. Peerani, E. Vendrell Vidal

Published in ESARDA 35th annual meeting - Symposium on safeguards and nuclear material management, 2013

This paper elaborated on ways to represent multiple kinds of shapes for radiation sources instead of the parallelepipeds used so far in previous versions, the proposed method used boundary representation with finite elements, and this corresponds to contents of chapter 4.7 of the thesis.

The results showed promising performance and therefore this method was included in the prototype application in its latest versions.

A Virtual Reality based Safeguards Surveillance Training Tool

T. Moltó Caracena, J.G.M. Gonçalves, S.E. Pickett

Presented and published in the proceedings of ESARDA 35th annual meeting - Symposium on safeguards and nuclear material management, 2013

This article further focused on the practical enhancements of the Surveillance simulation tool which received several upgrades since its prototype version was unveiled several years before.

These included simulation tools that permitted users to evaluate certain characteristics of their installation in much less time than an ordinary verification in a real scenario would take.

Real-time, Accurate Radioactive Source Representation for Virtual Reality based Training on Radiation Detection

T. Moltó Caracena, J.G.M. Gonçalves, P. Peerani, E. Vendrell Vidal

Published in Proceedings of INMM 54th Annual Meeting, July 2013.

This publication treats the topic or source representation oriented to a different audience with respect to the paper presented in ESARDA in the same year. This is due to the fact that the INMM (Institute of Nuclear Material Management) has a more industrial scope and is more interested in the practicality of the ideas proposes rather than the academic side of the proposal.

Furthermore the paper diverges on other projects which are only tangentially related to the PhD and are therefore not discussed in this context.

Hands-on training of IAEA Safeguards Surveillance Concepts using a VR based Application

T. Moltó Caracena, J.G.M. Gonçalves, S.E. Pickett

Published in the Proceedings of INMM 54th Annual Meeting, July 2013.

This article presents the latest novelties of the Safeguards Surveillance application adapting the content to the context of the meeting. Meaning that the practical aspect of tools presented is prioritised over the academic or scientific component of the work.

Therefore this article focused on the visual impact of the 3D models developed for the applications and the rest of software tools which emphasize the advantages of computer based training and the educational potential of these VR based tools in the field of Nuclear Safeguards and Security.

Lastly the paper narrates the experience with a real training session performed with one of these software tools to demonstrate its actual value and not just hypothesize about the potential of VR based tools.

A Variable Point Kernel Dosimetry Method for Virtual Reality Simulation Applications in Nuclear Safeguards and Security

Caracena T.M, Gonçalves J.G.M, Peerani P, Vidal E.V.

Published in IEEE Transactions on Nuclear Science, Vol. 60, Issue 5, October 2013.

Last, this article is the most in depth work published so far and gives a detailed view of the Octree non-regular Multi PK version of the application. This corresponds to the version described in chapter 4.5 of the thesis.

This article focused on the new characteristics of the prototype application in that version which are the use of a non-regular division of the radiation source volume, the solid angle check as a way of

evaluating the volume of the source and the dynamic nature of the automatic resolution choice of the algorithm.

With the results obtained it concluded that this was a valid approach to solving the problem of developing a VR based simulator of a portable radiation detector. Which is a conclusion shared with the thesis itself.